Research Report
KTC-05-21/SPR 238-02-1F

KENTUCKY TRANSPORTATION CENTER

College of Engineering

BEARING CAPACITY ANALYSIS AND DESIGN OF HIGHWAY BASE MATERIALS REINFORCED WITH GEOFABRICS

UNIVERSITY OF KENTUCKY

UNIVERSITY OF KENTUCKY
College of Engineering
Kentucky Transportation Center

Our Mission

We provide services to the transportation community through research, technology transfer and education. We create and participate in partnerships to promote safe and effective transportation systems.

We Value...

Teamwork -- Listening and Communicating, Along with Courtesy and Respect for Others
Honesty and Ethical Behavior
Delivering the Highest Quality Products and Services
Continuous Improvement in All That We Do

For more information or a complete publication list, contact us

KENTUCKY TRANSPORTATION CENTER
176 Raymond Building
University of Kentucky
Lexington, Kentucky 40506-0281

(859) 257-4513
(859) 257-1815 (FAX)
1-800-432-0719
www.ktc.uky.edu
ktc@engr.uky.edu

The University of Kentucky is an Equal Opportunity Organization

Research Report KTC- 05-21/SPR-238-02-1F
KYSPR-SPR-238-02

Bearing Capacity Analysis and Design of Highway Base Materials Reinforced with Geofabrics

by

Tommy C. Hopkins
Program Manager and
Chief Research Engineer

Liecheng Sun
Senior Research Engineer

and

Mikhail E. Slepak
Former Senior Research Engineer

Kentucky Transportation Center
College of Engineering
University of Kentucky

in cooperation with the
Kentucky Transportation Cabinet
The Commonwealth of Kentucky
and
Federal Highway Administration

The contents of this report reflect the views of the authors, who are responsible for the facts and accuracy of the data herein. The contents do not necessarily reflect the official views or policies of the University of Kentucky, Kentucky Transportation Cabinet, nor the Federal Highway Administration. This report does not constitute a standard, specification, or regulation.

August 2005

1. Report No. KTC- 05-21/SPR-238-02-1F	**2. Government Accession No.**	**3. Recipients catalog no**
4. Title and Subtitle **Bearing Capacity Analysis and Design of Highway Base Materials Reinforced with Geofabrics**		**5. Report Date** June 2005 **6. Performing Organization Report No.** KTC- 05-21/SPR-238-02-1F
7. Author(s) Tommy C. Hopkins, Liecheng Sun, and Mikhail Slepak		**8. Performing Organization Code** **9. Work Unit No. (TRAIS)**
10. Performing Organization Name and Address University of Kentucky, College of Engineering Kentucky Transportation Center University of Kentucky, 176 Oliver Raymond Building Lexington, Kentucky 40506-0281		**12. Contract or Grant No.** SPR-SPR-238-02 **13. Type of Report and Period Covered** Final
13. Sponsoring Agency name and address Kentucky Transportation Cabinet, 200 Mero Street Frankfort, KY 40622		**14. Sponsoring Agency Code**

15. Supplementary Notes
Prepared in cooperation with the Kentucky Transportation Cabinet and the United States Department of Transportation, Federal Highway Administration

16. Abstract
The primary objective of this study was to develop and implement mathematical bearing capacity models originally proposed by Hopkins (1988, 1991) and Slepak and Hopkins (1993; 1995). These advanced models, which are based on limit equilibrium and are operated together, can be used to analyze the bearing capacity, or stability, of early construction of loads on a single layer of material, two-layered problems involving a layer of base aggregate and subgrade, and a foundation involving multiple layers of different materials, such as a flexible asphalt pavement. A Prandlt-type shear surface is used in the model analyses of layered foundations. In this report, the models are extended to analyzing flexible pavements reinforced with tensile elements. Although the current model does not account for strain compatibility, the strength of the tensile elements may be input for assumed strain levels. Any number of tensile elements may be analyzed in a given problem. In the limit equilibrium approach, shear strengths, the angle of internal friction, N, and cohesion, c, are entered for each layer of material. Triaxial testing of the asphalt material is performed in a manner that the shear strength parameters, N and c, are developed as a function of temperature. Hence, if the temperature of the asphalt layer is known (or assumed) at a site, then values of N, and, c, may be calculated from the relationships between the shear strength parameters and temperature. Moreover, to facilitate and provide an efficient means of analyzing early construction cases and flexible pavements reinforced with geosynthetics, "Windows" software was developed. In the case of the asphalt layer, the entire layer is divided into finite layers because N and c varies with depth of asphalt. When the surface temperature of the asphalt is known (or assumed), a temperature distribution model is used to estimate the temperature at any depth below the asphalt layer surface. Consequently, the shear strength parameters are known at any depth (of each finite layer) below the surface. To establish the validity and reasonableness of the newly developed limit equilibrium models, bearing capacity factors are derived from the limit equilibrium methods and compared to classical bearing capacity factors, N_c and N_q, developed by Prandlt and Reissner. Differences range from 1 to 10 and 1 to 3 percent, respectively. The Slepak-Hopkins model yields values of $N_($ that are 12 to 38 larger than values published by Caquot and Kerisel. However, values of $N_($ from the Slepak-Hopkins model are only 3 to 11 percent larger than back calculated values obtained by Debeer and Ladanyi from experimental footing tests. The Slepak-Hopkins model was also used to analyzed 237 flexible pavement sections of the 1959-1960 AASHO Road Test. Factors of safety from the model analyses showed that very reasonable results were obtained and were in line with failures recorded at the test site. Finally, actual analyses of a stretch of roadway where failures occurred were analyzed. Three sections involved tensile elements.

17. Key Words Bearing Capacity, Reinforcement, Tensile Elements, Geofabrics, Pavements, Subgrades, Limit Equilibrium, Design, Theory		**18. Distribution Statement** Unlimited, with the approval of the Kentucky Transportation Cabinet	
19. Security Classif. (of this report)	**20. Security Classif. (of this page)**	21.No of Pages **119**	22. Price

TABLE OF CONTENTS

LIST OF FIGURES

LIST OF TABLES

EXECUTIVE SUMMARY

Mathematical bearing capacity models proposed and developed by Hopkins in 1986 and 1991 and Slepak and Hopkins in 1993 and 1995 were extended to analyzing flexible pavements reinforced with tensile elements. The models were initially developed for analyzing the stability of reinforced earthen walls and slopes. Those advanced models, which are based on limit equilibrium concepts and operate together in the computer software, can be used to analyze the bearing capacity, or stability, wheel loads resting on a single layer of pavement subgrade, two-layered problems involving a layer of base aggregate and subgrade, and a flexible asphalt pavement involving multiple layers of different materials. In bearing capacity problems, a Prandtl-type shear surface is used in the model analyses of layered foundations. Derivations of equations of the Hopkins and Slepak-Hopkins models are presented. Other limit equilibrium models are reviewed and discussed. The approach developed by Slepak and Hopkins (1993, 1995a,b), referred to as the Perturbation Method, is recommended when reinforcement is used. Either the Perturbation Method, or the Hopkins method, may be used in stability problems that do not involve reinforcement, or tensile elements. The Perturbation Method can be used to analyze all classes of stability problems involving circular or noncircular shear surfaces. Both effective and total stress analyses may be performed. Effective stress analyses may be performed in the stability analyses of flexible pavements if pore water pressures are known (or estimated) using the Perturbation Method.

Although the current model does not account for strain compatibility, the strength of the tensile elements may be input for assumed strain levels. Pullout resistance forces are computed for both active and passive zones. Those forces are compared to the strength entered by the user and the smaller value is used in the analyses. Any number of tensile elements may be analyzed in a given problem. In the limit equilibrium approach, shear strengths, the angle of internal friction, N, and cohesion, c, are entered for each layer of material. Triaxial testing of asphalt materials is performed in such a manner that the shear strength parameters, N and c, are developed as a function of temperature. Hence, if the temperature of the asphalt layer is known (or assumed) at a site, then values of N, and, c, may be calculated from the relationships between the shear strength parameters and temperature.

Moreover, to facilitate and provide an efficient means of analyzing early construction cases and flexible pavements reinforced with geosynthetics, "Windows" software was developed. The report includes a "user's guide" for operating the computer software. The limit equilibrium equations developed by the authors were originally coded in the Fortran language and data entry was difficult. However, to avoid recoding the Fortran software programs and to facilitate the use of the author's limit equilibrium models, PowerBuilder 8.0 was used to developed Graphical User Interface screens for the Windows program and data entry. The software was structured so that the old Fortran programs did not have to be recoded. The reliability of results from the old Fortran programs was enhanced since extensive "debugging" was not required. Moreover, results obtained from the older programs had been compared to results from many published stability examples on numerous occasions.

To establish the validity and reasonableness of results obtained form the author's limit equilibrium models, bearing capacity factors were derived from the author's programmed models and compared to classical bearing capacity factors, N_c and N_q, developed by Prandtl and Reissner in 1921. Differences in the bearing capacity factors from the author's Perturbation Method and those by and Reissner were only 1 to 10 and 1 to 3 percent, respectively. The Slepak-Hopkins Perturbation Model yielded values of $N_($ that are 12 to 38 percent larger than values published by Caquot and Kerisel. However, values of $N_($ from the Slepak-Hopkins model are only 3 to 11 percent larger than back-calculated values obtained by Debeer and Ladanyi from experimental footing tests.

The minimum shear strength (and CBR-value) of a soil subgrade needed to construct a flexible pavement was established from the Perturbation Model. The minimum CBR-value of the soil subgrade should be about 8 to 10 to safety construct a flexible pavement on a soil subgrade. Published field results of CBR verified results obtained from the theoretical model; essentially identical results were obtained. When should mechanical, such as reinforcing geogrids, or chemical stabilization be used? The model analyses showed that subgrade stabilization should be considered when the CBR (soaked) value of the subgrade is less than about 6 or 7. Those theoretical analyses were based on the assumption that the dual-wheel, contact stresses are 80 lbs/ft_2. The findings of this study and past studies by the author have been incorporated into recent pavement design standards of the Kentucky Transportation Cabinet.

The Slepak-Hopkins model was also used to analyze 237 flexible pavement sections of the 1959-1960 AASHO Road Test. Factors of safety from the model analyses showed that very reasonable results were obtained and were in line with failures recorded at the test site. Factors of safety of pavement sections that survived the AASHO Road Test two-year testing program (for ESALS ≥ 8 million equivalent single axle loads) generally exceeded 1.5.

Finally, actual analyses of a stretch of roadway where failures occurred were analyzed. Three sites of six test sites involved tensile elements. At three locations where tensile elements were used, and assuming tensile element mobilized strains of 2 percent, 5 percent, and ultimate strain, the factor of safety increased some 2-5 percent, 2–5 percent, and 6 to 12 percent, respectively, as shown by the Perturbation analyses. Geo-tensile elements with larger strengths than those used at those sites could produce larger factors of safety.

To advance the use and implementation of the limit equilibrium bearing capacity models described herein, the following recommendations were proposed:

- The Slepak-Hopkins Model, referred to as the Perturbation Method, proposed herein is recommended for general use in all classes of stability problems. In particular, the method is suitable for analyzing bearing capacity problems involving early pavement construction situations involving base aggregates reinforced with tensile elements. The approach, however, is suitable for analyzing completed flexible pavements reinforced with tensile elements. The method is also suitable for analyzing those situations where tensile elements are not used.

- To further validate and calibrate the model, additional field research studies need to be made that involve flexible pavements reinforced with tensile elements. Additional flexible pavement sites, however, where obvious pavement failures have occurred, need to be analyzed that do not involve tensile elements. In cases involving failures, the Perturbation Model should yield low values of factors of safety. The examples described herein appear to indicate that low factors of safety were obtained in areas where the flexible pavement showed distress.

- As deformation occurs under wheel loadings—bearing capacity problems--the strains of pavement layers and the strains of geofabrics are not necessarily the same, that is, there is incompatibility of strains. To mobilize the strength of the geofabric, sufficient strains must occur in the geofabric—and the pavement layers. Although the forces should be derived from the principle of strain compatibility, in this study, a simple assumption with respect to reinforcement forces was made, that is, the external forces of the geofabric act horizontal. Development of a strain compatibility model was much beyond the scope of this study and a new research proposal should be considered in the future to develop a

model. The assumption made in the Perturbation Model still allows the user to determine the factor of safety against failure if it assumed that a certain percentage of strain is mobilized in the tensile element.

- To fully implement the Perturbation computer software, it is recommended that a one- or two-day workshop be developed and taught to interested parties. The workshop should be geared toward teaching and explaining, in detail, the necessary parameters for performing bearing capacity analysis of reinforced flexible pavement. This workshop would be developed for practicing geotechnical engineers.

- For practicing engineers who are not totally versed in geotechnical engineering and are mainly interested in performing bearing capacity analyses of early construction and completed flexible pavements cases involving tensile element forces, it is recommended that simplified data entry screens be devised. In this case, the workshop could be shortened to one half-or one-day. The shortened version would basically be a "hands on" course for the user and include numerous examples.

INTRODUCTION

Problem Statement

Research by the University of Kentucky Transportation Center (Geotechnology Section) in the eighties and nineties helped establish a major subgrade stabilization program for the Kentucky Transportation Cabinet (Hopkins 1987; Hopkins et al, 1988; Hopkins and Hunsuckle, 1990; Hopkins and Allen, 1986a; Hopkins and Beckham 1995;). Techniques that evolved from the past research make use of chemical admixtures, such as hydrated lime and cement, to strengthen highway soil subgrades. As past research has shown (Hopkins, 1991; Hopkins and Beckham, 1995; Hopkins, et al, 1994a,b, c, d) soils generally used to construct highway pavement subgrades in Kentucky have large clay fractions and are usually very weak. Clay soils have a large affinity for moisture and they soften and become weak after water absorption. Although chemical stabilization has proven highly successful in increasing the strength of the natural soils some twenty to fifty times, and is used widely in the state, situations arise where those approaches cannot be used. For example, chemical stabilization cannot be used when the temperature is below 40^0F and in cases where traffic must be routed immediately onto the unfinished roadway. This particular problem is frequently encountered in urban areas, or high traffic areas. A curing period required in chemical stabilization is not available in these situations.

Hence, other techniques and alternatives must be considered and used to improve overall bearing capacity of the roadway during and after construction. As one alternative, and a method used by the Kentucky Transportation Cabinet (KyTC), an aggregate layer is placed on the soil subgrade, as illustrated by Case 1 in Figure 1. In this case, traffic can be routed onto the roadway immediately after the aggregate layer has been placed. However, when granular layers are placed on weak clayey subgrades that may soften and deflect under wheel stresses, tensile stresses may develop at the bottom of the granular layer and cause deep rutting and, eventually, pavement cracking (Hopkins and Sharpe, 1985; Hopkins and Beckham, 2000). To lessen, or prevent, rutting of the aggregate layer, or base, during construction and flexible pavement cracking due to base deflection after construction, geosynthetics may be placed at, or near, the bottom of the granular base (Case 2 in Figure 1), or on top of the finished subgrade. Additionally, by reinforcing the aggregate base with a geosynthetic fabric, the amount, Δt (= t_{wo}- t_w), of granular material required to yield the same pavement performance of a thicker aggregate base (without geosynthetic fabric) may be reduced.

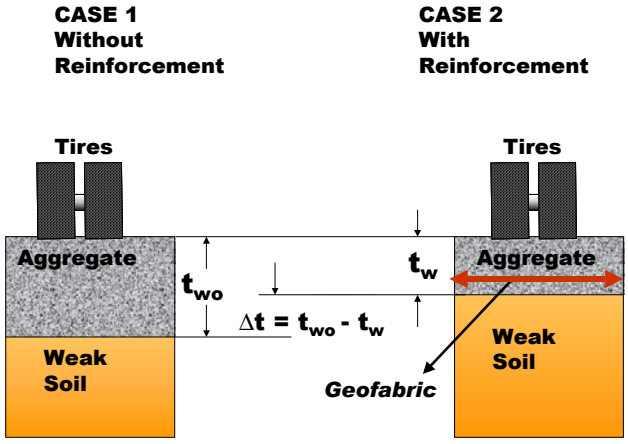

Figure 1. Mechanical stabilization of subgrade using aggregate without and with geosynthetic reinforcement.

According to some engineers in KyTC, the use of manufacturers' guidelines for designing an aggregate base reinforced with geosynthetics has yielded mixed results. This design problem has been identified as a problem that needs a full examination to determine the best design approach to this problem. Consequently, a need exists to develop a theoretical approach that can analyze the bearing capacity under traffic wheel stresses of base layers reinforced with geofabrics during construction. A design approach is needed to determine the required thickness of base aggregate

when it is reinforced with geofabrics. The designer needs guidelines and a design procedure (s) to select the required thickness of aggregate and the appropriate strength of geotextile for a given subgrade strength to prevent failure, or rutting, under traffic stresses. A design method and guidelines are needed to identify those situations where an aggregate reinforced base is needed. Also, the approach should allow a determination of how much the thickness of the aggregate base may be reduced when a geotextile is used. This reduced thickness is not a constant value; it varies with the strength of the soil subgrade and the strength of fabric.

Objectives and Scope

The primary objective of this study was to develop and implement mathematical bearing capacity models originally proposed by Hopkins (1986, 1991) and Slepak and Hopkins (1993; 1995a, b) and as visualized in Figure 2. Those models, which are based on limit equilibrium, can be used to analyze the bearing capacity, or stability, of the problem illustrated in Figure 2. They can be used to design the thickness of reinforced aggregate base required to avoid failure during and after construction. Other design procedures will be examined. The theoretical models developed by Hopkins and Slepak will be used to evaluate design procedures published by others. To facilitate and provide an efficient means of analyzing early construction cases and flexible pavements reinforced with geosynthetics, "Windows" software was developed. The methods have been stored in the Kentucky Geotechnical Database (Hopkins et al, 2004) so that the methods are in a client/server environment and are readily accessible to engineers and officials of the Kentucky Transportation Cabinet. A "stand along" version of the software was also written.

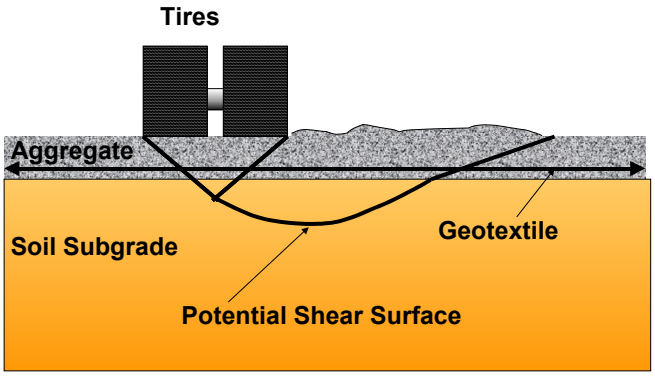

Figure 2. Configuration of bearing capacity model for analyzing highway aggregate bases reinforced with geofabrics.

BACKGROUND AND LIMIT EQUILIBRIUM METHODS FOR STABILITY OF EARTH STRUCTURES

General Definitions

Limit equilibrium approaches used to construct the bearing capacity model(s) have been described in full detail by Hopkins (1986, 1991) and Slepak and Hopkins (1993, 1995a,b) and the following discussion is basically a repeat of essentially elements of those works.

A mass of soil is considered to be in elasto-plastic equilibrium if the following conditions are satisfied within and at the boundary of a mass under consideration:

- stress equilibrium equations,
- stress-strain elasto-plastic constitutive relationships,
- compatibility equations relating strains and displacements, and appropriate boundary conditions, and

- appropriate boundary conditions.

Usual formulation of stress-strain elasto-plastic constitutive relationships involves a yield surface (f) and a flow rule. Elasto-plasic material is usually considered perfectly plastic for bearing capacity and stability problems. For a perfectly plastic material, f depends on the stress tensor, $F_{ij.}$ Plastic flow can occur only when the yield condition is satisfied, or

$$f(\sigma_{ij}) = 0. \tag{1}$$

Stress states for which f (F_{ij})>0 are excluded, and f(F_{ij})<0 corresponds to elastic behavior. In soil mechanics, yield function F_{ij} is usually assumed in the form:

$$f(\sigma_{ij}) = \tau - c' - \sigma' \tan\phi,' \tag{2}$$

first suggested by Coulomb (1773).

In Equation 2, it is assumed that plastic flow occurs when, on any plane, the stress J, reaches an amount that depends linearly upon cohesion, c,' and the effective normal stress

$$\sigma' = \sigma - u \tag{3}$$

where F is the total normal stress and u is a pore pressure.

The angle, N,' in Equation 2 is known as the angle of internal friction of a soil. Bearing capacity and stability problems can be formulated as the problems of finding collapse conditions. These collapse conditions correspond to the stage when the yielding of soil governed by the Coulomb criterion:

$$\tau = c' + \sigma' \tan\phi' \tag{4}$$

has spread to such an extent that the remaining elastic soil plays a relatively insignificant role in sustaining the load. This condition has been termed (Chen, 1975) uncontained or unrestricted plastic flow. This collapse condition can be used as a realistic basis for design.

Limit equilibrium methods have traditionally been used to obtain approximate solutions for the stability problems in soil mechanics. These methods can probably best be described as (Chen, 1975) approximate methods to the construction of a slip line field and generally entail an assumed failure surface of various simple shapes. With this assumption, each of the stability problems is reduced to one of finding the most dangerous position for the failure or slip surface of the shape chosen. According to limit equilibrium methods, a mass of soil (Figure 3) is considered to be in a state of limit equilibrium if Coulomb's failure condition (Equation 4) is satisfied along a potential slip surface, y (x) and if equilibrium equations are satisfied for the mass bounded by the slope surface Y(x), and the slip surface y(x). It is worth mentioning here (Chen, 1975) that none of the equations of solid mechanics mentioned is explicitly satisfied everywhere inside or outside the failure surface. The method gives no consideration to soil kinematics and does not satisfy Coulomb's failure criterion (Equation 4) everywhere inside or outside the failure surface. A solution obtained using the limit equilibrium method is not necessarily an upper bound or a lower bound. However, usage of the method quite often gives acceptable results.

As previously defined, and in general, a soil mass of given properties and geometry that is acted upon by a given set of loads is not in a state of limit equilibrium. To quantify the margin of safety

relative to a state of imminent failure, the soil's real strength parameters, c' and N,' may be replaced by artificial ones, c_f and N_f, for which a state of limiting equilibrium may be realized. There are many possible ways c' and N' may be related to c_f and N_f, and still realize a state of limiting equilibrium. It is customary, however (Baker and Garber, 1978), to adjust the real strength parameters by a single factor, F, in the following manner:

$$c_f = \frac{c'}{F}$$
$$\tan\phi_f = \frac{\tan\phi'}{F}. \qquad (5)$$

Proposed Theoretical Approaches

None of the equations of solid mechanics is explicitly satisfied everywhere inside or outside the failure surface. As an alternative to equilibrium equations of solid mechanics, the limit equilibrium method considers either equations of equilibrium for vertical slices, shown in Figure 3, or overall equilibrium equations bounded by the slope surface and the shear surface. Consequently, two equivalent formulations of a stability problem may be formulated.

Bearing capacity models developed by Hopkins (1986; 1991) and Slepak and Hopkins (1993; 1995a, b), which are based on limit equilibrium concepts, were used to evaluate the stability of aggregate bases reinforced with geosynthetics. The approach was used to determine the amount of thickness that a granular base can be reduced when geotextile reinforcement is used. The bearing capacity model used to analyze the fabric-reinforced aggregate base, under wheel contact stresses, calculates the factor of safety against failure. The concept of using limiting equilibrium methods in bearing capacity analysis of partially completed and completed flexible pavements has been demonstrated in reports and papers published previously by UKTC geotechnical engineers. The original model (method of slices) developed by Hopkins (1986,1991) is especially useful for analyzing the bearing capacity of early construction stages of flexible pavements and low volume roads. However, the model, which is based on the method of slices, has been formulated in such a manner that the bearing capacity of a flexible pavement containing any number of layers can be analyzed. Ultimate strengths of the materials in each pavement layer are used. Algorithms were developed to simulate any given uniform contact tire stress. Shear strengths, N and c, the angle of internal friction and cohesion, respectively are used to describe each layer of the flexible pavement, base, and soil subgrade. Strength parameters used in the problems analyzed below were assumed and based on triaxial test results previously obtained.

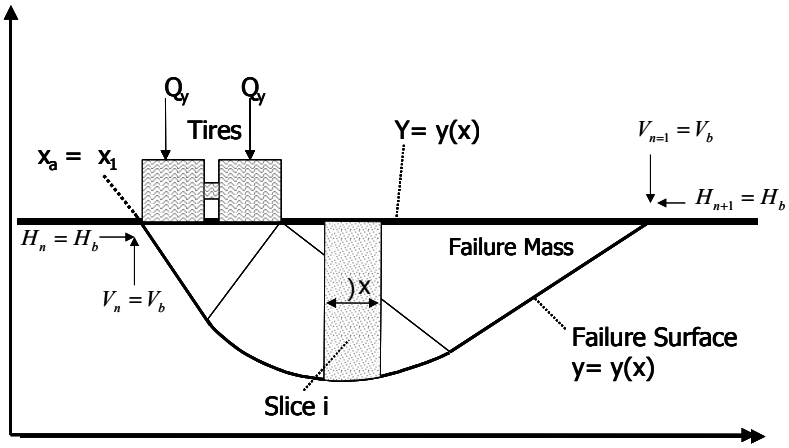

Figure 3. Failure surface and division of failure mass into slices in limit equilibrium analysis.

The idea of using limit equilibrium methods was extended to the case of a bearing capacity analysis of unreinforced flexible pavements. Later, the proposed method for analyzing the bearing capacity of unreinforced pavements was extended to the case of reinforced analysis. The approach is based on a perturbation method (Slepak and Hopkins, 1993; 1995a, b) and the formulation of the equations is based on consideration of the overall equilibrium of the mass bounded by the slope surface and the shear surface. The initial approximation of normal stresses acting along the failure surface is estimated from the Hopkins' Approach (1986, 1991). The final distribution of normal stresses is sought as a function of the initial approximation of normal stresses, reinforced forces, and two unknown parameters. Substituting this function into equations of equilibrium of a failure mass produces a system of three nonlinear equations with respect to the unknown parameters and a safety factor. The perturbation method has been used in a number of cases of bearing capacity and stability analysis of embankments reinforced with geosynthetics. In all cases, the proposed method showed rapid convergence and yielded reasonable factors of safety; the solution required only a few iterations (typically two - three) to converge. It is important to note that the proposed method is statically consistent since it satisfies the three equations of equilibrium. Raulin et al (1974) described the original perturbation method. In 1993, Slepak and Hopkins added additional theory to the approach so that a wider variety of problems could be solved than those that could be solved by Raulin's original method. The two approaches are described below.

HOPKINS LIMIT EQUILIBRIUM MODEL

The pavement bearing capacity model developed in previous research and used to calculate the factor of safety against failure is a generalized limit equilibrium procedure of slices. The pavement mathematical model is an adaptation of a slope stability model developed by Hopkins in 1986. The mathematical model has been formulated in such a manner that the factor of safety of a multi-layered flexible pavement system may be calculated. The factor of safety may be calculated of a pavement system containing as many as 25 (arbitrarily selected) different layers. In the procedure, the potential failure mass is divided into a series of vertical slices; the equilibrium of each slice and the equilibrium of the entire mass is considered. In the approach, the ultimate strengths of the materials in each pavement layer are used. Algorithms were developed to simulate any given contact tire stress. The theoretical equations presented herein were written in the FORTRAN language. Development of the pavement bearing capacity mathematical model is presented as follows.

Statical indeterminacy

Determining the stability of a potentially unstable mass based on a limit equilibrium approach is indeterminate as shown in Table 1. There are more unknown quantities than known quantities. To make the pavement stability problem determinate, certain assumptions must be made. Known quantities and assumptions required to achieve statical equilibrium of the pavement bearing capacity model are summarized in Table 2. The location of the line passing through the points of action of the interslice forces, or the line of thrust (Bishop 1955; Janbu1954) is assumed. This assumption is unique. In other limit equilibrium procedures of slices, such as those by Morgenstern and Price (1965), Spencer (1967), Spencer (1973), and Hardin (1984), the locations of the points of action of the interslice forces are computed as part of the solution. Although variation of the interslice points of location on the sides of slices causes changes in computed values of the factor of safety, the slight variations do not appear to affect the reasonableness of solutions obtained from the model analyses.

Table 1. Unknowns and equations for n slices.

Unknowns Associated With force Equilibrium		
1	Factor of safety	
n	Normal Forces (N_i) on the base of each slice	
n-1	Normal Forces (E_i) on each interface between slices	Resultant Forces (Z_i) of E_i and (or) T_i on each interface between slices
n-1	Shear forces (T_i) on each interface between slices	Angles –which express the relationships between E_i and T on each interface between slices
Unknowns Associated With Moment Equilibrium		
n	Coordinates bi locating the normal forces on the base of each slice	
n-1	Coordinates ai locating the normal forces Ei on each interface between slides	
2n-1	Unknowns versus n equations	
Totals Unknowns		
5n-2	Unknowns versus 3n equations	

Table 2. Janbu's Approach (1954) –unknowns and equations for n slices.

Unknowns Associated With Force Equilibrium	
1	Factor of safety
n	Normal Forces (N_i) on the base of each slice
n-1	Normal Forces (E_i) on each interface between slices
Assume (initially) $T_i = 0$	Shear forces (Ti) on each interface between slices
2n	Unknowns versus 2n Equations
Unknowns Associated With Moment Equilibrium	
n	Coordinates b_i locating the normal forces on the base of each slice
Assume	Coordinates a_i locating the normal forces E_i on each interface between slides
n	Unknowns versus n equations
Total Unknowns	
3n	Unknowns versus 3n equations

Basic Assumptions

Fundamental assumptions made in the formulation of the pavement bearing capacity model are as follows:

- A line, or thrust line (Bishop 1955) passing the points of action of the interslice forces is known or assumed.
- The materials forming the layers of the pavement of the potentially unstable mass conform to the Terzaghi-Coulomb shear strength formula (Terzaghi 1943).
- For each pavement cross section, the stability problem is treated as two dimensional (plain strain). The shear strength of the materials in the pavement layers may be expressed in terms of effective stress or total stress (Terzaghi 1943).
- For each pavement cross-section, the stability problem is treated as two-dimensional (plain strain).
- The factor of safety of the cohesive component of strength and the frictional component are equal.
- The factor of safety is the same for all slices. It is expressed as the ratio of the total shear strength available on the shear surface to the total shear strength mobilized to maintain statical equilibrium (Bishop 1954). This assumption implies there is mutual support between adjacent slices. It implies the existence of interslice forces.
- Since vehicles are normally in motion, the assumption is made that contact tire stresses are in motion and that the imposed contact stresses act similar to an infinitely long strip loading. While this assumption may not be strictly correct, the assumption is considered to be conservative in nature since end effects of the loaded area are not included. Forces due to acceleration, a, or deceleration are not considered in this study (a = o).

Theoretical equations

A cross section of a pavement subgrade showing the external loading of wheel loads and the potential failure mass and bearing capacity shear surface is shown in Figure 3. The potential failure mass located between the potential failure surface and grade elevation is divided into slices by vertical lines. The forces acting on the four boundaries of an individual slice are shown in Figure 4. The sign convention used in formulating equations is shown in the upper right portion of that figure.

Geometry

The method used to describe the geometry of a pavement section and the arrangements of different types of layers is illustrated in Figure 5. The computer program can only solve two-dimensional problems. Geometry of the section is defined by x- and y- coordinates and line segments. The x-coordinate direction must be horizontal and increases positively from left to right. The y- coordinate direction is vertical and must increase positively from bottom to top. The origin of the coordinate system is located to the left and below the section.

Straight-line segments approximate the entire cross section. This applies to the ground line surface, layer boundary interfaces, water table surface, or piezometric lines, shear surface, and thrust line (Bishop 1954). The uppermost line segments are identified in the computer solution as the ground line surface (grade elevation). In the example shown in Figure 5, the ground line is defined

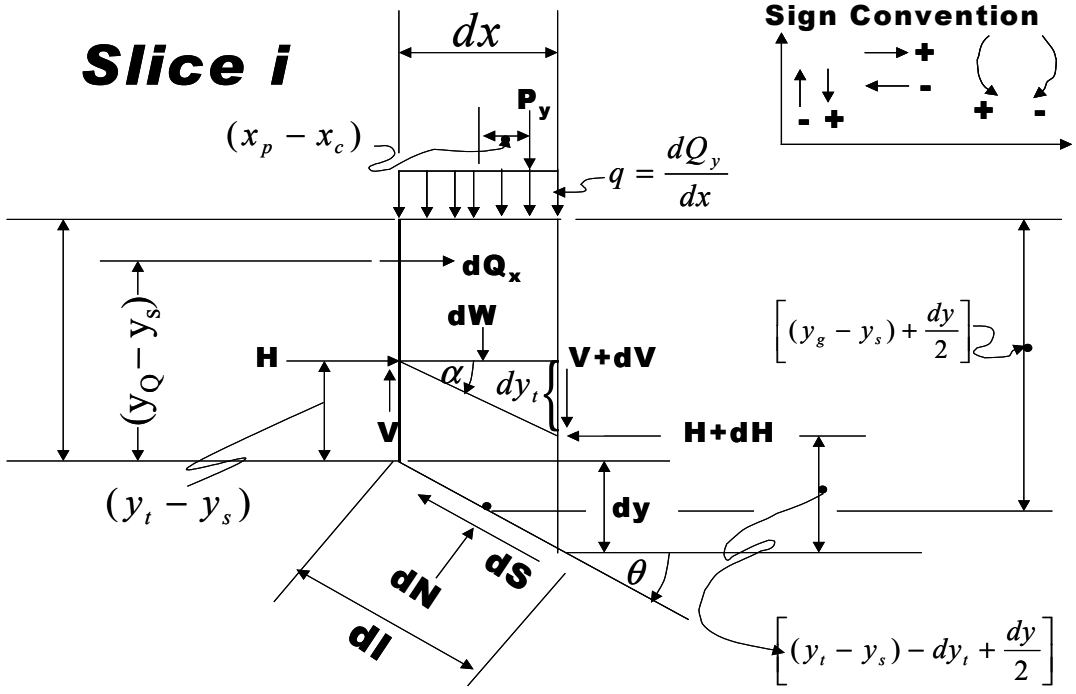

Figure 4. Forces acting on slice i.

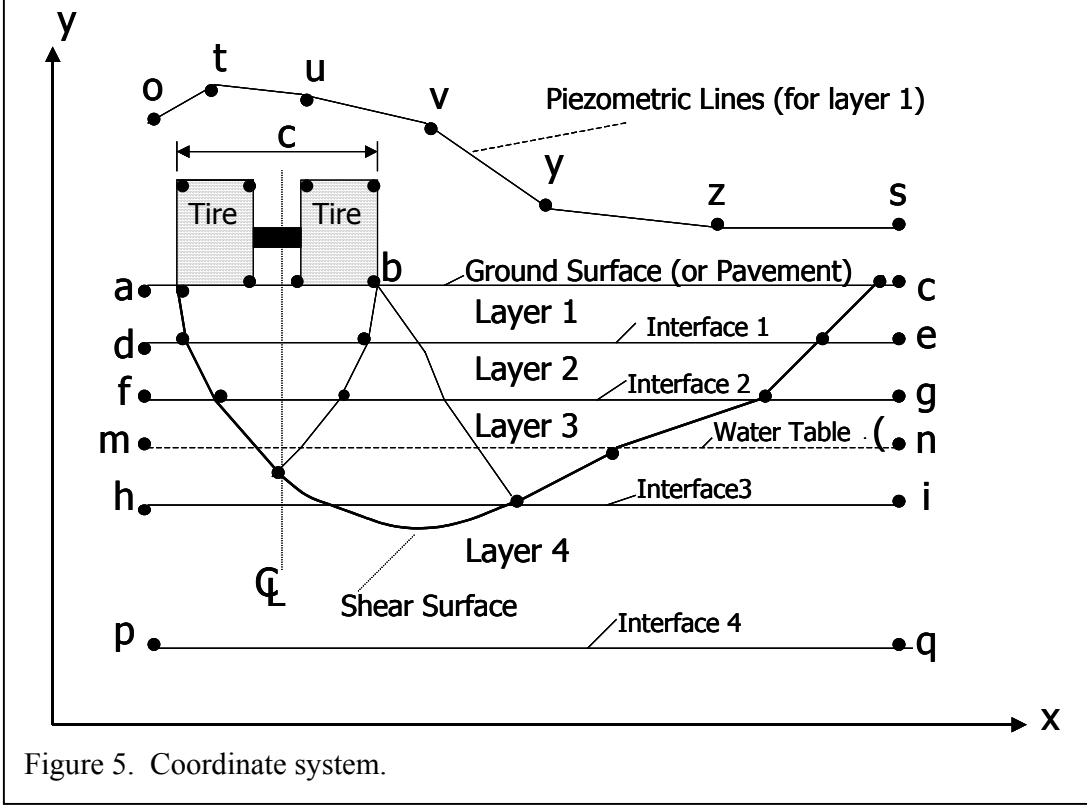

Figure 5. Coordinate system.

by x- and y- coordinates of points a, b, and c. Layer number 1 lies between the line segments of the ground line surface and line segments of boundary interface number 1. Boundary interface number 1 is described by x- and y- coordinates of Points d and e. Layer number 2 lies between boundary interface number 1 (Points d and e) and boundary interface number 2. This interface is described by x- and y- coordinates of Points f and g in the example. Layer number 3 lies between boundary interface number 2 and boundary interface number 3. Interface number 3 is described by x- and - coordinates of Points h and i. For additional layers of material, this pattern is repeated. In the present version of the computer model (HOPKIB, version 1.0), a maximum of 25 (arbitrarily selected) layers of material may be specified.

Additionally, the ground surface and all boundary interfaces must be horizontal -- this condition does not seriously affect the solution since most pavement layers are essentially horizontal (subsequent versions of the computer model will remove this condition).

As shown in Figure 5, the water table is defined by x- and y- coordinates of Points m and n. Alternatively, the pore pressures in any given layer of material may be defined by x- and y- piezometric coordinates (identified as Points o, t, u, v, y, z and s in Figure 5). As another option, pore pressures may be defined for each layer of material using a pore pressure ratio (Daehn and Hilt 1951),

$$r_u = \frac{u}{\sigma_v}. \tag{6}$$

This parameter (a dimensionless parameter) is the ratio of the pore pressure, u, to the vertical stress, σ_v, above the element under consideration. In the computer solution, pore pressures in one layer may be defined by piezometric coordinates while in another layer they may be defined by specifying a value of r_u. Line segments of the water table, piezometric coordinates, thrust line, or shear surface need not be horizontal. A maximum of twenty-five coordinates may be used to describe a given piezometric level or water table. A set of piezometric lines may be used to define the pore pressures for each layer of material. Piezometric lines and pore pressure ratios may be intermixed.

A summary and definitions of the forces acting on an individual slice (Figure 4) are as follows:

dx = finite width of slice i
P_y = external vertical point load acting on the surface of slice i
P_x = horizontal external point load acting at the surface of slice i
dQ_x = horizontal force acting at the surface or in the interior of the soil mass (earthquake force)
dQ_y = vertical force acting at the surface or in the interior of the soil mass (in the analysis performed herein,
dQ_y = qdx) is assumed to be the force acting on a single tire).
$dW\gamma$ = denotes the weight of the slice
dN = normal force acting perpendicular to the base of slice i (see Figure 4 and 6)
dN_y = normal force component acting vertically at the base of slice i
dN_x = normal force component acting horizontal at the base of slice i
dS = shear force acting along the base of slice i (see Figures 4 and 6)
dS_y = component of the shear force acting vertically at the base of slice i
dS_x = component of the shear force acting horizontally at the base of slice i
H = resultant of the total horizontal interslice force
V = resultant of the total vertical interslice force

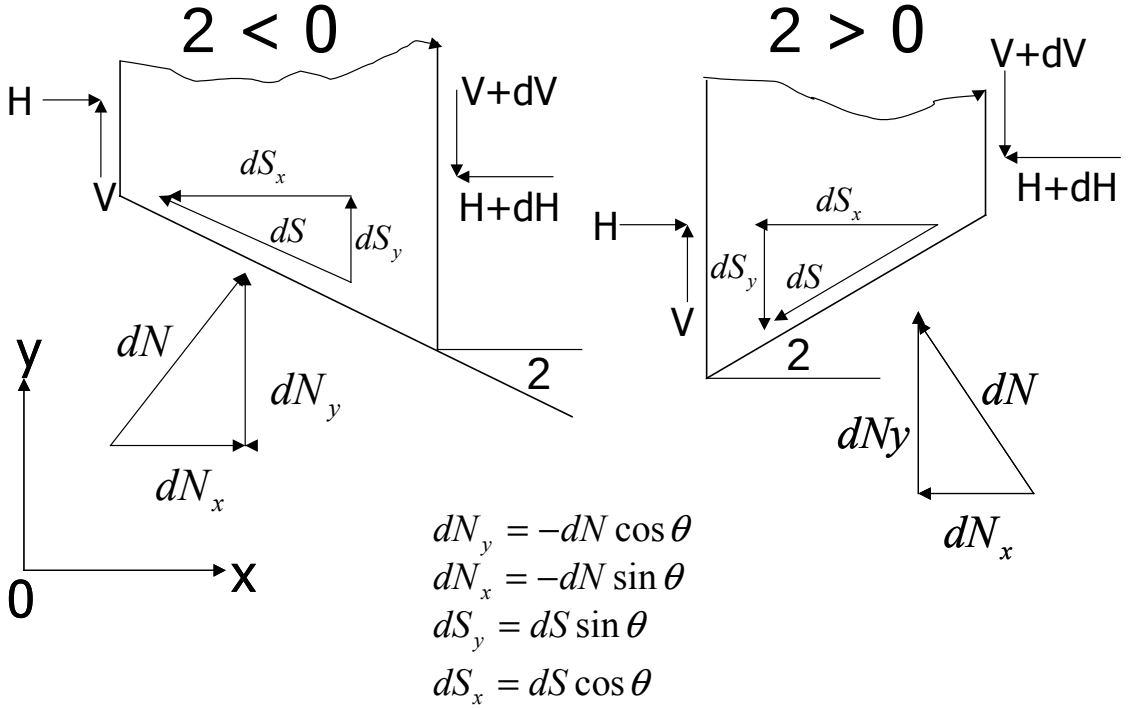

Figure 6. Projections of the forces dN and dS when 2> 0 and 2<0.

dl = length of slice i along its base
S_c = seismic coefficient
Tanα = slope of line of thrust
tan θ = slope of shear surface
(y_t-y_s) = vertical distance between shear surface and line of thrust
dy = vertical distance between the shear surface at the left side of slice i and the shear surface at the right side of slice i
(y_Q-y_s) = distance that dQ_x acts above the assumed shear surface
(y_g-y_s) = distance that P_x acts above the assumed shear surface (also, the vertical distance between ground surface and shear surface at the side of slice i)
σ = normal stress acting perpendicular to the base of slice i
τ = shear stress acting along the shear surface
F = average factor of safety
C = tensile element resultant force acting at the base of slice i (see Figure 8).
C_x = tensile element component force acting horizontal at the base of slice i
Cy = tensile element component force acting vertical at the base of slice i.

Projections of the forces, dN and dS, when θ is greater than zero and when θ is less than zero are shown in Figure 6. The tensile element force, C, acting at the base of slice i and projections of this force, C_x and C_y, are considered in Figure 7. The directions of the force C when θ is greater than zero and when θ is less than zero are shown in Figure 7. When θ is less than zero, the force C acts at some angle, η (as shown in the left portion of Figure 7) where η is assumed to be some value between 180 + θ and 180 degrees. When θ is greater than zero, the force C is assumed to act at angle, η, that lies

between 180 + θ degrees and 270 degrees, as shown in the right portion of Figure 8 (equations have been derived that relate the direction -- or angle η -- of force C in terms of the angle θ and the failure strain, E_f, or a selected value of E, of the tensile element that intersects the base of slice i). Although the derivations given below consider the force C, the HOPKIB bearing capacity computer model does not include these algorithms.

Derivations

The equation of equilibrium in the horizontal direction (see Figure 4) is:

□ HORIZONTAL FORCES = 0:

$$H - (H + dH) + dN_x + dS_x + dQ_x + P_x + C_x = 0 \tag{7}$$

$$dN_x = dH - dS_x - dQ_x - P_x - C_x \tag{8}$$

Equilibrium in the vertical direction is:

Σ VERTICAL FORCES = 0:

$$dQ_y + P_y + dW - V + (V + dV) + dS_y + dN_y + C_y = 0 \tag{9}$$

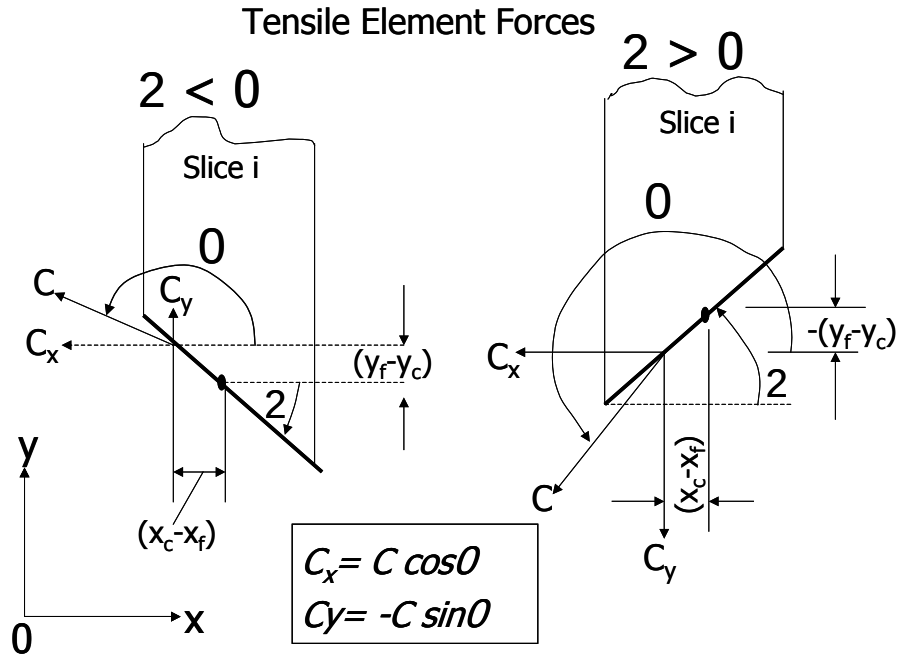

Figure 7. Projections of tensile element forces acting at the base of slice i when 2> 0 and 2 <0.

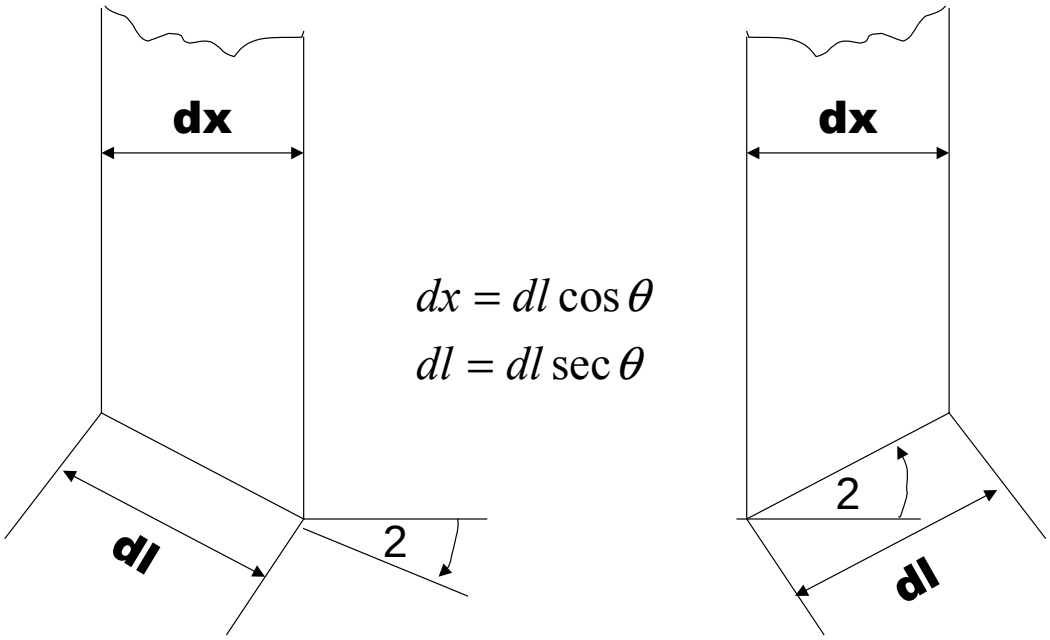

Figure 8. Relationship between dx and dl.

Solving for dN:

$$dN_y = -dQ_y - P_y - dW - dV - dS_y - C_y \tag{10}$$

Equation 9 may be used to develop an expression for the normal stress, F, which acts perpendicular to the base of slice i. Since

$$dN_y = -dN\cos\theta \text{ , and} \tag{11}$$

$$dS_y = dS\sin\theta \text{ , then} \tag{12}$$

$$-dN\cos\theta = -dQ_y - P_y - dW - dV - dS\sin\theta + C\sin\eta \tag{13}$$

$$dN = [\, dQ_y + P_y + dW + dV - C\sin\eta \,]\sec\theta + dS\tan\theta \tag{14}$$

(See Figure 8) then:

$$dN = \sigma dl = \sigma dx\sec\theta \text{ , and} \tag{15}$$
$$dS = \tau dl = \tau dx\sec\theta \text{ , then} \tag{16}$$

$$\sigma dx \sec\theta = [\, dQ_y + P_y + dW + dV - C \sin\eta \,] \sec\theta + \tau dx \sec\theta \tan\theta \tag{17}$$

Solving for F:

$$\sigma = \frac{[\, dQ_y + P_y + dW + dV - C \sin\eta \,] \sec\theta}{dx \sec\theta} + \frac{\tau dx \sec\theta \tan\theta}{dx \sec\theta} \tag{18}$$

$$\sigma = \left[\frac{dQ_y}{dx} + \frac{P_y}{dx} + \frac{dW}{dx} + \frac{dV}{dx} - \frac{C \sin\eta}{dx} \right] + \tau \tan\theta \tag{19}$$

By definition, the equation defining limit equilibrium and the mobilized shear stress, J is:

$$\tau = \frac{c'}{F} + \frac{(\sigma - u) \tan\phi'}{F} \tag{20}$$

Introducing Equation 19 into Equation 20, an expression for J is:

$$\tau = \frac{c'}{F} + \left(\left[\frac{dQ_y}{dx} + \frac{P_y}{dx} + \frac{dW}{dx} + \frac{dV}{dx} - \frac{C \sin\eta}{dx} \right] + \tau \tan\theta - u \right) \frac{\tan\phi'}{F} \tag{21}$$

Let

$$M = \left[\frac{dQ_y}{dx} + \frac{P_y}{dx} + \frac{dW}{dx} + \frac{dV}{dx} - \frac{C \sin\eta}{dx} \right] \tag{22}$$

then

$$\tau = \frac{c'}{F} + \frac{M \tan\phi'}{F} - u \frac{\tan\phi'}{F} + \frac{\tau \tan\theta \tan\phi'}{F} \tag{23}$$

$$\tau = \frac{c'}{F} + \left[(M + \tau \tan\theta) - u \right] \frac{\tan\phi'}{F} \tag{24}$$

$$\tau - \frac{\tau \tan\theta \tan\phi'}{F} = \frac{c'}{F} + \frac{M \tan\phi'}{F} - u \frac{\tan\phi'}{F} \tag{25}$$

Equations 8 and 10 may be used to obtain an expression for the differential horizontal force, dH, by eliminating dN. By making the substitution,

$$dN_x = -dN \sin\theta \tag{26}$$

$$\tau\left(1-\frac{\tan\theta\tan\phi'}{F}\right)=\frac{c'}{F}+\frac{M\tan\phi'}{F}-u\frac{\tan\phi'}{F} \tag{27}$$

$$\tau_f=\frac{c'+\left(\left[\frac{dQ_y}{dx}+\frac{P_y}{dx}+\frac{dW}{dx}+\frac{dV}{dx}-\frac{C\sin\eta}{dx}\right]-u\right)\tan\phi'}{\left(1-\frac{\tan\theta\tan\phi'}{F}\right)} \tag{28}$$

Equation 10 becomes:

$$dN_x=-dN\sin\theta=dH-dS_x-dQ_x-P_x-C_x \tag{29}$$

$$dN=(-dH+dS_x+dQ_x+P_x+C_x)\csc\theta \tag{30}$$

Making the substitution:

$$dN_y=-dN\cos\theta, \tag{31}$$

Equation 10 becomes:

$$dN_y=-dN\cos\theta=-dQ_y-P_y-dW-dV-dS_y-C_y \tag{32}$$

$$dN=(dQ_y+P_y+dW+dV+dS_y+C_y)\sec\theta \tag{33}$$

Setting Equation 30 equal to equation 33, an expression for the differential interslice horizontal forces may be developed as follows:

$$(-dH+dS_x+dQ_x+P_x+C_x)\csc\theta=(dQ_y+P_y+dW+dV+dS_y+C_y)\sec\theta \tag{34}$$

$$(-dH+dS_x+dQ_x+P_x+C_x)=(dQ_y+P_y+dW+dV+dS_y+C_y)\tan\theta \tag{35}$$

$$-dH=-dS_x+dS_y\tan\theta-dQ_x-P_x-C_x+(dQ_y+P_y+dW+dV+C_y)\tan\theta \tag{36}$$

$$-dH=(-dS_x-dQ_x-P_x-C_x)+(dQ_y+P_y+dW+dV+dS_y+C_y)\tan\theta \tag{37}$$

$$-dH=dS\cos\theta+dS\sin\theta\tan\theta-dQ_x-P_x-C_x+(dQ_y+P_y+dW+dV+C_y)\tan\theta \tag{38}$$

$$-dH = \tau dx(\sec\theta\cos\theta + \sec\theta\sin\theta\tan\theta) - dQ_x - P_x - C_x + (dQ_y + P_y + dW + dV + C_y)\tan\theta \quad (39)$$

$$-dH = \tau dx\sec\theta\cos\theta + \tau dx\sec\theta\sin\theta\tan\theta - dQ_x - P_x - C_x + (dQ_y + P_y + dW + dV + C_y)\tan\theta \quad (40)$$

$$-dH = \tau dx(1+\tan^2\theta) - dQ_x - P_x - C_x + (dQ_y + P_y + dW + dV + C_y)\tan\theta \quad (41)$$

$$-dH = \tau dx\sec^2\theta - dQx - Px - Cx + (dQy + Py + dW + dV + Cy)\tan\theta \quad (42)$$

At any interface, x_i, as shown in figures 3 and 4, the side force, H_i, at any distance from x_i, may be calculated in the following manner:

$$H_i - H_1 = \int_{x_1}^{x_i} dH\,, \quad (43)$$

or (introducing Equation 37 into Equation 38),

$$H_i = H_1 - \int_{x_1}^{x_i} \tau dx(\sec^2\theta) - dQ_x - P_x - C\cos\eta + \left(\frac{dQ_y}{dx} + \frac{P_y}{dx} + \frac{dW}{dx} + \frac{dV}{dX} - \frac{C\sin\eta}{dx}\right)dx\tan\theta \quad (44)$$

An expression for calculating the vertical shear force at any interface, x_i, may be obtained by considering moment equilibrium about point **a** of slice i, as shown in Figure 4. Moment equilibrium about the assumed point of application (point **a** in Figure 4) of the normal forces, dN, is:

Σ MOMENTS = O

$$\begin{gathered} H\left[(Y_t - y_s) - \frac{dx\tan\theta}{2}\right] - (H+dH)\left[(y_t - y_s) + dx\tan\alpha - \frac{dx\tan\theta}{2}\right] + \\ V_i\frac{dx}{2} + (V_i + dV)\frac{dx}{2} + P_x\left[(y_g - y_s) - \frac{dx\tan\theta}{2}\right] + \\ dQ_X(Y_Q - Y_s) - \frac{dQ_x\,dx\tan\theta}{2} + P_y(X_p - X_c) - C_y(X_c - X_f) + \\ C_x(Y_f - Y_c) = O \end{gathered} \quad (45)$$

Multiplying terms,

$$H(Y_t - Y_s) - H\frac{dx\tan\theta}{2} - H\left[(y_t - y_s) + dx\tan\alpha - \frac{dx\tan\theta}{2}\right] -$$
$$dH\left[(y_t - y_s) + dx\tan\alpha - \frac{dx\tan\theta}{2}\right] + V_i\frac{dx}{2} + V_i\frac{dx}{2} + dV\frac{dx}{2} +$$
$$P_x\left[(y_g - y_s) - \frac{dx\tan\theta}{2}\right] + dQ_x(y_Q - y_s) - \frac{dQ_x\,dx\tan\theta}{2} + P_y(x_p - x_c) + \quad (46)$$
$$C\cos\eta(y_f - y_c) + C\sin\eta(x_c - x_f) = O$$

rearranging terms, Equation 46 may be written as:

$$H(y_t - y_s) - H\frac{dx\tan\theta}{2} - H(y_t - y_s) - Hdx\tan\alpha + H\frac{dx\tan\theta}{2} -$$
$$dH(y_t - Y_s) - dHdx\tan\alpha + dH\frac{dx\tan\theta}{2} + V_i\frac{dx}{2} + V_i\frac{dx}{2} + dV\frac{dx}{2} +$$
$$P_x\left[(y_g - y_s) - \frac{dx\tan\theta}{2}\right] + dQ_x(y_Q - y_s) - \frac{dQ_x dx\tan\theta}{2} + P_y(x_p - x_c) + \quad (47)$$
$$C\cos\eta(y_f - y_c) + C\sin\eta(x_c - x_f) = O$$

Neglecting second order term $dQ_x dx\tan 2/2$, Equation 47 becomes:

$$-Hdx\tan\alpha - dH(y_t - Y_s) - dHdx\tan\alpha + dH\frac{dx\tan\theta}{2} + dV\frac{dx}{2}$$
$$+V_i\,dx + P_x(y_g - Y_s) - P_x\frac{dx\tan\theta}{2} + dQ_x(y_Q - y_s) + P_y(x_p - x_c) \quad (48)$$
$$+C\cos\eta(y_f - y_c) + C\sin\eta(x_c - x_f) = O$$

When concentrated loads are not considered ($P_x = P_y = C_x = C_y = 0$) the values of dH and dV are of the same order as dx. Here, Equation 48 can be further simplified and an expression for V_i is:

$$V_i = H\tan\alpha + \frac{dH}{dx}(y_t - y_s) - \frac{dQ_x}{dx}(y_Q - y_s) \quad (49)$$

At any interface, x_i, as sown in Figures 3 and 4, the differential vertical force dV, at any distance from x_i, may be calculated as follows:

$$\int_{X_i}^{X_I} dV = V_I - V_i \quad (50)$$

When concentrated loads are present an expression for dV can be obtained by solving the system of Equations 48, 42, and 28 with respect to dH and dV.

An expression for the average factor of safety may be developed from the equation by solving the equation for overall horizontal equilibrium, or

$$H_{n+1} - H_1 = \int_{x_1}^{X_{n+1}} dH \tag{51}$$

Substituting the expression, Equation 42, for the differential horizontal interslice forces, Equation 51 becomes :

$$H_1 - H_{n+1} = \int_{x_1}^{x_{n+1}} \frac{\tau_f}{F} dx(1+\tan^2\theta) - dQ_x - P_x - C_x + (dQ_y + P_y + dW + dV + C_y)\tan\theta \tag{52}$$

Rearranging terms,

$$H_1 - H_{n+1} + \int_{x_1}^{x_{n+1}} dQ_x + P_x + C_x - \left(\frac{dQ_y}{dx} + \frac{P_y}{dx} + \frac{dW}{dx} + \frac{dV}{dx} + \frac{C_y}{dx}\right) dx \tan\theta = \frac{1}{F}\int_{x_1}^{x_{n+1}} \tau_f \, dx(1+\tan^2\theta) \tag{53}$$

and solving for the average factor of safety, or

$$F = \frac{\int_{x_1}^{x_{n+1}} \tau_f \, dx(1+\tan^2\theta)}{H_1 - H_{n+1} + \int_{x_1}^{x_{n+1}} dQ_x + P_x + C_x - \left(\frac{dQ_y}{dx} + \frac{P_y}{dx} + \frac{dW}{dx} + \frac{dV}{dx} + \frac{C_y}{dx}\right) dx \tan\theta} \tag{54}$$

Substituting the expression for J_f (Equation 28*),* Equation 54 becomes*:*

$$F = \frac{\int_{x_1}^{x_{n+1}} \frac{\left(c' + \left(\left[\left(\frac{dQ_y}{dx} + \frac{P_y}{dx} + \frac{dW}{dx} + \frac{dV}{dx} + \frac{C_y}{dx}\right)\right] - u\right)\tan\phi'\right) dx(1+\tan^2\theta)}{\left(1 - \frac{\tan\theta\tan\phi'}{F}\right)}}{H_1 - H_{n+1} + \int_{x_1}^{x_{n+1}} dQ_x + P_x + C\cos\eta - \left(\left(\frac{dQ_y}{dx} + \frac{P_y}{dx} + \frac{dW}{dx} + \frac{dV}{dx} + \frac{C_y}{dx}\right)\right) dx \tan\theta} \tag{55}$$

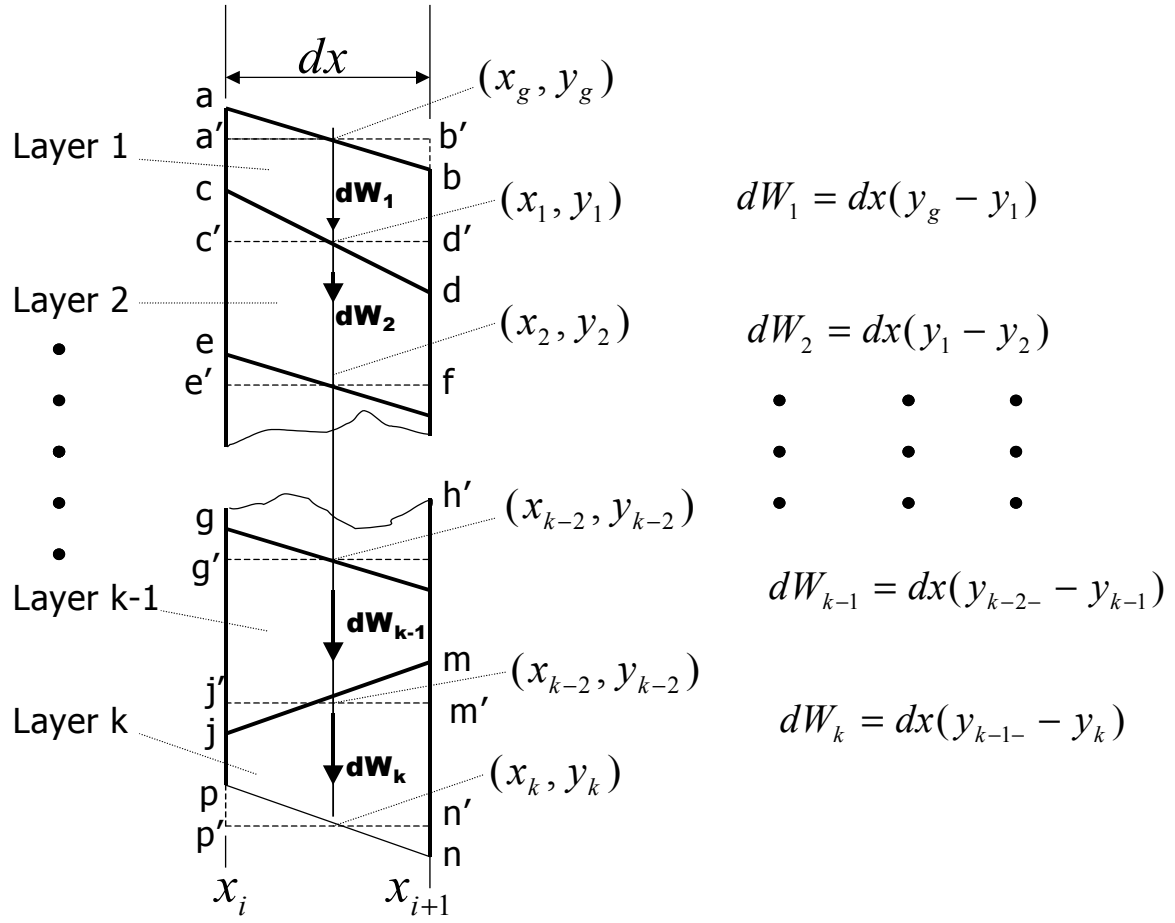

Figure 9. Scheme for estimating the force, dW_i, for a multilayered bearing medium.

Solution of Equations

There are many considerations and steps involved in calculating the factor of safety from Equation 55. A full description and complete details of the solution are much beyond the scope of this report. Many details and geometric considerations have been given elsewhere (Hopkins 1985). A brief summary of the steps necessary to solve Equation 55 is described below.

The force, dW, may be approximated as shown in Figure 9 and the expressions

$$dW^i \approx \Delta W_i \approx dW_1 + dW_2 + ,...,+ dW_{K-1} + dW_k \tag{56}$$

$$\approx \gamma_1 a_1 + \gamma_2 a_2 + ,...,+ \gamma_{K-1} a_{k-1} + \gamma_K a_K \tag{57}$$

$$\approx \gamma_1 dx(y_g - y_1) + \gamma_2 dx(y_1 - y_2) + ... + \gamma_{K-1} dx(y_{K-2} - y_{K-1}) + \gamma_K dx(y_{K-1} - Y_K) \tag{58}$$

where y_g, y_1, ..., y_{K-2}, y_{K-1}, and y_K = y- coordinates at the intersections of the center of slice i and the bottom of each layer of material and γ_1, γ_2, ..., γ_{K-1}, and γ_K = unit weights of Layers 1, 2, ..., K-1, K (K is equal to the total number of layers of the bearing media).

The actual areas bounded by the boundary layer interfaces and the x- coordinates of the sides of the slices are approximated by rectangles. For example, in Figure 9, the actual area, identified as bcd (Layer 1) is approximated by the rectangular area identified as **a'b'd'c**'. Similarly, the actual area (Layer 2) identified as **cdef** is approximated by the rectangular area **c'd'e'f'.** Although this scheme introduces some error in calculating the actual area of a slice (and the force dW^i), the error becomes essentially insignificant when a large number of slices are used (in solutions shown herein, the potential failure masses were divided into 598 slices). The derivative, dW/dx, may be approximated from the following expression:

$$\frac{dW^i}{dx} \approx \frac{\Delta W^i}{\Delta x} \tag{59}$$

where $\Delta x = x_{i-1} - x_i$.

The scheme for considering distributed loads due to the tire force, dQ_y, is illustrated in Figures 10 and 11. The contact area of the tire resting on the pavement is assumed to be essentially a square. It is assumed that the length of the contact area is infinitely long since the vehicle is normally in motion. The distributed stress may be computed from the relationship:

$$q = \frac{Q_y}{a_c}, \tag{60}$$

where

q = tire contact stress,
a_c = unit ground contact area.

For example, in the AASHO Road Test (1962), the gross tire unit contact area for the vehicles on lane one, loop four, (18-Kip single-axle loads) was 67.8 pounds per square inches (For loops 3, 4, 5, and six of the AASHO Road Test, the unit tire contact stress was about 87 to 90 percent of the tire inflation pressure). The force (dQ_y) per tire was 4,580 pounds. The unit stress was

$$q_u = \frac{4580lbs}{67.8\ in^2} = 67.5lb/in^2 \tag{61}$$

In the computer analyses shown herein, the stress, q_u, was assumed to be uniformly distributed, as shown in Figure 10. While this assumption is not strictly correct, the assumption simplifies the setup of the equations. Uniformly distributed load (or stress) was assumed to extend the width of the tire and to extend 1 inch into the page (perpendicular to the section). Hence, the distributed load is 67.5 lb/inch (inch) (note: other units may be used). The units of all data entered into the computer model must be consistent. The numerical value and units specified for the unit weight of water control the units of all other input data. For example, if the unit weight of water is specified to be 0.0361 pounds per cubic inch, then x- and y- coordinates must be in inches; values of the strength component,

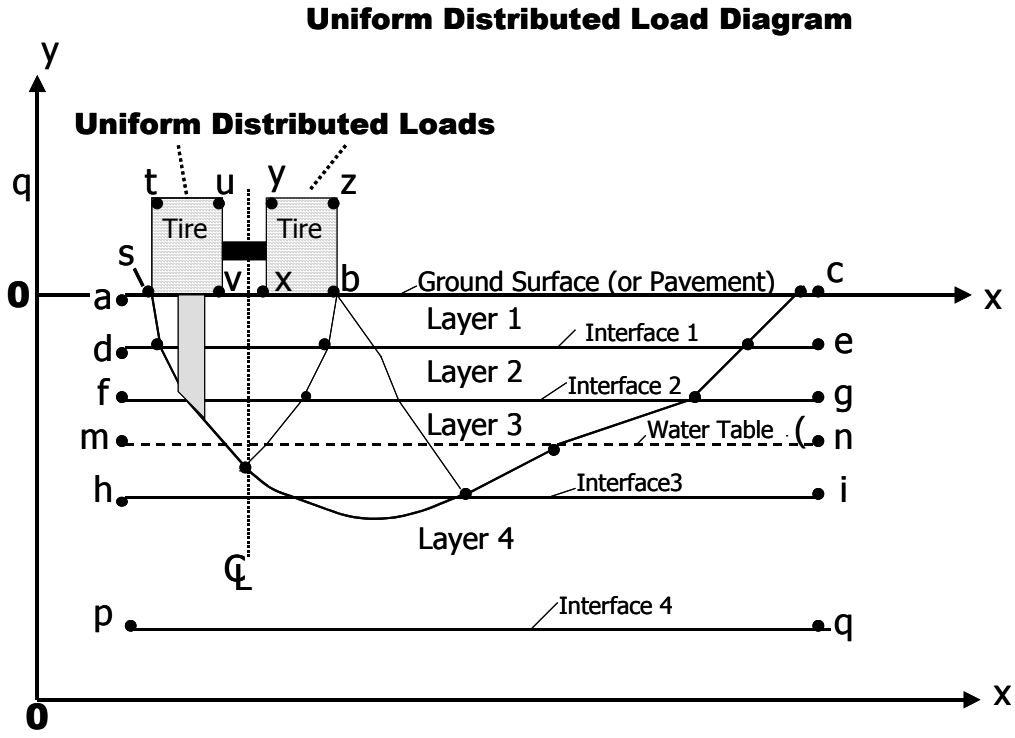

Figure 10. Method for describing distributed loads.

cohesion, c, must be in pounds per square inch; and unit weights of layer materials must be specified as pounds per cubic inch. These units were used in all problems shown herein since these units are convenient to use when working with pavement layers and considering that thicknesses of pavement layers and tire inflation pressures are usually stated in units of inches and pounds per square inch, respectively.

As shown in Figure 10, the externally acting distributed loads, q, due to wheel loadings are entered into the computer model by specifying values of q at specified values of the x-coordinate. For example, the distributed load in the example in Figure 10 is described by q- and x- coordinates of Points **a, s, t, u, v, x, y, z, b,** and **c**. For instance, if q equals 67.5, then the following coordinates would be entered (the q_u - x coordinates must extend the full length of the ground line surface):

x_a 00.0
x_s 00.0
x_t 67.5
x_u 67.5
x_v 00.0
x_x 00.0
x_y 67.5
x_z 67.5
x_b 00.0
x_c 00.0

Internally, in the computer program, for each slice located between the end points, x_i and x_{i+1}, the portion of the load diagram lying immediately above slice i is divided into ten slices (an arbitrarily selected value), as illustrated in Figure 11, or

$$\Delta X_{si} = \frac{x_{i+1} - x_i}{10} \tag{62}$$

For each small slice, ΔX_{si}, point loads, $P_{\Delta xs}$, are computed from:

$$P_{\Delta xsi} = q \bullet \Delta x_{si} \tag{63}$$

Since $P_{\Delta xsi}$ values occur on both sides of the center of slice i at the base (point a in Figure 11 there are moments about point Q. For a given slice, the moments due to the $P_{\Delta xs}$ forces to the left of Point **a** and moments to the right of Point **a** cancel each other, since the area of a given slice is approximated by a rectangle. At the ends of the load (q > o) and in the case where the loaded portion does not coincide with the x-coordinate, x_i or x_{i+1}, there are unbalanced moments. There is some error introduced, but may be made small by using a large number of slices (Note: by formulating the scheme in the manner described above, irregularly-shaped distributed loads, q, may be solved; however, in the present version -- HOPKIB 1.0 -- of the computer solution, only uniformly distributed loads may be solved since the moments due to $P_{\Delta xs}$ are not considered in the present version. When irregularly-shaped distributed loads are used, the unbalanced moments need to be considered. Future versions will rectify this situation so that irregularly shaped distributed loads may be considered). The derivative dQ_y/dx is

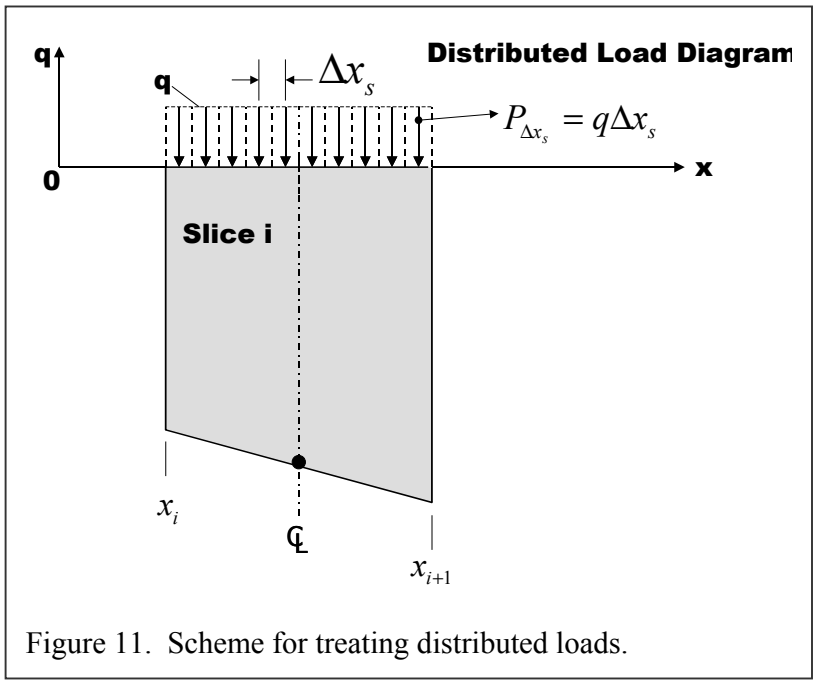

Figure 11. Scheme for treating distributed loads.

$$\frac{dQ_y}{dx} = q \tag{64}$$

The force, Q_x (considered herein as an earthquake force acting at the side of each slice), may be approximated from the expression:

$$dQ_x \approx dW \bullet S_c \tag{65}$$

The force dQ_x for each slice is plotted as a function of x_i for each slice. Numerical differentiation is used to obtain a value of dQ_x/dx at the side (x_i - coordinate) of each slice (these calculations are performed internally in the computer model solution).

The end boundary forces, H_1, H_{n+1}, V_1, and V_{n+1} are assumed to be known quantities (these quantities, when known or estimated, may be entered into the computer program). In the analyses shown herein, these forces are assumed equal to zero.

The forces, P_y, P_x, and dQ_y are assumed to be known quantities. The derivative, dQ_y/dx, is approximated as follows:

$$\frac{dQ_y}{dx} \approx \frac{\Delta Q_y}{\Delta x} \tag{66}$$

The quantity, P_x/dx (or P_y/dx), containing concentrated load, P_x (or P_y), does not represent a real derivative. This is a generalized δ-function that makes sense only under the integral sign:

$$\left.\begin{aligned} \int_{a_x}^{b_x} \frac{P_x}{dx}\,dx = \int_{a_x}^{b_x} P_x\,\delta(X - C_x)dx = P_x \\ \int_{a_y}^{b_y} \frac{P_y}{dx}\,dx = \int_{a_y}^{b_y} P_y\,\delta(X - C_y)dx = P_y \end{aligned}\right\} \tag{67}$$

where (a_x, B_x) or (a_y, B_y) is any interval containing the point C_x (or C_y) of application of the concentrated load P_x (or P_y).

The value of the tensile element force, C, is assumed to be known. Angle, η, must be assumed. This angle ranges between the angles 180 + θ (see Figure 7) and 180 degrees for θ<0, and between 180+0 and 270 degrees for θ>0. The terms, C sinη/dx, and C cosη/dx are of the same nature as P_x and P_y, so they are estimated as follows:

$$\int_{a_c}^{b_c} \frac{C\sin\eta}{dx}\,dx = C\sin\eta \tag{68}$$

and

$$\int_{a_c}^{b_c} \frac{C\cos\eta}{dx}\,dx = C\cos\eta \tag{69}$$

where (a_c, b_c) is any interval, containing the point of application of the tensile force C.

(The present version of the HOPKIB computer program (version 1.0) does not contain these logarithms. Future versions will consider tensile element forces.) The values of φ' and c' (or the total stress parameters, φ and c) must be determined for each layer of the multi-layered bearing medium.

Location of the points of action (thrust line -- Bishop 1955) of the interslice forces on the sides of the slices is assumed. In the computer model solution, only one parameter, λ, needs to be entered. The parameter, λ, is defined as follows (see Figure 4):

$$\lambda = \frac{Y_t - y_s}{Y_g - y_s}, \tag{70}$$

$$(y_t - y_s) = \lambda(y_g - y_s) \tag{71}$$

In the solutions shown herein, a value of 0.33 was assumed for λ.

The quantities, tan θ and tan α, are computed from geometric considerations. The factor of safety, F, must be obtained by iteration since the factor of safety appears on both sides of Equation 55. The derivative, dv/dx, appearing in Equation 55 for each slice is unknown. The values of V_i cannot be defined until values of the derivative, dH/dx, and H_i are known. To obtain estimates of the derivatives, dV/dx and dH/dx, and the quantities V_i and H_i, the following procedure may be used. Let

$$N = \frac{1 - \frac{\tan\theta \tan\phi'}{F}}{1 + \tan^2\theta} \tag{72}$$

$$dM = \left(C' + \left(\left[\frac{dQ_y}{dx} + \frac{P_y}{dx} + \frac{dW}{dx} + \frac{dV}{dx} - \frac{C\sin\eta}{dx} \right] - u \right) \tan\phi' \right) \frac{dx}{N} \tag{73}$$

$$dL = dQ_x + P_x + C\cos\eta - \left(\frac{dQ_y}{dx} + \frac{P_y}{dx} + \frac{dW}{dx} + \frac{dv}{dx} - \frac{c\sin\eta}{dx} \right) dx \tan\theta \tag{74}$$

Equation 58 becomes:

$$F = \frac{\int_{x_1}^{x_{n+1}} dM}{H_1 - H_{n+1} + \int_{x_1}^{x_{n+1}} dL} \tag{75}$$

Using the new variables, M and L, Equation 28 may be rewritten

$$\tau_f = \frac{\frac{dM}{dx}}{1 + \tan^2\theta}, \tag{76}$$

Since, by definition

$$\tau = \frac{\tau_f}{F}, \tag{77}$$

then Equation 42 for the differential horizontal interslice forces, dH, is

$$dH = dL - \frac{dM}{F} \tag{78}$$

An expression may be developed for computing the differential horizontal interslice forces. The vertical interslice forces, V_i, and the derivatives, dv/dx, are unknown in Equation 78. Iteration may be used to obtain a first approximation of the factor of safety, F_o. This operation is done by setting the derivatives, dv/dx, equal to zero. Iteration is performed on Equation 75 by first assuming that values of dv/dx are equal to zero and by using an assumed value of F_o. Iteration is completed when the condition,

$$| F_{on+1} - F_{on} | \leq \varepsilon \tag{79}$$

is satisfied. The parameter, ε, is a selected error. In all computations shown herein, ε is set equal to 0.001. That is, the iteration is considered successful when the absolute difference in successive factors of safety is equal to or less than 0.001. Convergence of the solution to the factor of safety, F_o, usually occurs in three to six iterations.

The second stage of the computations involves the introduction of interslice forces, H_i and V_i, and the derivatives, dv/dx and dH/dx, into the equations and performing iteration on Equation 75. Using F_o, the first set of the horizontal interslice force differentials, dH, may be computed from Equation 78 for each slice. At any interslice boundary x_i, the horizontal force may be computed from the expression:

$$H_i = H_1 + \int_{x_1}^{x_i} dH \, . \tag{80}$$

The values of H_i are plotted as functions of the values of x_i. Based on this curve, numerical differentiation may be used to compute the derivative, dH/dx, at a selected value of x_i. Using the computed derivative at a selected value of x_i, the vertical interslice force, Vi, may be computed from Equations 48 or 49. Values V_i are plotted as a function of x_i. Based on this relationship, the derivative dv/dx may be computed using numerical differentiation techniques. Using the computed values of dv/dx, a new factor of safety is computed -- F_1. Based on F_1, the process is repeated: new

values of dH, dH/dX, V_i, and dV/dX are obtained. Based on these subsequent sets of values, a new safety factor is obtained. The iterative scheme is continued until the condition,

$$| F_n - F_{n+1} \; | \leq \varepsilon \,, \tag{81}$$

is satisfied. The term, , , is an error selected by the user. Usually the value in this case is 0.001.

Classes of Bearing Capacity Analysis

Bearing capacity analyses of pavements and soil subgrades may be divided into two main classes of problems. In the first class, the pore pressures acting within each structural layer of pavement (asphalt concrete, base, subbase, and soil subgrade) are independent of the magnitude of total stresses acting in each layer of the pavement regime. The pore pressures are independent variables and the analyses are performed in terms of effective stress using the shear strength parameters, φ' and c'. The values of φ' and c' may be obtained from consolidated-drained triaxial tests (Bishop and Henkel 1964) or consolidated-undrained triaxial tests with pore pressure measurements. To analyze the stability of pavements using the effective stress approach requires knowledge of the pore pressures acting within each layer of material. To conduct this type of analysis would require estimating pore pressures using (perhaps) methods proposed by Skempton (1954); or Ching and Fredlund (1983); Fredlund and Rahardjo (1985); Fredlund (1985) -- future versions will consider methods involving unsaturated soils.

In the second class of analyses, the pore pressures acting in each layer are a function of stress changes within each layer. The analyses are conducted in terms of total stress using the total stress parameters, φ_u and c_u. The values of φ_u and c_u are obtained from unconsolidated-undrained triaxial tests. If the soil subgrade is saturated, then the total stress parameters of the soil may be obtained from the unconfined triaxial (ASTM) compression test -- a form of the unconsolidated-undrained triaxial compression test. In this case, the total stress parameter, φ_u, is zero and the undrained strength is defined as c_u.

At the present stage in the development of the current pavement bearing capacity computer model, the stability analyses shown herein were performed using total stress analyses. Unconsolidated-undrained triaxial compression tests were performed on the asphalt concrete and base (and subbase) to define the total stress parameters, φ_u and c_u. Unconfined compression tests were used to define the shear strength of the soil subgrade (when these were available). Alternately, a relationship developed during the course of this study between the CBR strength and the undrained shear strength, c_u, or S_u, was used to define the undrained shear strength when CBR data were available (although total stress analyses were used herein, the bearing capacity problem may be solved using the effective stress technique). Use of this method of analyses was beyond the scope of this study because of the complexity of determining values of pore pressures. Perhaps, in future research, an examination of techniques necessary to define pore pressures in each pavement layer could be made. For example, consolidated-undrained triaxial compression tests with pore pressure measurements could be performed on saturated specimens of asphalt concrete to define the effective stress parameters, φ' and c'. Additionally, consolidated-undrained triaxial compression tests with pore pressure measurements could be performed on base (and subbase materials), and the subgrade soils to define the effective stress parameters, φ' and c'. To perform the analysis in terms of effective

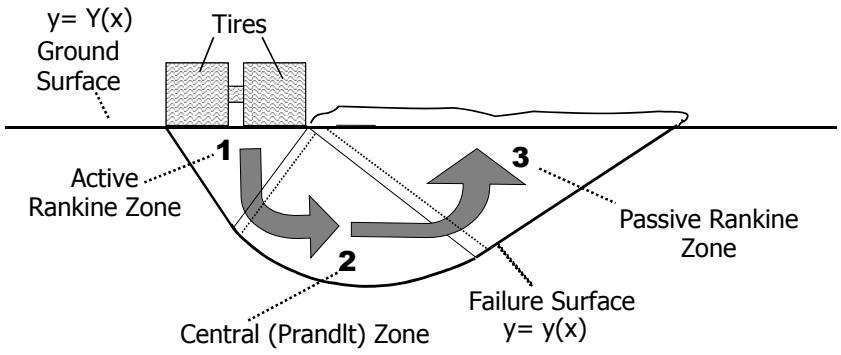

Figure 12. Assumed failure patterns and block movements**.**

stress, pore pressures acting within each pavement layer and subgrade could be estimated or measured -- a complex task.

More sophisticated techniques of shear strength testing than used herein could be examined to define the shear strengths of the different pavement components. For example, consolidated-drained, or consolidated-undrained triaxial compression tests with pore pressure measurements could be used to estimate the effective stress parameters, φ_a and c_a, for the portion of the shear surface along the active wedge. Simple shear tests, torsional tests, or direct shear tests could be performed to estimate the shear strength along the portion of the shear surface of the central wedge. Triaxial extension tests could be performed to define the shear strength along the portion of the shear surface of the passive wedge. These series of tests would be performed on each member or layer of the pavement regime. To a certain degree, the research version of the HOPKIB model has been developed to consider this approach. However, full development of this approach is much beyond the scope of this study.

Shear Surface Used in Bearing Capacity Analysis

Shear surfaces of various shapes or failure patterns may be assumed in performing bearing capacity analysis. For example, circular and wedge-type shear surfaces may be used. However, basic bearing capacity solutions by Prandtl in 1921 and Reissner in 1924 show that the failure pattern should consist of three distinctive zones as shown in Figure 12. These three zones are identified as zones 1, 2, and 3. Zone 1 is an active Rankine zone. This zone pushes the radial Prandtl Zone 2 sideways and the passive Rankine Zone 3 in an upward direction as shown in Figure 12. The basic Prandtl-type failure pattern was assumed in developing the pavement bearing capacity mathematical model. Basic failure patterns and equations for one, homogeneous layer and a multi-layered system are described as follows.

One, Homogeneous Layer

The shear surface assumed in the model analysis for a homogeneous layer of material consists of a lower boundary, identified in Figure 13, as **abcd**. This surface consists of two straight lines, **ab** and **cd**. The portion of the shear surface shown as line **ab** is inclined at an angle, α_1 to the horizontal, or

$$\alpha_1 = 45 + \frac{\phi}{2} \tag{82}$$

while line **cd** is inclined at an angle, α_2 to the horizontal, or

$$\alpha_2 = 45 - \frac{\phi}{2} \tag{83}$$

According to Vesic' (c.f. Winterhorn 1975), the shape of curve **bc** connecting the two straight lines of the shear surface depends on the angle of internal friction, φ, and the ratio, γC/q, where

- γ = unit weight of the bearing layer of material,
- C = width of the loaded area, or footing, and
- q = distributed load acting on the surface of the bearing layer.

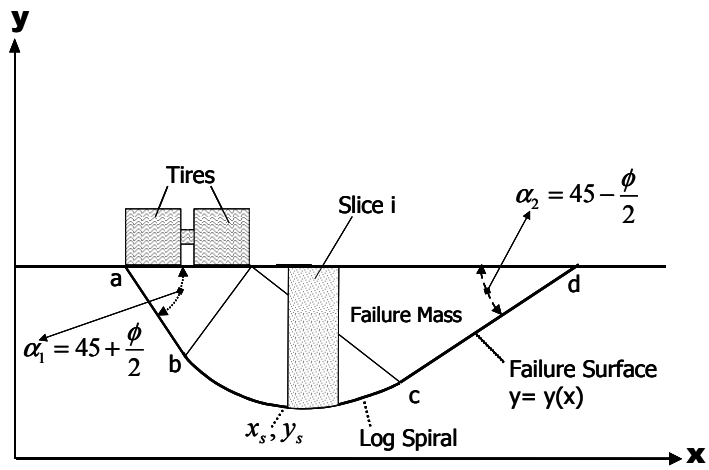

Figure 13. Exit and entry angles for a homogeneous bearing media.

When the ratio γC/q approaches a value of zero, the connecting curve becomes a logarithmic spiral in which γ equal zero degenerates into a circle. If the term, γC, is not zero, the connecting curve lies between a spiral and a circle when the value of φ is not zero. If the soil is frictionless (φ equal to zero), then the connecting curve is a circle. According to Vesic' (c.f. Winterhorn and Fang 1975), these findings have been confirmed experimentally.

To describe the shape of the shear surface **abcd** in Figure 14 for use in the pavement bearing capacity computer model, the x- and y- coordinates of points **a**, **o**, **b**, **c**, and **d** must be established. After these points have been defined, the coordinates, x_s (the x-coordinates of the sides of the slices) and y_s (the y-coordinates of the shear surface at the sides of the slices) may be determined. The coordinates of point **a**, x_a, and y_a are assumed. The x- coordinate of point (**o**, x_o) is assumed and depends on the width of the footing, C, or

$$C = x_o - x_a , \tag{84}$$

and

$$x_o = C + x_a . \tag{85}$$

The y- coordinate, y_o, is arbitrarily selected, or assumed. The coordinates of point **b**, x_{tn}, y_{tn}, may be defined by first computing the radius, r_1, of the spiral,

$$r_1 = \frac{C \bullet \sin \alpha_1}{\sin \Psi} \tag{86}$$

where Ψ = 90 - φ. Line **ab** is assumed to be tangent to the log spiral curve at point **b**. After determining r_1, the coordinates of point **b** are defined as:

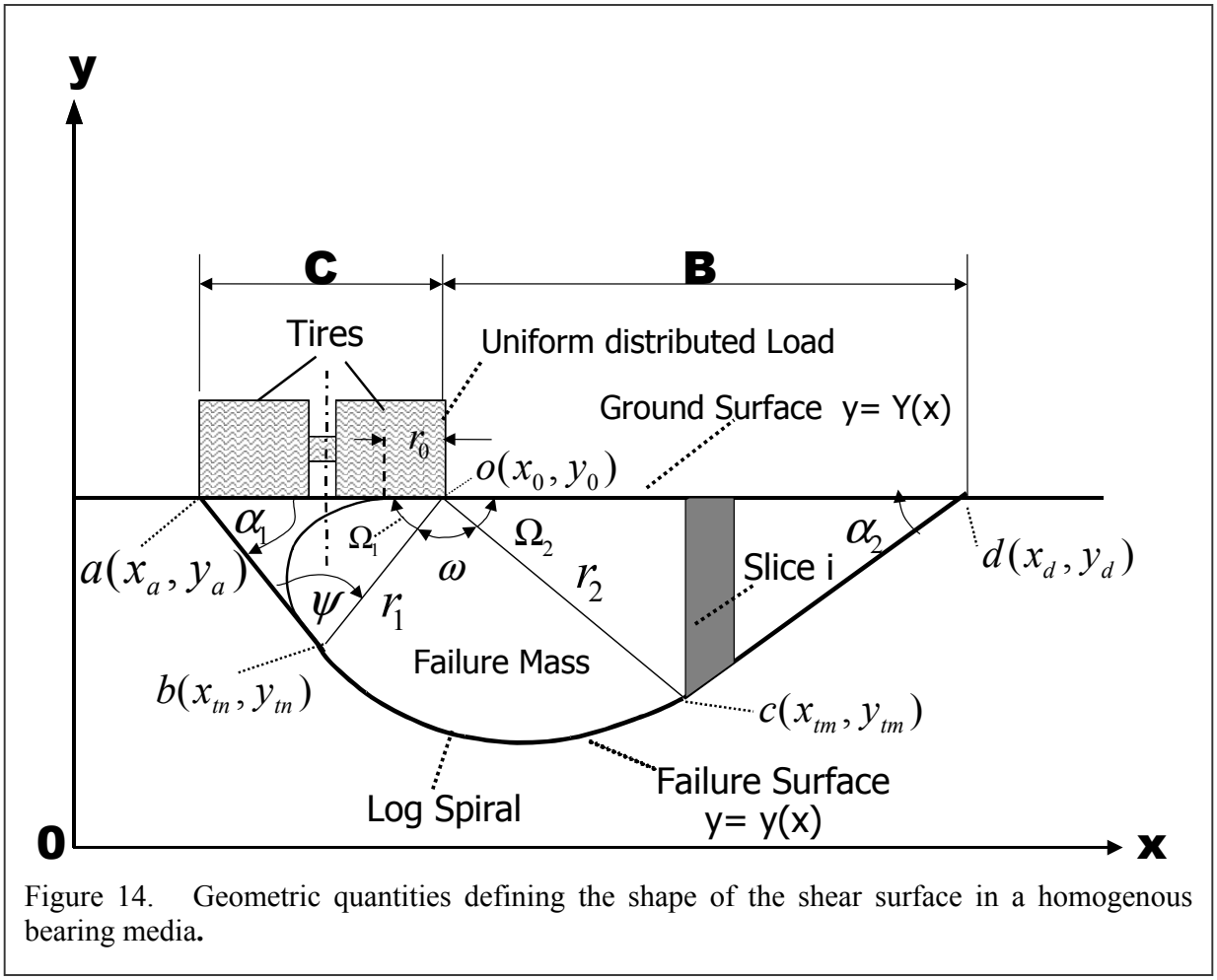

Figure 14. Geometric quantities defining the shape of the shear surface in a homogenous bearing media**.**

$$x_{tn} = x_o - r_1 \cos \Omega_1 \tag{87}$$

and

$$y_{tn} = y_o - r_1 \sin \Omega_1 \tag{88}$$

where

$$\Omega_1 = 180 - \alpha_1 - \Psi. \tag{89}$$

The initial radius, r_o, of the logarithmic spiral, at the top of the bearing surface (see Figure 14) is defined by the expression:

$$r_o = r_1 \bullet e^{(-\Omega_1 \bullet \tan \phi)} \tag{90}$$

Line **cd** is assumed to be tangent to the logarithmic spiral at point **c**. The coordinates of point **c** may be defined after the spiral radius, r_2, is determined. This radius is obtained from the expression:

$$r_2 = r_o \bullet e^{(180-\Omega_2)\bullet \tan\phi}, \tag{91}$$

where

$$\Omega_2 = \Psi - \alpha_2 \tag{92}$$

Coordinates of point **c** may now be defined by the following expressions:

$$x_{tm} = x_o + r_2 \bullet \cos(\Omega_2) \tag{93}$$

and

$$y_{tm} = y_o + r_2 \bullet \sin(\Omega_2) \tag{94}$$

The x-coordinate, x_d, of the point **d** may be determined by first computing the value of r_2 in Equation 84 (Figure 14). After r_2 is determined, the distance B may be calculated using the law of sines, or

$$B = \frac{r_2 \bullet \sin(180 - \Psi)}{\sin \alpha_2} \tag{95}$$

Hence,

$$x_d = x_o + B \tag{96}$$

The y-coordinate, y_d, may be found from the following expression:

$$y_d = y_{tm} + (x_d - x_{tm}) \tan \alpha_2 \tag{97}$$

After the coordinates **a**, **b**, **c**, and **d** are defined, the y-coordinate, y_s, of the intersection of the x-coordinate of the side of any given slice **i** and the shear surface may be determined. The potential failure mass is divided into a selected number of slices, **n**, as shown in Figure 15, or

$$\Delta x = \frac{x_a - x_d}{n}. \tag{98}$$

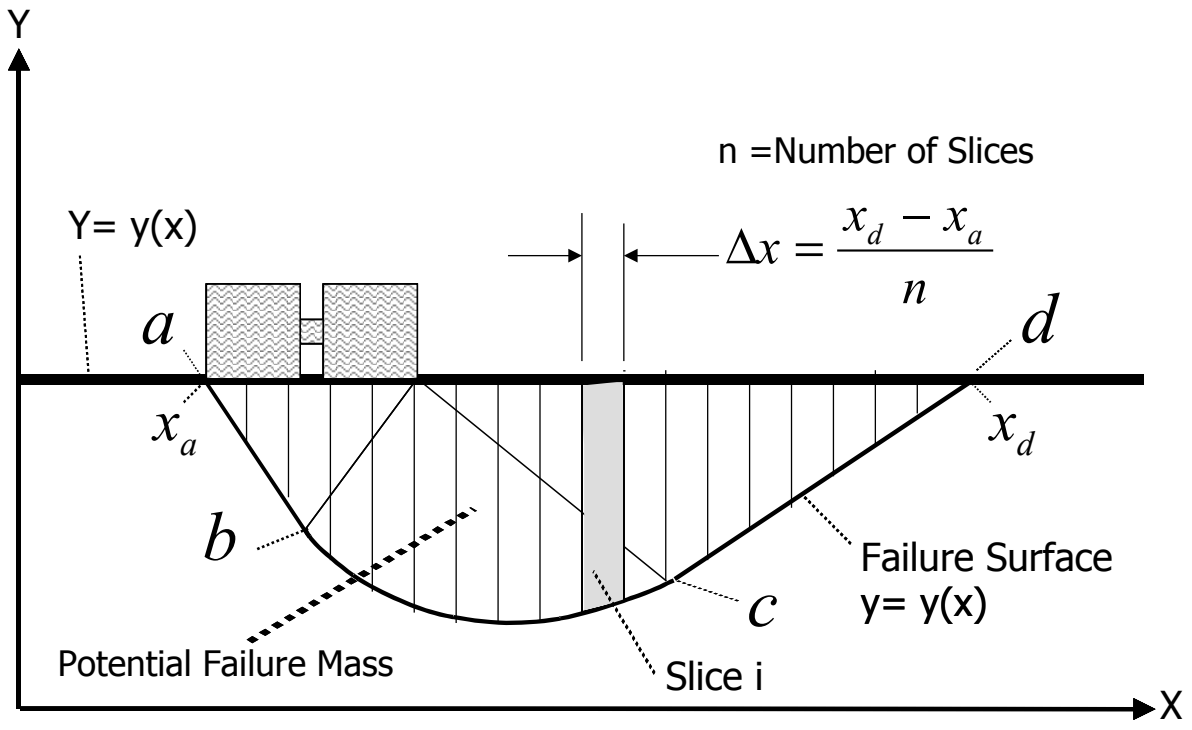

Figure 15. Division of theoretical failure mass into a number of slices and method of computing the width of each slice.

where Δx is equal to the width of each slice. For the x-coordinates, x_s, at the sides of slices that lie between points **a** and **b**, the y-coordinates, y_s, may be computed from the expression:

$$y_s = y_a - (y_{tm} + y_o)\tan\alpha_1 \qquad (x_a < x_i < x_{tn}). \tag{99}$$

Similarly, for the x-coordinates, x_s, at the sides of slices that lie between x_{tm} and x_b, the y-coordinates, y_s, located on the shear surface may be computed from the expression:

$$y_s = y_{tm} + (x_b - x_{tm})\tan\delta_2 \qquad (x_{tm} < x_i < x_{tn}) \tag{100}$$

For the x-coordinates at sides of slices that intersect the shear surface between points **b** and **c** (the connecting logarithmic spiral), the corresponding y-coordinates, y_s, cannot be computed straightforwardly since the angle, ω_{xi}, corresponding to a given x-coordinate of the side of slice i is unknown. The problem may be solved by using an iterative scheme. The iterative scheme is

performed by assuming, initially, a value of the angle, ω_{xi}, and a value of y_{si}. To start the iteration for the first x-coordinate, x_s, which lies between x_{tn} and x_{tm}, the following assumptions are made

$$y_s = y_{tn} \tag{101}$$

and

$$\Omega_n = \Psi_1 . \tag{102}$$

Iteration is performed on the following expression:

$$\Omega_{(n+1)} = \Omega_n - \frac{(x_o - x_s) - \left[e^{(\Omega_1 \tan\phi)}\right] r_{ocdot} \cos\Omega_1}{r_o \left[e^{\Omega_1 \tan\phi)}\right]\left[\sin\Omega_1 - \cos\Omega_1 \bullet \tan\phi\right]} . \tag{103}$$

When

$$\left| \left[(x_0 - x_s) - \left[e^{(\Omega_n \tan\phi}\right] r_0 \cos\Omega_n\right] \right| \leq \Delta, \tag{104}$$

where) = a selected value, then

$$\Omega_{(n+1)} \approx \Omega_n , \tag{105}$$

and the correct angle, ω_{xi}, is found that corresponds to the x-coordinate of slice i. A selected value of 0.0001 is used for Δ in the bearing capacity computer program. The y-coordinate, y_s, may be computed from the following expression:

$$y_s = y_o - \left[r_o e^{(\Omega_{(n+1)} \bullet \tan\phi)}\right] \sin\Omega_{n+1} . \tag{106}$$

For each x-coordinate of the side of each slice that lies between the x-coordinates, x_{tn} and x_{tm}, the iterative scheme is repeated so that corresponding y-coordinates, y_s, may be determined. Convergence is very rapid using this scheme.

Multilayered Bearing Medium

Bearing capacity calculations involve a certain degree of uncertainty and complexity when the problem involves more than one layer of material. The failure pattern, or the shape of the shear surface, of a multilayered medium is not as evident as the shear surface shape associated with only one layer of material. No bearing capacity, experimental information concerning the failure patterns of multilayered systems could be located in published literature. An approach was assumed, as shown in Figure 16. The approach adopted for approximating the failure pattern, or shear surface, of the multilayered medium is based partly on theoretical considerations. For a given multilayered

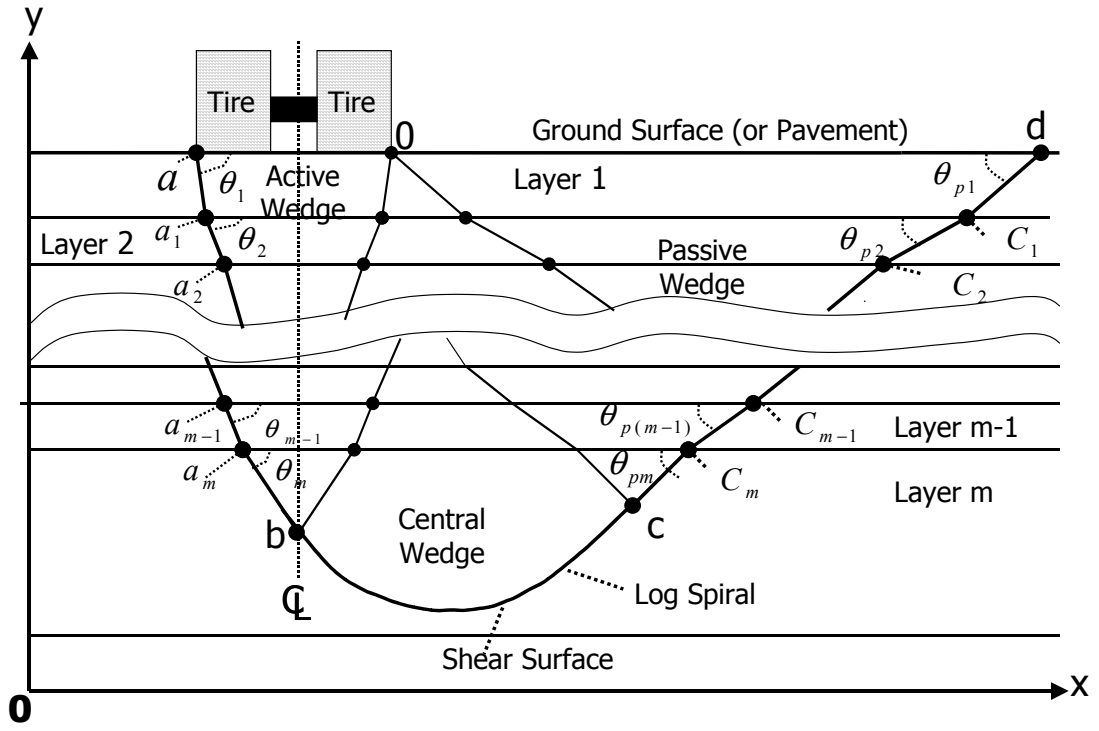

Figure 16. Assumed shear surface of the active wedge in a multilayered bearing medium.

bearing medium, the shear surfaces, identified as lines $\mathbf{aa_1}$,…....$\mathbf{a_{m-1}a_m}$, and $\mathbf{a_mb}$ in Figure 16, are assumed to lie at angles to the horizontal as follows:

$$\theta_{a_2} = 45 + \frac{\phi_1}{2} \qquad (Line\ aa_1) \tag{107}$$

$$\theta_{a_2} = 45 + \frac{\phi_2}{2} \qquad (Line\ a_1a_2) \tag{108}$$

$$\theta_{a_3} = 45 + \frac{\phi_1}{2} \qquad (Line\ a_2a_3) \tag{109}$$

$$\vdots \qquad \vdots \qquad \vdots$$

$$\theta_{a_{(m-1)}} = 45 + \frac{\phi_{(m-1)}}{2} \qquad (Line\ a_{(m-1)}a_m) \tag{110}$$

$$\theta_{am} = 45 + \frac{\phi_m}{2} \qquad (Line\ a_m b\ ), \tag{111}$$

where **m** is the total number of layers of the multi-layered bearing medium and φ_1, φ_2,.....$\varphi_{(m-1)}$, and φ_m are the angles of internal friction of the individual layers, respectively, of the bearing medium. The angles, θ_1, θ_2,....., $\theta_{(m-1)}$, and θ_m are the entry angles of the shear surface of the active block (number 1 in Figure 16).

At point **a**, the x-and y-coordinates are known, or assumed. The problem consists of determining the points of intersections (points $\mathbf{a_1}$, $\mathbf{a_2}$,…….$\mathbf{a_{(m-1)}}$) of the shear surfaces passing through the individual layers and the boundary layer lines. The y-coordinates of these points of intersections are known since the elevations of the boundary layer lines are known. Boundary layer lines are assumed to be horizontal. The x-coordinates of the points of intersection may be determined from the following equations:

$$x_{a1} = \frac{y_a - y_{a1} + \tan\theta_{a1}}{\tan\theta_{a1}} \tag{112}$$

$$x_{a2} = \frac{y_{a1} - y_{a2} + \tan\theta_{a2}}{\tan\theta_{a1}} \tag{113}$$

$$\vdots \qquad \vdots \qquad \vdots$$

$$x_m = \frac{y_{m-1} - y_n + \tan\theta_{(m-1)}}{\tan\theta_{(m-1)}} \tag{114}$$

Since the active block is assumed to be symmetrical, the x-coordinate of point **b** is determined from Equation 114. The y-coordinate of point **b** is calculated from the following equation:

$$y_b = y_{tn} = y_n + (x_n - x_{tn})\tan\theta_{am} \tag{115}$$

The points (identified as $\mathbf{c_m}$, $\mathbf{c_{(m-1)}}$, ..., $\mathbf{c_2}$, and $\mathbf{c_1}$, in Figure 17, of the intersection of the shear surface (passive wedge 3) passing through each layer of the bearing medium and the boundary layer lines cannot be defined until the x-and y-coordinates of point **c** are determined. Although the assumption is made that points **b** and **c** are connected by a logarithmic spiral, the spiral terminating at point **c** cannot be computed since it is uncertain which φ value should be used to compute the spiral radius, r_2. There may be several different φ values in a multi-layered medium. To overcome this problem, and for approximating the size of the passive wedge, an effective φ-value is calculated and used to compute the coordinates of point **c** in Figure 17. This value, $\varphi_{\theta eff}$, is an angle between an imaginary line connecting points **a** and **b** and the horizontal line and is estimated in the following manner (see Figure 17):

$$\theta_{eff} = 45 + \frac{\phi_{eff}}{2} \tag{116}$$

and, rearranging terms,

$$\phi_{eff} = 2(\theta_{eff} - 45) = \tan^{-1}\left(\frac{y_{tn} - y_a}{x_{tn} - x_a}\right) \tag{117}$$

After computing φ_{eff}, r_o and r_1 may be determined from Equations 86 through 91. The φ_{eff} value obtained from Equation 85 is used in these equations. The radius, r_2 (an imaginary line connecting Points **o** and **c**) is computed from Equation 91 using the value of φ_{eff}. After r_2 is found, the x-and y-coordinates of Point **c** are calculated from Equations 96 and 97. Starting at Point **c**, the x-and y coordinates of $\mathbf{c_m}$, $\mathbf{c_{m-1}}$, ..., $\mathbf{c_2}$, $\mathbf{c_1}$ may be computed. The y-coordinates of these points are known since the boundary layer lines are assumed to be horizontal and the elevations of these points are the same as the elevations of boundary layer lines. The x-coordinates of Points $\mathbf{c_m}$, $\mathbf{c_{m-1}}$, ... $\mathbf{c_2}$, and $\mathbf{c_1}$ may be computed from the following expressions:

$$x_{cm} = \frac{(y_{cm} - y_{tm}) + x_{tm}\tan\theta_{pm}}{\tan\theta_m}, (line\ cc_m) \tag{118}$$

$$x_{c(m-1)} = \frac{(y_{c(m-1)} - y_{c(m-2)}) + x_c\tan\theta_{p(m-1)}}{\tan\theta_{p(m-1)}}, (LineC_mC_{m-1}) \tag{119}$$

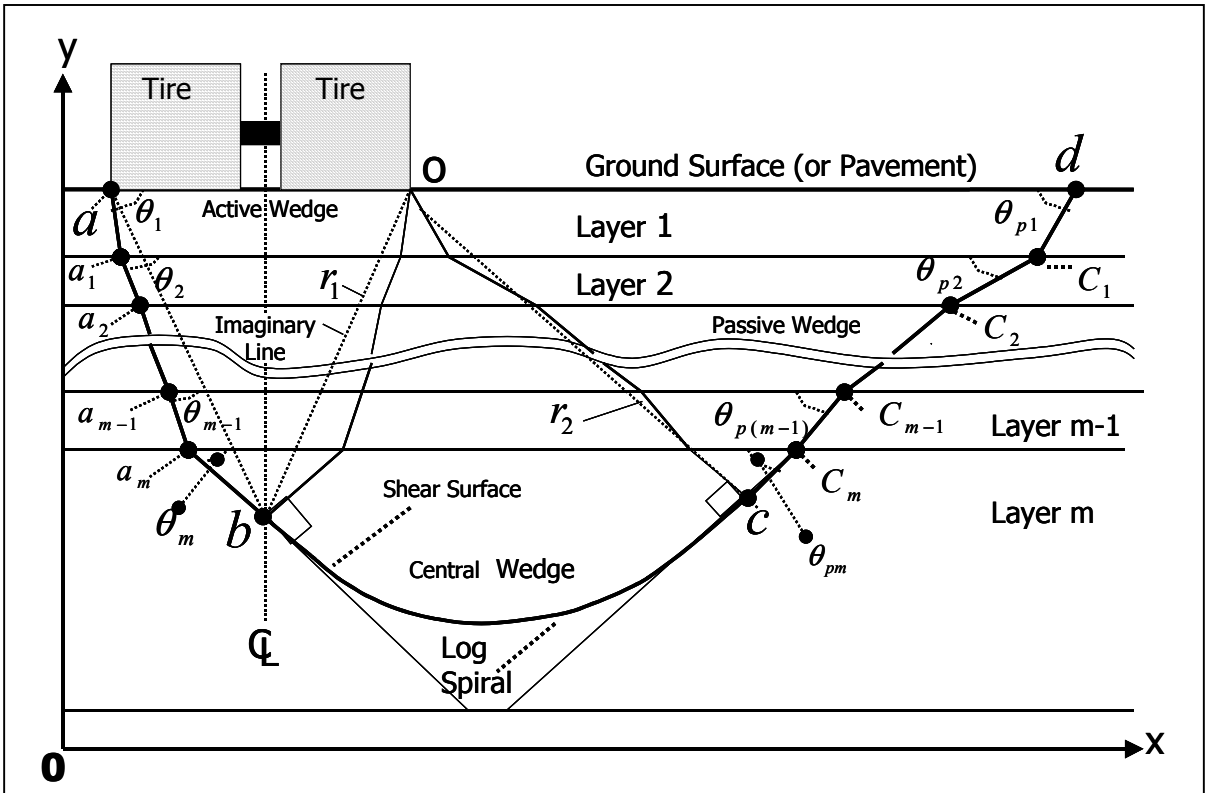

Figure 17. Method for estimating the effective value of N_{eff}.

$$x_1 = \frac{(y_{c1} - y_{c2}) + x_{c2} \bullet \tan\theta_{p2}}{\tan\theta_{p2}}, (Line C_2 C_1) \tag{120}$$

$$x_d = \frac{(y_d - y_{c1}) + x_{c1} \bullet \tan\theta_{p1}}{\tan\theta_{p1}}, (Line C_1 d) \tag{121}$$

Equations 107 through 121 are used to determine the x-and y-coordinates at Points $\mathbf{a_1}$, $\mathbf{a_2}$, ..., $\mathbf{a_{(m-1)}}$, $\mathbf{a_m}$, **b**, **c**, $\mathbf{c_m}$, $\mathbf{c_{m-1}}$, ..., $\mathbf{c_2}$, $\mathbf{c_1}$, and **d** and to define the general shape of the shear surface passing through the multilayered bearing medium. After these coordinates are determined, the potential failure mass is divided into a selected number of slices, **n**, or

$$n = \frac{x_d - x_a}{\Delta x} \tag{122}$$

and

$$x_{si} = x_a + \Delta x \bullet n \tag{123}$$

where x_{si} is defined as the side of any given slice i. After the sides of the slices are defined, the y-coordinates, y_s, which lie on the shear surface at the intersection of the sides of the slice, x_s, and the shear surface may be computed in a fashion similar to the one described previously for the homogeneous case. Each segment of the shear surface passing through each layer is considered. Since the potential failure mass is divided into rectangular slices and considering that the thicknesses of individual layers of the multilayered medium may be very thin, a large number of slices are used. In the analyses shown herein, the potential failure masses were divided into 598 slices (any even number of slices may be used).

To facilitate the use of the approach proposed by Hopkins, all algorithms were programmed for the computer using the Fortran language (Hopkins 1986). The Hopkins limit equilibrium approach has been used very successful in solving hundreds of a variety of slope stability and bearing capacity problems involving no tensile forces (Hopkins 1986, 1991; Slepak and Hopkins 1993, 1995a, and 1995b). The model yields solutions that are within about 1-3 percent of solutions obtained from the Morgenstern-Price and Bishop models. The model has been used extensively in developing remedial solutions for a number of major landslides in Kentucky. Later comprehensive studies by Slepak and Hopkins (1993 and 1995a) showed that, in some cases, the proposed approach did not always converge when tensile reinforcement forces were introduced in the Hopkins' equations, although convergent problems did not occur for stability problems that did not involve reinforcement. Consequently, studies were refocused to finding an approach that would permit the introduction of tensile element forces without divergence.

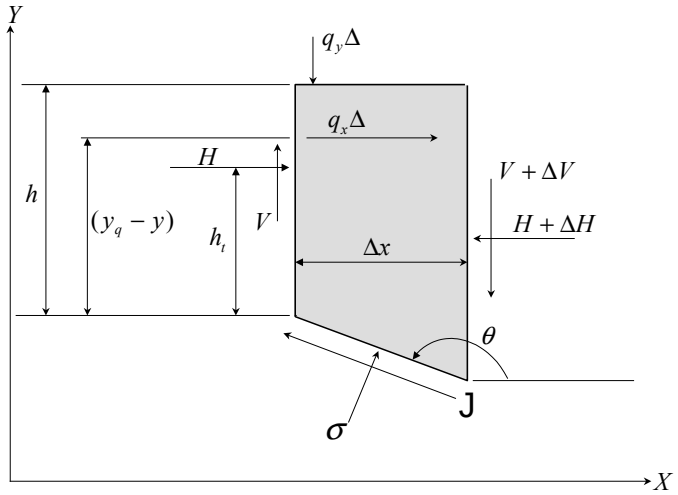

Figure 18. Forces acting on a vertical slice.

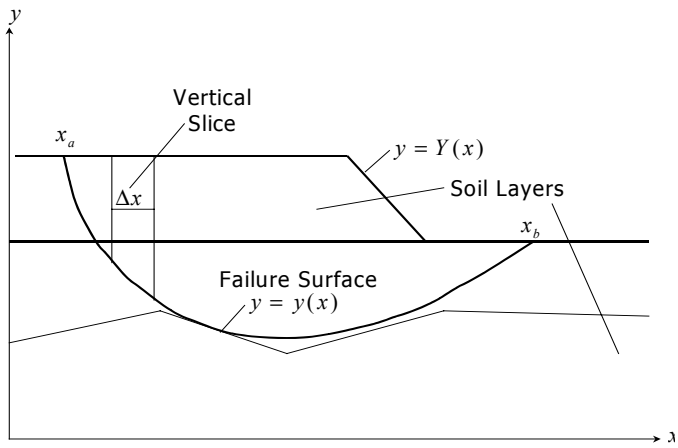

Figure 19. Failure surface in limit equilibrium analysis.

In studies conducted by Slepak and Hopkins, several different approaches were attempted (Slepak and Hopkins 1993, 1995a, and 1995b) in finding a suitable mathematical model that would solve stability problems involving tensile forces. The development of a model where tensile element forces could be included in the system of equations is described and discussed below. Much of this discussion is essentially a recast of the work reported in detail by Slepak and Hopkins (1993, 1995a, and 1995b).

SLEPAK-HOPKINS LIMIT EQUILIBRIUM MODEL

As mentioned earlier, none of the equations of solid mechanics satisfy explicitly everywhere inside or outside the failure surface. The limit equilibrium method represents an alternative to equilibrium equations of solid mechanics. As an alternative to equilibrium equations of solid mechanics, the limit equilibrium method considers either equations of equilibrium for vertical slices, or equilibrium equations for a soil mass bounded by the slope surface and the shear surface, as depicted in Figures 18 and 19. Consequently, two equivalent formulations of a slope stability problem are possible.

As one approach, referred to hereafter as Formulation 1, the equilibrium method may consider the equilibrium equations for vertical slices shown previously in Figure 4, or depicted in Figure 18 in a slightly different form. Details of Formulation 1, referred to as the "slices" method was presented above and will be recast in an integral form below. The soil mass bounded by the slope surface and failure mass is divided into slices, as illustrated in Figure 3, or Figure 19. A second approach may be formulated by considering the overall equilibrium equations of the soil mass bounded by the slope and shear surface. Both Formulations 1 and 2 are described below.

Limit Equilibrium Method. Formulation 1 (Without Tensile Forces)

Taking into consideration Equations 4 and 5, the slice equilibrium equations for the soil mass bounded by the slope surface Y (x) and any particular shear surface y (x) could be written in a form (Janbu, 1954; Morgenstern and Price, 1965; and Hopkins, 1986, 1991):

$$\frac{dH}{dx} = -(\tau + \sigma \tan\theta) + q_x \tag{124}$$

$$\frac{dv}{dx} = \sigma - \tau \tan\theta - (q_y + \gamma_{av} h) \tag{125}$$

$$\frac{d(Hh_t)}{dx} = V - H \tan\theta + q_x (y_Q - y) \tag{126}$$

where

$$\tau = \frac{c' + (\sigma - u)\tan\phi'}{F}, \tag{127}$$

q_x *and* q_y = distributed horizontal and vertical external forces, psf,

H and V = horizontal and vertical interslice forces, lbs/ft.

$h_t = y_t - y, ft,$

$y_t = y$ -coordinates of the thrust line, ft,

$y_Q = y -$ coordinates of points of application of qx, ft,

θ = angle between the tangent to the failure surface and horizontal,

γ_{av} = the distribution of the average total unit weight of the soil above y (x), pcf.

This quantity is related to the conventional unit weight (( ), by the relation

$$\gamma_{av} = \frac{\int_{y(x)}^{Y(x)} \gamma dy}{h} \tag{128}$$

$$h = Y(x) - y(x) \tag{129}$$

where h = height of slices, ft.

All of the variables in Equation 124 through 129 are shown in Figures 19 and 20. Appropriate boundary conditions should be added to the system of Equations 124 to 127, namely:

$$H(x_a) = H_a$$
$$H(x_b) = H_b$$
$$V(x_a) = V_a \quad (130)$$
$$V(x_b) = V_b$$

The system of Equations 124 to 127, with the boundary conditions Equation 130, is statically indeterminate because there are only four equations available to determine five unknowns functions H (x), V (x), F(x), J(x), and h_t (x). This system of equations may have an infinite number of solutions. To narrow the range of possible solutions, some physical admissibility criteria are usually considered (Chen and Morgenstern, 1983). Two additional functions related to the set of original unknown functions are the thrust ratio,

$$\eta = \frac{h_t}{h} \quad (131)$$

and the average factors of safety on vertical slides of slices:

$$F_v = \frac{c_{av} + (H - u_{av}h)\tan\phi_{av}}{V} \quad (132)$$

where c_{av}, N_{av}, and u_{av} are the average weighted values of c', N', and u, respectively.

It is required usually that:

$$0 \le \eta \le 1 \quad (133)$$

$$F_{ve} = \frac{F_v}{F} \quad (134)$$

where F is defined by Equation 127.

It should be mentioned that taking account of admissibility criteria, Equations 133 and 134, does not necessarily lead to a rigorous solution of t problem because this solution is still obtained within the framework of approximations of a limit equilibrium method (see above). At the same time, however, any rigorous solutions of a problem formulated as a problem of plasticity theory will satisfy both criteria 133 and 134.

Admissibility criteria, Equations 133 and 134, narrow a range of possible solutions of the system, 124 to 127 Equations and Equation 130, but this system still remains statically indeterminate. To provide statical determinacy to the system under consideration, some additional assumptions are usually required. These assumptions will be considered next. It is only emphasized that any additional assumption that leads to a statical determinacy of the system of equations, 124 to 127 and 130, automatically defines a function F(x) of a normal stress distribution along the slip line, y (x).

Therefore, the factor F in Equation 127 that is completely defined by the functions F(x) and y (x) represents a functional of two functions:

$$F = F\{ y(x),\ \sigma(x)\}. \tag{135}$$

This functional is termed (Baker and Garber, 1978) the safety functional, to be distinguished from the factor of safety F_s, which is the minimum value of F:

$$F_s = \min F\{ y(x),\ \sigma(x)\}. \tag{136}$$

Consequently, a stability problem may be formulated in the following way:

> Formulation 1: Among all functions $y(x)$, $H(x)$, $V(x)$, $\sigma(x), and\ \tau(x)$ that satisfy equilibrium Equations 124 to 127 and boundary conditions 130, find the functions that provide the minimum value F_s of the safety functional, Equation 135, and meet admissibility conditions, Equations 133 and 134.

Limit Equilibrium Method. Formulation 2

The stability problem may be formulated in another manner using the limit equilibrium method. In this approach, the overall equilibrium equations for a soil mass bounded by the slope surface, Y (x), and s, slip surface y (x), with Coulomb's failure criterion, Equation 127, satisfied along the slip surface (Baker and Garber, 1978):

$$-\int_{x_a}^{x_b}(c' - u\tan\phi')dx - \int_{x_a}^{x_b}\sigma(\tan\phi' + F\tan\theta)dx + F\int_{x_a}^{x_b} q_z dx = 0 \tag{137}$$

$$\int_{x_a}^{x_b}(c' - u\tan\phi')\tan\theta dx - \int_{x_a}^{x_b}\sigma(F - \tan\phi'\tan\theta)dx + F\int_{x_a}^{x_b}(q_y + \gamma_{av}h)dx = 0 \tag{138}$$

$$\int_{x_a}^{x_b}(c' - u\tan\phi')(y - x\tan\theta)dx + \int_{x_a}^{x_b}\left[(\sigma_y(\tan\phi' + F\tan\theta) + \sigma_x(F - \tan\phi'\tan\theta)dx\right] -$$

$$F\int_{x_a}^{x_b} y_Q q_z dx - F\int_{x_a}^{x_b} x(\gamma_{av}h + q_y)dx = 0\,. \tag{139}$$

Variables in these equations have the same meaning as before. The quantity F depends on the functions y (x) and F(x). Therefore, F can be again considered as a safety functional, Equation 136, of two functions y (x) and F(x). So far, there was no attention paid to interslice forces and Equations

124 through 130. At the same time it is to see that any assumption made with respect to selecting a function F(x) will lead to a certain set of functions H, V, and h_t, and the admissibility criteria given by Equations 133 and 134 may not be satisfied. In other words, admissibility criteria expressed by Equations 133 and 134 put some restrictions to selecting a function of normal stress distribution F(x). Hence, a stability problem can be formulated in the following way:

> Formulation 2: Among all functions y (x) and F(x) that satisfy Equations of overall equilibrium 137 –139, find the functions which provide the minimum value F_s of the safety functional 135 and physically admissible interslice characteristics H, V, and h_t (Equations 133 and 134).

Formulations 1 and 2 of a stability problem are equivalent to each other. In the following sections, different limit equilibrium methods are discussed.

Limit Equilibrium Methods Based on Formulation 1

Several methods have been developed for the stability of slopes in which the failure surface may have any arbitrary shape and the differential equations of equilibrium, 124 to 127, are satisfied. In each method, however, additional assumptions are made to render a statical determinacy to the system under consideration. Slepak and Hopkins reviewed several limit equilibrium methods in efforts to select an appropriate procedure to use without and with tensile forces.

In Janbu (1954, 1957), the thrust line h_t is assumed. This assumption makes the problem statically determinate, because for four unknown functions H, V, F, and J, four equations 124 through 127 are available. Using the overall horizontal equilibrium equation as a stability criterion, an iterative procedure was developed for the factor of safety determination. It was shown by Morgenstern and Price (1965) that convergence problems may arise using Janbu's method, especially in cases with high cohesion. To overcome these difficulties, Hopkins (1986, 1991) used a special numerical technique to obtain derivatives of interslice forces involved in the Janbu's iterative procedure. In contrast to the original Janbu's method, Hopkins' method provides rapid convergence for a wide range of practical problems (Hopkins, 1986, 1991).

Another assumption to make the problem statically determinate was made by Morgenstern and Price (1965). They assumed a linear relationship between interslice forces:

$$V = \lambda f(x) H \tag{140}$$

where 8- is an unknown parameter;

f(x)- is an assumed but known function.

By substituting Equation 140 into the original system of equations 124 through 127 the system finally results in a system of two equations with respect to 8 and F:

$$H_{x_b} = (\lambda, F) = H_b$$
$$M_{x_b} = (\lambda, F) = 0 \tag{141}$$

where

$$H_{x_b} = H(x_b)$$

$$M_{x_b} = M(x_b) \tag{142}$$

$$M(x) = H(x)h_t(x).$$

To obtain a solution of the system 141, initial approximations for 8 and F are assumed. Successive approximations are obtained using the Newton-Raphson technique.

Hardin proposed a similar approach (1984). He used the same assumption 140 as in the Morgenstern and Prices's method but another equation to obtain 8 and F. Instead of Equations 143, he used overall equilibrium equations.

Spencer (1967, 1973) proposed a method that assumes the interslice forces to be parallel. He found the results to be fairly accurate and gave some attention to obtaining an acceptable position for the line of thrust in terms of effective stresses.

The most detailed discussion of the admissibility criteria (Equations 133 and 134) is by Chen and Morgenstern (1983). They extended the original generalized method of slices (Morgenstern and Price, 1965) and developed special numerical procedure for formally exploring the bounds of the factor of safety within the limits of physical admissibility. It was shown that, consistent with earlier studies, the variation in the factor of safety when subjected to conditions of physical admissibility is small for all practical purposes. This analysis confirms the view that variations in the factor of safety between several methods in common use are of little practical significance.

Limit Equilibrium Methods Based On Formulation 2.

In this class of methods, overall equilibrium equations are considered as main equations. Differential equations of equilibrium for interslice forces should be considered to check admissibility criteria.

Taylor's method (Taylor 1937) satisfies all equilibrium requirements, but makes arbitrary assumptions with respect to both the kinematical function y (x) and the stress function F(x). Taylor's method is based on the assumption that kinematical function represents a circular arc, while the stress function is distributed as sin x.

Another group of methods is represented by logarithmic-spiral methods (Rendulic, 1935; Taylor, 1937; Frolich, 1935; Wright, 1969; Huang and Avery, 1976). Log-spiral methods are based on the properties of log-spiral functions that the resultant of the elementary normal and frictional forces passes through the pole of the spiral. Consequently, in this case the moment equation about the pole is independent of F and may be used for the determination of the factor of safety regardless of the normal stress distribution; i.e., the problem of sliding along a logarithmic spiral is statically determinate. Furthermore, the stress function F(x) can always be selected to satisfy admissibility criteria (Equations 125 and 126). That makes log-spiral methods not only statically consistent but also physically admissible. Therefore, these methods could be good independent checks for other methods. It is necessary to note that log-spiral methods are only applicable in the case of homogeneous soils with c' equal to a constant, and tan N' equal to a constant.

The first attempt to formulate the slope stability problem as a variational problem in terms of Formulation 2 (see above) was made by Kopacsy (1955). A reappraisal of Kopacsy's analysis by Baker and Garber (1977a) shows that this analysis contains a number of serious errors and misconceptions. An improved variational formulation of the slope stability problem was presented by Baker and Garber (1977b). This formulation applies to the case of homogeneous and isotropic

soil, without pore water pressure or external loads. Baker and Garber (1978) later extended their approach to the general case of non-homogeneous, non-isotropic soil with arbitrary distribution of pore pressure and external loads. They proved that the minimal factor had to occur on slip surfaces with a special geometrical property. The geometrical property ensures that the resultant of the infinitesimal and frictional forces either pass through a common point or are parallel to a common direction. It is shown that as a result of this geometrical property the minimal factor of safety is independent of the normal stress distribution along the critical slip surface. In the homogeneous and isotropic case, the analysis shows that the critical slip surface may be either a lo-spiral (rotational failure mode) or a straight line (translational failure mode). In a layered profile, the critical slip surface may consist of a series of log-spirals that have a common pole or a series of straight lines. In some cases, the boundary between layers may be part of the critical slip surface. Baker and Garber (1978) suggested a simple computational scheme for the determination of the factor of safety and the critical slip surface. This computational scheme is only slightly more laborious than generally used simplified Bishop's method. It was also proved by Baker and Garber (1978) that for the homogeneous and isotropic case, without pore water pressure or external loads, the solutions provided by Rendulic (log-spiral) and Culmann (straight-line) are not only convenient, but also correct. The two methods are related to the two possible modes of failure (rotational and translational).

It is necessary to note that those variational formulations of the problem are criticized by some researchers (De jong, 1980, 1981; Luceno and Castillo, 1981). According to De Jong (1980), the variational approach leads to a weak extremum (or no extremum at all and therefore it produces unsafe predictions for slope stability problems. At the same time, it was shown by Castillo and Luceno (1983) and Leshcinsky et al. (1985) that the procedure based on variational formulation of the problem yields a result that is equivalent to an upper-bound solution in the strict framework of limit analyses of plasticity. Subsequently, although the variationally obtained y(x) signifies a stationary result by virtue of satisfying Euler's equation, it may actually yield a local minimum or inflection value of F_s in the context of limit analysis (Leshchinsky, 1990).

At the same time, encouraging results were obtained by Leschinsky (1990). Based on the results by baker and Garber (1978), he developed an approximate procedure for evaluation safety factors for any kind of arbitrarily selected slip surfaces. For each arbitrarily selected y (x), Leshchinsky (1990) used Euler's equation for normal stress distribution F(x) obtained by Baker and Garber (1978). The specified y (x) that yields the minimum F_s is considered the critical surface. Using this approach, however, it is explicitly being assumed that among all possible stress distributions, the variationally determined F(x) leads to F_s, which is a genuine minimum for all specified y(x). Leshchinsky considered three example problems. For all three examples, he found the line of thrust to be reasonable. This result indirectly supports the original variational approach by Baker and Garber (1978).

Another group of methods which is based on overall equilibrium equations is known as a group of perturbation methods Raulin et al, 1974). In these methods, any arbitrarily selected slip line can be analyzed. As first step, an approximation for the normal stress distribution is considered:

$$\sigma_0(x) = (\gamma_{av} h + q_y)\cos^2 + q_x \sin\theta\cos\theta. \tag{143}$$

Equation 143 is based on the assumption that the normal stress distribution is not affected by interslice forces. The real normal stress distribution is assumed in the following form:

$$\sigma(x) = \omega(x) + \sigma_o(x) \tag{144}$$

where T(x) is a perturbation coefficient. Raulin et al (1974) considered three possible expressions for T(x):

$$\omega(x) = \lambda + \mu \tan\theta \tag{145}$$

$$\omega(x) = \lambda + \mu \tan^2\theta \tag{146}$$

$$\omega(x) = \lambda \tan\theta + \mu \tan^2\theta . \tag{147}$$

By substituting any of expressions 145 to 147 into Equation 144 and then into equilibrium equations, one can obtain three algebraic equations with respect to three unknowns λ, μ *and* F.

It was shown by Raulin et al (1974) that all three perturbation methods based on Equations 175, 146, or 147 provide practically the same values of factors of safety.

Simplified Limit Equilibrium Methods

The methods considered above were statically consistent. That is, three equilibrium equations, either overall or differential) were always satisfied. Some methods satisfy some of the equilibrium equations and ignore the others. Those approaches are referred to as simplified methods.

Ordinary Method of Slices

Ordinary method of slides, which is also called Fellenius' (1927, 1936) method, satisfies only one condition of equilibrium, that is, overall moment equilibrium around the center of a circular slip surface –the method is only applicable to a circular slip surface. In this method, resultant of all side forces on any slice acts parallel to the base of a slice. Ordinary method of slices does not satisfy either horizontal or vertical force equilibrium for the mass above the slip surface, but it provides a simple procedure for the determination of the safety factor.

Bishop's (1955) modified method provides a more rigorous approach by including the interslice forces in the equations of equilibrium of a typical slice. This method satisfies the overall moment equilibrium equations around the center of the circle and vertical equilibrium equation for each slice. However, the method is applicable only to circular slip surfaces. The method does not satisfy horizontal force equilibrium or individual slice moment equilibrium equations. The solution of the problem is obtained by iteration.

Bishop's Method

Bishop's modified method provides a more rigorous approach by including the interslice forces in the equations of equilibrium of a typical slice. This method satisfies the overall moment equilibrium equation around the center of the circle (the method is only applicable to circular slip surfaces) and vertical equilibrium equation for each slice. The method doses not satisfy horizontal force

equilibrium or individual slice moment equilibrium equations. The solution of the problem is obtained by iteration.

Force Equilibrium Methods

Another group consists of methods that use only force equilibrium conditions. These include a method proposed by Lowe and Karafiath (1960), a method developed by Seed and Sultan (1967) and various methods in which the slip surface is assumed to consist of two or three plane segments (Chowdhury, 1978) –commonly referred to as "wedge" or "sliding block' methods, and any other methods that satisfy only force (not moment) equilibrium. In all such methods, the analysis can be accomplished by trial-and-error graphical procedures wherein a value of F is assumed and a trial force polygon is drawn for each slice or wedge. If the last slice is in equilibrium, the assumed value of F is correct. The analysis may be accomplished by a numerical equivalent of this graphical procedure.

Comparison of Different Limit Equilibrium Methods

According to Duncan and Wright (1980), methods that satisfy all conditions of equilibrium (log spiral, Janbu's, Spencer's, and Morgenstern and Price's methods) all give essentially the same value of F_s. Studies of non-homogeneous slopes and dams, and non-circular slip surfaces, show a slightly wider disparity in the values of F_s calculated by those methods. Those studies indicate that for any practical slope stability problem, any method which satisfies all conditions of equilibrium will give a value of F_s which differs by no more than "5 percent from what may be considered the "correct" answer. Thus, although there is no mathematical proof that the values of F_s calculated from Janbu's, Morgenstern-Price's, and Spencer's methods are rigorously correct, from a practical point of view there is no doubt that they may be considered to be correct for all practical purposes.

Bishop's method, which does not satisfy all conditions of equilibrium, gives virtually the same value of F_s as methods that satisfy all conditions of equilibrium. Thus, for analyses of circular slip surfaces, no more elaborate method need to be used (Morgenstern and Price, 1965; Duncan and Wright, 1980).

Ordinary method of slices which is applicable only to circular slip surfaces gives values of F_s that are lower than those calculated by more accurate methods. For u (pore water pressure) equal to zero conditions (in practical terms these would be total stress analyses), the inaccuracy is no more than a few percent. For effective stress analyses with high pore pressures, the inaccuracy may be as much as 50 percent. Thus, while ordinary method of slides may be applied to total stress analysis, it should not be used for effective stress analyses with high pore pressure (Duncan and Wright, 1980).

For N' = 0 conditions, any method which satisfies moment equilibrium around the center of a circular slip surface will give the correct value of Fs, regardless of what other equilibrium conditions it does or does not satisfy (Duncan and Wright, 1980). Thus, the ordinary method of slices, Bishop's method, Morgenstern-Price's method, and Spencer's method all give the same value of Fs for circular slip surfaces and N' = 0 conditions.

The factor of safety calculated by force equilibrium procedures is significantly affected by the assumed side force inclination (Duncan and Wright, 1980). Of all the possible assumed inclinations for these forces, the one suggested by Lowe and Karafiath (1960) appears to be the most generally applicable. They proposed that the side force inclination at the interslice boundary should be assumed to be the average of:

- the inclination of the ground interslice surface at the top of the interslice boundary and
- the inclination of the slip surface at the bottom of the interslice boundary.

Use of Limit Equilibrium Methods in the Stability Analysis of Reinforced Earth Structures

The concept of reinforcing an earth structure by incorporating geosynthetics that possess a much higher tensile strength than soil, and the capability to bond with soil through friction has gained great popularity in recent years. Polymer based soil reinforcing materials are finding increased use in permanent, critical applications, such as reinforced flexible asphalt pavements, reinforced soil retaining walls, steep fills, and earth dams. Those uses are in contrast to earlier soil reinforcement applications such as unpaved roads, temporary retaining walls, and low-height embankments where the reinforcement function was often temporary or where the consequences of failure were not severe.

In walls reinforced with geosynthetics, the sheets of geosynthetics are used to wrap layers of compacted soil producing a stable composite structure. Advantages of reinforced walls over conventional concrete walls include (Leshchinsky and Perry, 1987):

- in many cases, the reinforced wall economics compares favorably with convential walls –usually the cost is much less;
- the construction of reinforced walls is simple and rapid; and
- the reinforced wall is flexible, thus it can undergo significant deformation or sustain significant dynamic impacts.

Moreover, tensile elements --geosynthetics reinforcement materials-- have expanded the practical options for design of soil slopes. Those materials permit construction of slopes at angles steeper than the angle of repose of the soil fill, thereby reducing land requirements for slope construction and often eliminating the need for retaining walls. Steep reinforced soil slopes frequently provide economic advantages over traditional design alternatives.

The main performance criterion for a reinforced structure is stability against sliding of the soils comprising the structure. The common practice concerning reinforced soil structures analysis consists in utilizing traditional limiting equilibrium methods originally developed for unreinforced soil stability analysis. Reinforcing forces are treated as known external forces.

Two Definitions of the Factor of Safety

Commonly, two approaches for incorporating the factor of design into limiting equilibrium design equations (Bonaparte et al., 1987). The factor of safety can be defined as the ratio of the resistance (forces or moments) of the soil structure and foundation to the applied loading effects. This approach is usually used in methods that treat the unstable soil zone as a rigid body (Schneider and Holtz, 1986; Verduin and Holtz, 1989; Jewell, 1982; Ingold, 1982; Murray, 1982). For example, in the case of a circular analysis, this definition will lead to a following expression for the factor of safety (Langston and Williams, 1989):

$$F = \frac{M_{res+} M_q}{M_{dr}} \tag{148}$$

where M_{res} and M_{dr} are resisting and driving moments correspondingly (the same values as in unreinforced soil stability analysis) and M_g is the geosynthetics resisting moment.

Alternatively, the factor of safety can be applied to the soil shear strength to produce shear strength parameters. This is the approach when the soil is considered to behave as a continuum (Schmertmann et al., 1987; Leshchinsky and Reinschmidt, 1985; Giroud and Beech, 1989; Gourc et al., 1989; Leschinsky and Perry, 1987). In this case, the factor of safety is defined using the same expression, Equation 127, as in unreinforced stability analysis.

Those two approaches give answers that are close to each other for cases in which the soil weight and soil shear strength are the major destabilizing and stabilizing forces, respectively (Bonaparte et al., 1987). For reinforced soil structure, the reinforcement forces can be large, and the two cited methods for calculating the factor of safety give different answers (Bonaparte et al., 1987). In fact, since the soil and reinforcement often exhibit markedly different stress-strain behavior, no meaningful overall factor of safety can be defined for the reinforced soil structure. That is why Bonaparte et al. (1987) recommended applying the factor of safety to the soil shear strength, i. e. to use the second definition of the factor of safety based on Equation 127.

Treatment of Reinforcement Forces in Stability Analysis

Internal failure may result from reinforcement rupture, reinforcement pullout, or a combination of the both. Reinforcement rupture can occur when the tensile force required to maintain equilibrium at any elevation within the slope exceeds the available tensile force required to maintain equilibrium at any elevation within the slope, wall, or pavement exceeds the available tensile strength of the reinforcement. Reinforcement pullout can occur when the frictional forces in active and passive zone (Figure xx) are less than the tensile forces required to maintain equilibrium. The direction of the reinforcement resistance, T, is characterized by the angle $ (0# $#2). In most applications, reinforcement forces are assumed horizontal ($ = 0) and their magnitude is assumed equal to long-term tensile strength of a geosynthetics sheet under consideration.

However, since geosynthetics have no significant lateral stiffness and T is activated by soil differential movement, it is obvious that T is not horizontal ($>0). Leshchinsky and Reinschmidt (1985), Leshchinsky and Perry (1987) assume that when failure of the composite structure occurs, the membrane at the slip surface will be inclined so as to contribute the most resistance, that is, be most effective. A more rigorous approach is based on the principle of strain compatibility. Although limiting equilibrium methods don't allow taking strains in account, in the last few years, the importance of strains in the design of reinforced structures had been recognized (McGown et al., 1984; Bonaparte et al. 1987; Beech, 1987; Wallace and Fluet, 1987; Delmas et al., 1986; Gourc et al., 1989). One of the primary reasons for this is that various types of strains are involved in the soil and reinforcement). Since soil and reinforcement have different deformations, their strength cannot usually be mobilized at the same strains. Consequently, both magnitude and direction of the geosynthetics resistance will depend on soil strains or displacements along the potential slip surface. In other words, strains of soil and reinforcement must be compatible. The most rigorous limit equilibrium procedure accounting for strain compatibility was developed by Delmas et al. (1986) and Gourc et al. (1986, 1989). In this method, the relationship between the displacement along the potential slip surface and inclination of the geosynthetic sheets at the points of intersection with the slip surface is established accounting for both rupture and pullout resistance of geosynthetics. This allows calculation of the magnitude and the direction of the geosynthetics at any displacement) of a sliding soil mass. In the proposed procedure the factor of safety F_s is referenced to the soil strength parameters only (Equation 122). The required value of F_s of the factor of safety is chosen (e.g. F_{sr} = 1.5). Different slip surfaces having initial values of $F_s = F_{so} < F_{sr}$ for) = 0 are considered.

Calculations stop when $F_s = F_{sr}$. The slip surface having a maximum value of) (maximum values of mobilized reinforcement resistance) is considered critical.

Another possibility for estimating the reinforcement forces consists of using finite element solutions of the plasticity theory. This possibility is discussed by Rowe (12984), Rowe and Soderman (1985, 1987), Rowe and Myllerville (1989). Rowe and Soderman (1985) developed a method of estimating the short-term stability of reinforced embankments constructed on a uniform purely cohesive foundation. This approach maintains the simplicity of simple limit equilibrium techniques while incorporating the effects of soil-geosynthetic interaction in terms of allowable compatible strain for the geosynthetics. This allowable compatible strain may be deduced from a design chart and depends on the foundation stiffness, the embankment geometry, the deposit depth, the unit weight of the fill, and the critical height of an unreinforced embankment. As it was shown further (Rowe and Soderman, 1987; Rowe and Mylleville, 1989), this approach worked well since the reinforced collapse mechanism was similar to the unreinforced collapse mechanism. However, this is not the case when embankments are constructed on a foundation where there is a significant strength increase with depth.

Methods Commonly used in Reinforced Earth Stability Analysis

Most methods commonly used in reinforced earth stability analysis are based on either force equilibrium methods (Tensar technical note, 1986a, b; Steward et al., 1977; Bonpaparte et al, 1987; Murray, 1982; Schneider and Holtz, 1986; Jewell et al., 1986; Schmertmann et al., 1987) or circular slip methods (Ingold, 1982; Jewell, 1982; Verduin and Holtz, 1989: berg et al., 1989).

Some authors used statically consistent methods. For example, investigations performed by Leshchinsky (1984,1985), Leshchinsky and Reinschmidt (1985), Leschinsky and Boedeker (1989) are based on a variational approach proposed by baker and Garber (1978). Gourc et al. (1989) used a perturbation method.

A comparative analysis of different methods for reinforced soil stability analysis was performed by Langston and Williams (1989) and Wright and Duncan (1991). It was shown that methods that satisfy all conditions of equilibrium result in essentially the same value of factor of safety regardless of the assumptions they might involve. Bishop's method, although it does not satisfy all conditions of equilibrium, results in values of safety factors that are essentially the same as values calculated using methods that do satisfy all conditions of equilibrium. As in the case of unreinforced analysis, force equilibrium methods provide safety factors that are strongly affected by the assumed inclination of side forces.

Major Intent of This Study

As described previously by Slepak and Hopkins (1993), there are different methods available for evaluating the stability of reinforced structures. All methods built within the framework of limit equilibrium methods are approximate. Research performed by Slepak and Hopkins was focused on finding a method that provided reasonable accuracy and at the same time could be easily used by practitioners. The final method developed and proposed by Slepak and Hopkins, after an exhaustive literature review, has been described elsewhere (1983) and portions of this work are described in the following sections. The merits based on a comprehensive comparative analysis ant the shortcomings of each method were outlined. The intents of the current study were to extend the Slepak and Hopkins model to solve the different bearing classes of problems involving layered soils reinforced with geosynthetics. In particular, the following cases were of interest (in this current study):

- Early construction of pavements involving aggregate bases reinforced with geosynthetics.
- After construction cases involving flexible pavements reinforced with geosynthetics.

In developing a method of solving the above classes of problems it should be noted that the Slepak and Hopkins model provides solutions to a variety of the following problems:

- Embankments, and other geotechnical structures, resting on unreinforced and reinforced foundations containing layered soils.
- Embankment slopes reinforced (as well as unreinforced) with geosynthetics.
- Earth walls reinforced with geosynthetics.

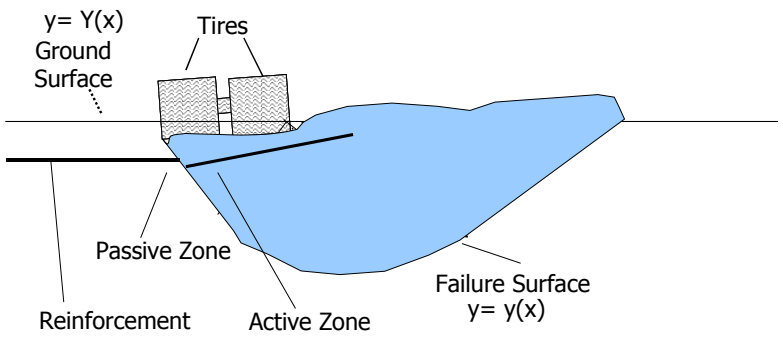

Figure 20. Treatment of reinforcement force(s) in bearing capacity analysis.

To make the works readily useful to practitioners, windows software was written (L. Sun) using Sybase PowerBuilder 8.0 (1999a, b, c). Use of this software is detailed herein in a later section of this report. Some important aspects of the mathematical theories developed by Slepak and Hopkins is detained below. Portions of this work are repeated so that the user may understand how and why this model and computer software were structured.

DEVELOPMENT OF MULTIPURPOSE LIMIT EQUILIBRIUM COMPUTER PROGRAM FOR REINFORCED EARTH STABILITY ANALYSIS

General features of the program

The computer program developed by Hopkins (1986, 1991) is used as a basis for the proposed multipurpose limit equilibrium approach. In the adopted approach, calculations are based on assumptions that the safety factor is referred to the soil shear strength only and the reinforcement forces are treated as known external forces. Although the forces should be derived from the principle of strain compatibility, in this study, a simple assumption with respect to reinforcement forces is made and, based on that assumption; the most reliable equilibrium method is selected. After the basic equilibrium method is developed, extensions to this method can be made including more rigorous calculations of reinforcement forces based on a principle of strain compatibility. Complete implementation of this principle is beyond the scope of this study, however, and may be considered as a proposal in the future.

Reinforcement forces, T, are considered horizontal and equal to (see Figure 20):

$$T = \min(T_r, T_a, T_p) \tag{149}$$

where

$T_r = is\ a\ long-term\ strength\ of\ a\ fabric$
$T_a = is\ \ a\ pullout\ \ resistance\ \ of\ \ a\ \ fabric\ in\ an\ active\ zone$
$T_p = is\ a\ pullout\ resistance\ of\ \ a\ \ fabric\ in\ a\ \ passive\ zone$

and

$$T_a = k_1 \sum_{l_a} (c_i^{'} + \sigma_i^{'} \tan \phi_i^{'}) \Delta x_i + k_2 \sum_{l_a} (C_j^{'} + \sigma_j^{'} \tan \psi_i^{'}) \Delta x_j \tag{150}$$

$$T_p = k_1 \sum_{l_p} (c_i^{'} + \sigma_i^{'} \tan \phi_i^{'}) \Delta x_i + k_2 \sum_{l_p} (C_j^{'} + \sigma_j^{'} \tan \psi_i^{'}) \Delta x_j \tag{151}$$

where

$l_a\ and\ l_p$ $= lengths\ \ of\ \ a\ \ fabric\ \ in\ \ an\ active\ and\ \ passive\ zone\ correspondingly$;
$c_i^{'}\ and\ \phi_i^{'}$ $= the\ soil\ effective\ strength\ parameters\ above\ the\ \ fabric$
$C_j^{'}\ and\ \psi_j^{'}$ $= the\ soil\ effective\ strength\ parameters\ below\ the\ \ fabric$;
$k_1\ and\ k_2$ $= the\ soil-fabric\ \ interaction\ coefficients\ \ for\ soils\ above\ and\ below\ the$
$fabric\ correspondingly$;

$$\sigma_i^{'} = \sigma_i + u_i = effective\ normal\ stress; \tag{152}$$

$u_i = pore\ pressure$;

$$\sigma_i = \gamma_{av} h_i + q_y^i. \tag{153}$$

Though the assumptions expressed by Equations 149 to 153 simplify the problem, very often they may lead to reasonable results. This research is basically methodological and it is the authors' belief that from the methodological viewpoint these assumptions should work very well.

The computer program was originally structured in such a way that it can use different limit equilibrium methods according to the user's choice. All of these methods assume a two- dimensional failure mechanism. These methods are discussed in the following sections. Detailed information about the computer program is included in the user's manual (Section entitled " Windows Computer Software for Computing the Stability of Unreinforced and Reinforced Earth Structures").

Limit Equilibrium Methods Used in the Computer Program

Basic Equations

Differential and integral equations appearing in the section entitled "Slepak-Hopkins Limit Equilibrium Model" to account for reinforcement forces, which are treated as known external concentrated forces, are shown below. The differential equations of equilibrium are as follows:

$$\frac{dH}{dx} = -(\tau + \sigma \tan\theta) + q_x - t(x) \tag{154}$$

$$\frac{dv}{dx} = \sigma - \tau \tan\theta - (q_y + \gamma_{av} h) \tag{155}$$

$$\frac{d(Hh_t)}{dx} = V - H \tan\theta + q_x (y_Q - y) \tag{156}$$

$$\tau = \frac{c' + (\sigma - u)\tan\phi'}{F}. \tag{157}$$

Integral equations of equilibrium are as follows:

$$-\int_{x_a}^{x_b} (c' - u\tan\phi')dx - \int_{x_a}^{x_b} \sigma(\tan\phi' + F\tan\theta)dx + F\int_{x_a}^{x_b} q_z dx - F\sum T_i = 0 \tag{158}$$

$$\int_{x_a}^{x_b} (c' - u\tan\phi')\tan\theta dx - \int_{x_a}^{x_b} \sigma(F - \tan\phi'\tan\theta)dx + F\int_{x_a}^{x_b} (q_y + \gamma_{av} h)dx = 0 \tag{159}$$

$$\int_{x_a}^{x_b} (c' - u\tan\phi')(y - x\tan\theta)dx + \int_{x_a}^{x_b} \left[(\sigma_y(\tan\phi' + F\tan\theta) + \sigma_x(F - \tan\phi'\tan\theta)dx\right] -$$
$$F\int_{x_a}^{x_b} y_Q q_z dx - F\int_{x_a}^{x_b} x(\gamma_{av} h + q_y)dx + F\sum T_i y_r^i = 0 \tag{160}$$

In Equations 154 to 160, reinforcement forces, T_i, are treated here as known external forces applied at points between the potential failure surface and geosynthetics sheets:

$$t(x) = \sum T_i \delta(x - x_r^i); \tag{161}$$

$x_r^i \; and \; y_r^i$ are x-and y-coordinates of points of intersection between an assumed failure surface and geosynthetic sheets;

$\delta(x) - Delt - function$:

$$\delta(x) = \begin{cases} 0, if \; x \neq 0; \\ 1, if \; x=0; \end{cases} \tag{162}$$

and

$$\int_{-\varepsilon}^{\varepsilon} \delta(x)dx = 1, \tag{163}$$

for any $\varepsilon > 0$.

After eliminating $\sigma \; and \; \tau$, differential Equations 154 through 157 can be rewritten:

$$-\frac{dH}{dx} = \frac{1}{F} \frac{c' + (q_y + \gamma_{av} h + \frac{dv}{dx} - u)\tan\phi'}{1 - \frac{\tan\theta \tan\varphi'}{F}} \sec^2\theta - q_x + t(x) + (q_y + \gamma_{av} h + \frac{dv}{dv})\tan\theta \tag{164}$$

$$\frac{d(Hh_t)}{dx} = V - Htan\theta + q_x(y_Q - y). \tag{165}$$

Equations 164 and 165 are used in methods formulated by Janbu, Hopkins, and Morgenstern and Price's.

Hopkins' Method

Hopkins' method (1986, 1991) involves the same assumption as the original Janbu's method (1954, 1957). It assumes the thrust ratio, 0, and consequently, the values of h_t. Then Equations 164 and 165 become a system of two equations having two unknown functions, H and V. As in the original Janbu's method, Hopkins uses an overall horizontal equilibrium equation for the determination of the factor of safety:

$$F = \frac{\int_{x_a}^{x_b} A\,dx}{H_a - H_b + \int_{x_a}^{x_b} B dx} \tag{166}$$

where

$$A = \frac{(c' + (q_y + \gamma_{av} h + \frac{dV}{dx} - u)\tan\phi')(1 + \tan^2\theta)dx}{1 - \frac{\tan\theta\tan\phi'}{F}} \tag{167}$$

$$B = q_x - t(x) - (q_y + \gamma_{av} h + \frac{dv}{dx})\tan\theta\,. \tag{168}$$

In Equation 166, the factor of safety, F, appears in both parts of the equation; therefore, iterations are needed to solve it. As a first approximation both Janbu and Hopkins, start with an assumption that

$$\frac{dv}{dx} = 0 (x_a \le x \le x_b)\,. \tag{169}$$

With this assumption, Equation 166 leads to a simple iteration procedure and allows the obtainment of an initial approximation for F:

$$F_0 = F\,|_{\frac{dv}{dx}=0} \tag{170}$$

This approximation is used to obtain a more rigorous solution through the following steps:

1. Determine $\frac{dH}{dV}$ and H from the Equation 164 based on F=F_0 and $\frac{dH}{dV} = 0$;

2. Determine V and $\frac{dV}{dx}$ from Equation 165;

3. Substitute $\frac{dV}{dx}$ into Equation 166 to obtain the next approximation of F;

4. Repeat steps 1 through 3 until the difference between subsequent approximations of F becomes appropriately small, or the iterative scheme is continued until the condition

$$|F_n - F_{n+1}| \leq \varepsilon, \tag{171}$$

is satisfied. The term, , , is an error selected by the user. Usually the value in this case is 0.001.

Steps 1 through 4 are involved in both the original Janbu's and Hopkins' procedures. However, Hopkins uses a special smoothing technique to obtain dH/dx and dV/dx in steps 1 and 2. As shown by Hopkins (1986,1991), with this smoothing technique, his method converged for a big variety of practical problems for unreinforced earth stability analysis. It was shown, however, by Slepak and Hopkins (1993) that this method is applicable for reinforced earth stability analysis but it has convergence problems in some particular cases.

Morgenstern-Price's Method

Similar to the original Morgenstern and Price's (1965) method, this version for the reinforced case uses the basic Equations 164 and 165 and the assumption of Equation 140, which makes the problem statically determinate:

$$V = \lambda f(x) H. \tag{172}$$

With this assumption, Equation 164 takes the form:

$$\begin{aligned}\frac{dH}{dx} = &\{(c' - u\tan\phi')\sec^2\theta + t(x)(F - \tan\theta\tan\phi') + \\ &(q_y + \gamma_{av}h)(\tan\phi' + F\tan\theta) + \\ &\lambda(\tan\phi' + F\tan\theta) f'(x) H\} / \{\tan\theta\tan\phi' - F - \lambda(\tan\phi' + F\tan\theta) f(x)\}.\end{aligned} \tag{173}$$

As in the original Morgenstern and Price's method, this equation can be solved with respect to H with an initial condition

$$H(x_a) = H_a. \tag{174}$$

By substituting H (x) into Equation 165, the value of M (x) = H (x) ht(x) can be easily determined. Finally, equations 141 are used as criteria to obtain the values of λ and F.

Three options were initially considered in the program based on different definitions of f (x):

$$f(x) = 1 \tag{175}$$

$$f(x) = \sin\frac{\pi(x - x_a)}{x_b - x_a} - half\ \sin wave \tag{176}$$

$$f(x) = \left[\sin\frac{\pi(x - x_a)}{x_b - x_a}\right]^2 - full\ \sin wave. \tag{177}$$

Bishop's Method

Bishop's method is not a statically consistent method and it was classified as a simplified method. However, it was proven that this method gives reasonable answers.

The original Bishop's method (for unreinforced analysis) consists of finding the safety factor, F., by subsequent approximation based on the following equation:

$$F = \frac{M_{res}}{M_{dr}}, \tag{178}$$

where M_{res} is a resisting moment with respect to the center of a trial circle;

$$M_{res} = \sum \frac{(c' + (q_y + \gamma_{av} h - u)\tan\phi')\Delta x}{\cos\theta\left(1 - \frac{\tan\theta\tan\phi'}{F}\right)} \tag{179}$$

and M_{dr} is a driving moment;

$$M_{dr} = -\sum \sin\theta(\gamma_{av} h + q_{y)}\Delta x. \tag{180}$$

Ingold (1982) first proposed an extension of the original Bishop's method to take account for reinforcing fabrics. He proposed the following equation:

$$F = \frac{M_{res} + \sum T\cos\theta}{M_{dr}}, \tag{181}$$

where the term $\sum T\cos\theta$ is an additional resisting moment provided by the fabric.

An approach based on Equation 181 does not strictly follow the logic involved in Bishop's method. Bishop's method satisfies the overall moment equilibrium condition and the vertical equilibrium condition for each slice. An approach proposed by Ingold (1982) satisfies the overall condition moment equilibrium condition but it doesn't satisfy the vertical equilibrium condition. To overcome this misconception, all of the derivations involved in Bishop's method should be considered in treating reinforcement forces as known external forces. It is easy to show that this approach will lead to an equation different than the one proposed by Ingold, or

$$F = \frac{M_{res}}{M_{dr} - \sum T\cos\theta} \tag{182}$$

where M_{res} and M_{dr} are described by the same Equations 179 and 180. The method based on Equation 182 will be referred to as Bishop's incorrect method while the second method based on Equation 181 will be referred to as Bishop's correct method. Many authors use Bishop's incorrect method following the original work by Ingold (1982), but in a recent publication (Wright and Duncan, 1991) the necessity of using Bishop's correct method is strongly emphasized. Slepak and Hopkins (1993) have shown that the difference between Bishop's correct and incorrect methods may be very large. Comparing Equations 181 and 182, both methods only yield the same results in two special cases: when F=1 or when T=0 (unreinforced case).

Perturbation Methods—Slepak and Hopkins' Model

In contrast to the method of slices, perturbation methods use overall equilibrium equations in an integral form (see section entitled " *Limit equilibrium methods based on formulation 2").* In the original perturbation method proposed by Raulin et al (1974), basic approximation for the normal stress distribution is chosen in the form of Equation 143. A modification of this approximation for reinforced analyses was made by Gourc et al (1989):

$$\sigma_o(x) = (\gamma_{av}h + q_y)\cos^2\theta + q_x\sin\theta\cos\theta - t(x)\sin\theta\cos\theta \tag{183}$$

where t (x) is described by Equation 161.

As shown by Raulin et al (1974), all three modifications expressed by Equations 145, 146, and 147 of the perturbation method with the same basic function, Equation 143, yield essentially the same results. Therefore, the authors considered only one version decribed by Equation 145. Instead two other versions were introduced. Those versions consider normal stress distribution obtained by Hopkins' (1986, 1991) method for the unreinforced case. It was mentioned in the section, " Hopkins method" above, that Hopkins' method provided reasonable answers in unreinforced earth stability analysis and therefore the normal distribution obtained by this method may be a good initial approximation for perturbation methods. The authors in the earlier works (1993, 1995) considered three perturbation methods, as follows:

Method 1. (After Gourc et al, 1989).

$$\sigma = (\lambda + \mu \tan\theta)\sigma_o \tag{184}$$

Where σ_o is described by Equation 183

Method 2.

$$\sigma = \lambda\sigma^* - \mu t(x)\sin\theta\cos\theta \tag{185}$$

where σ^* is the normal stress distribution in a corresponding unreinforced problem obtained according to the Hopkins' method (1986, 1991).

Method 3.

$$\sigma = (\lambda + \mu \tan\theta)(\sigma^* - t(x)\sin\theta\cos\theta) \tag{186}$$

where σ^* is defined in the same way as in Method 2. On substituting any of expressions 184,185, or 186 into the system of equilibrium Equations 158 to 160, the following system of nonlinear algebraic equations with respect to $\lambda, \mu,$ *and* F :

$$\begin{aligned} &a_{11}\lambda + a_{12}\mu + a_{13}\lambda F + a_{14}\mu F + a_{15}F - b_1 = 0 \\ &a_{21}\lambda + a_{22}\mu + a_{23}\lambda F + a_{24}\mu F + a_{25}F - b_2 = 0 \\ &a_{31}\lambda + a_{32}\mu + a_{33}\lambda F + a_{34}\mu F + a_{35}F - b_3 = 0. \end{aligned} \tag{187}$$

Expressions for a_{ij} *and* b_i for each of the above mentioned methods are given elsewhere (see Slepak and Hopkins, 1993 in an Appendix). The system 187 is solved by the Newton-Raphson method.

In the study performed by Slepak and Hopkins (1993), applications of the above methods to reinforced earth stability analyses were performed. Numerous published stability problems involving tensile reinforcement were performed using the perturbation method and the three different assumptions expressed by Equations 184 to 186. One published example (a reinforced slope) was taken from Tensar Technical Note (1986a). For comparison, results published by Wright and Duncan (11991) for the same example were compared to results using the three different perturbation approaches. Wright and Duncan solved the problem using stability methods by Spencer, Bishop (correct approach), Force Equilibrium, and Log Spiral. In addition to the perturbation methods, the authors solved the problem using Bishop's correct and incorrect methods, and Hopkins' method. All methods gave almost identical results (F=1.44-1.46) except the Force Equilibrium method (F=1.30) and Bishop's incorrect method (F=1.36).

Several generic reinforced slopes of different degrees (30^0,45^0, 60^0, and 80^0) were performed using Morgenstern and Price's method, Hopkins' method, Bishop's correct and incorrect methods, and the perturbation methods using three different approaches. In all cases statically consistent methods gave reasonable thrust ratios and the difference between answers were practically insignificant. Morgenstern and Price's method was found to be very sensitive to initial approximations of 8 and F. Depending on how close those approximations are to the "true" answer, this method may or may not converge. Bishop's incorrect methods gave lower answers than the other methods. Depending on the number of reinforcement sheets, the differences in factors of safety provided by Bishop's correct and incorrect methods varied from 0 to 47 % where 0% represented the case when there were no intersections between a selected failure surface and reinforcement sheets. Occasionally, the Hopkins's method for the reinforcement case did not converge.

Other published cases include a load test of a large –scale geotextile retaining wall (Billilard and Wu, 1991), RMC load test of a large scale model geogrids-reinforced wall (Bathurst et al, 1988). In both cases, the perturbation, Bishop's correct, and Hopkins' methods yielded results that agreed with failure conditions, that is the factor of safety were very close to 1.0).

Slepak and Hopkins (1993) also examined the stability of reinforced embankments on soft clay foundations. Three published examples were analyzed and included examples published by Wright and Duncan (1991), Rowe et al (1984), and Hadj-Hamou et al (1990). These cases were examined using admissibility criterion, Equation 128, or: $0 \le \eta \le 1$. Detailed analysis of these examples were made by Slepak and Hopkins using the admissibility criterion, Equation 128. The analysis were performed by using the following defined value:

$$\varepsilon = \frac{\int_{x_a}^{x_b} \eta^*(x)dx}{x_b - x_a} \tag{188}$$

where

$$\eta^* = \begin{cases} 0, & \text{if} \quad 0 \le \eta \le 1 \\ 1, & \text{if either } \eta \prec 0 \text{ or } \eta \succ 1 \end{cases} \tag{189}$$

For an admissible thrust ratio, the value of $\varepsilon = 0$; a thrust ratio that violates the admissibility criterion at all points $x(x_a \le x \le x_b)$, $\varepsilon = 1$. For all intermediate cases, $0 \le \varepsilon \le 1$. In the case of a reinforced embankment on a soft foundation, Slepak and Hopkins (1993) concluded that different limit equilibrium methods may lead to essentially different values of factors of safety, especially in the case of noncircular slip surfaces. Using the admissibility criterion given by equations 93 and 94, it was shown that in both circular and noncircular analyses only the Perturbation Method 3 proposed in their report appeared to be statically consistent and physically admissible. Perturbation Method 3 was recommended for practical use and as a universal limit equilibrium method. Moreover, the

method works reasonably in the case of internal stability of reinforced slopes and retaining walls as well as reinforced slopes in the case of a reinforced embankment on a soft foundation involving deep failure surfaces. The method does not have any restrictions to the kind of failure surface and, in all cases, rapid convergences were observed by the authors. The authors also noted that Bishop's method and all statically consistent methods, such as Hopkins' method, Morgenstern and Price's method, the original Perturbation method, and new Perturbation methods, as proposed by the authors, provide reasonable factors of safety for internal analyses of reinforced slopes and retaining walls. However, Hopkins' method on occasions does not converge and Morgenstern and Price's method appears very sensitive to the initial approximations of λ and F parameters as well as the function *f (x)*.

Based on the findings of Slepak and Hopkins, three different stability methods were included in the computer software for analyzing reinforced slopes and retaining walls, and the extension of the software to include the bearing capacity of reinforced flexible pavements. Perturbation Method 3, Hopkins' method, and Bishop's correct method were included in the newly developed Windows software. The Hopkins' method was included in the software since this method provides the first estimate of normal stresses that are used in the Perturbation method 3. Also, the Hopkins method can also be used to analyze all classes of stability problems (circular and noncircular) that do not involve reinforcement. In the software, the user is not allowed to use the Hopkins' method in solving problems involving reinforcement. Bishop's correct method was included for comparative purposes. However, the user should be cautious in using this approach for solving problems involving deep failures. The Perturbation method was recommended for solving all classes of problems, including the analyses of flexible pavements reinforced with tensile elements.

DEFINING SHEAR STRENGTH PARAMETERS OF FLEXIBLE PAVEMENT LAYERS

Shear strength Parameters of Asphalt Cores

Because shear strength of asphalt materials varies with temperature and temperatures within the asphalt concrete materials vary with pavement depth, the shear strength varies with pavement depth (Hopkins, 1991; Hopkins and Beckham 1995). To examine the variation of shear strength with temperature, unconsolidated-undrained triaxial compression tests were performed on asphalt core specimens obtained from an asphalt concrete pavement site in Kentucky. As a means of varying the temperature of the asphalt specimens, coiled, copper tubing

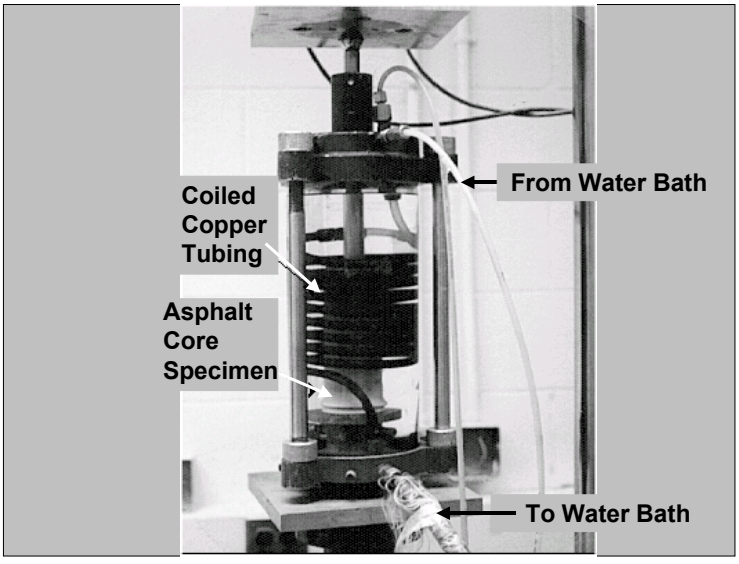

Figure 21. Close-up view of triaxial chamber, triaxial specimen of asphalt core, and copper tubing.

(Figure 21) was fitted around each core specimen in the triaxial chamber. The copper tubing was connected to a temperature-controlled, water bath. Water was circulated from the water bath through the copper coils and back to the water bath. A close-up view of the triaxial chamber is shown in Figure 22. After several hours, the temperature of the water in the triaxial chamber (and asphalt core specimen) becomes the same as the circulating water from the water bath.

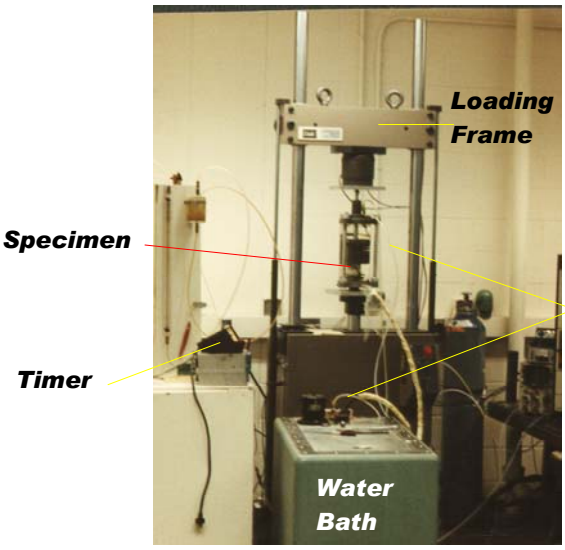

Figure 22. Triaxial equipment for testing asphalt pavement cores, aggregates, and soil subgrades.

A minimum of three specimens was tested at a selected temperature. Selected temperatures ranged from 25 to 60^0 C. Variations of the total stress parameters, angle of internal friction, N, and cohesion, c, with temperature are shown in Figures 23and 24 respectively. The value of N increases from 26 to 44 degrees as the temperature increases from 25^0 to 60^0 C. The value of c decreases from about 386 to 51 kPa.

Shear Strength Parameters of Aggregate Base Materials

Shear strength parameters, ϕ and c, of the base material (crushed limestone) were estimated to be 43 degrees and zero, respectively. This assumption was based on actual triaxial test results obtained from testing similar compacted aggregates.

Shear Strength of Soil Subgrades

The shear strength of a soil subgrade may be expressed in terms of the effective stress parameters, $\phi' and\ c'$ or the undrained shear strength, S_u. To use the effective stress parameters requires knowledge of the pore pressures in the soil subgrade. Although pore pressure measurements could be performed in situ to obtain this information, the effort would require extensile efforts. This certainly could be the subject of a

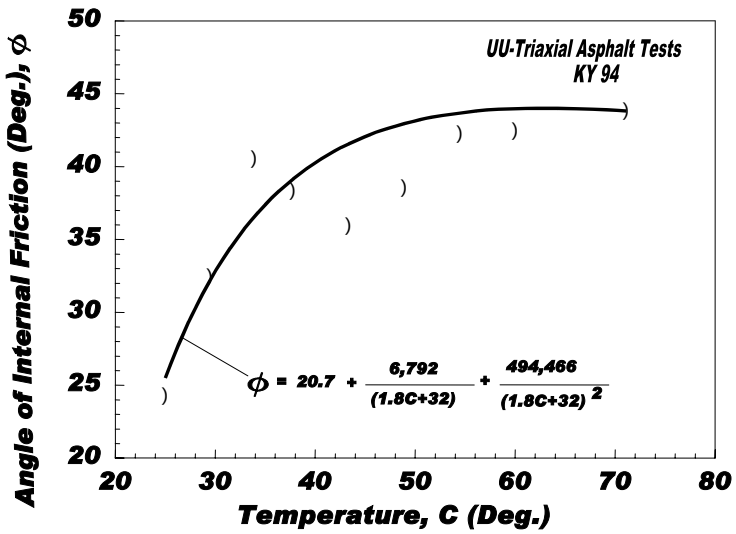

Figure 23. Angle of internal friction of asphalt core specimens as function of temperature.

future research study and is beyond the scope of this research effort. However, if the pore pressure behavior is known, than the Slepak-Hopkins and Hopkins models could be used to perform an effective stress analysis. The pore pressures acting in the soil subgrade under wheel loadings could also be estimated from triaxial tests, but with a great deal of uncertainty. Because traffic loadings are almost instantaneous, the analysis could be performed using the undrained shear strength of the soil subgrades, or assuming a total stress analysis. In this study this approach was adopted. Moreover, the undrained shear strength of the subgrade during the life of the pavement is largely unknown. However, the CBR bearing strength of the compacted soil is usually available, or it can be measured in situ. Consequently, Hopkins (1991) developed a relationship between undrained shear strength and CBR, or

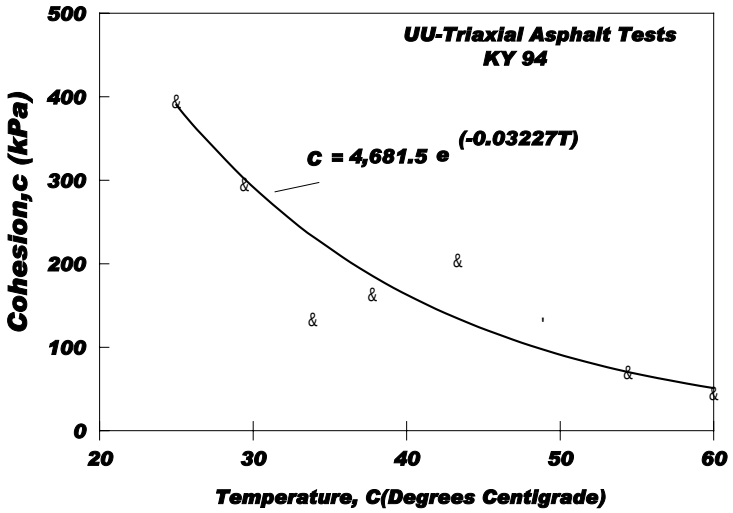

Figure 24. Cohesion, c, as function of asphalt temperature.

$$S_u = 2.173 CBR^{0.979}. \tag{190}$$

MULTIPURPOSE LIMIT EQUILIBRIUM COMPUTER PROGAM GENERAL GUIDE TO DATA ENTRY

Originally, the computer program developed by Hopkins (1986, 1991) was written in the Fortran language. Later Slepak and Hopkins (1993 and 1995) revised that software and included other stability methods. Stability models by Morgenstern-Price, Bishop, Hopkins, and Slepak-Hopkins were included in the revised Fortran version. However, to make the software "user friendly" the software was revised again in this study. To avoid rewriting the different model equations (programmed in Fortran), PowerBuilder 8.0® (Synbase 1999a, b, and c) was used to develop graphical user interfaces (GUIs). Those Graphical user interfaces were coupled with the old Fortran program. This approach avoided also the need for testing the software since many hundreds of comparisons have made in past studies. This approach also essentially eliminated the need to "debug" the Fortran software. Basic data entry and output are described below.

Main Menu

The stability models developed by Hopkins (1986, 1991) and Slepak and Hopkins (1993, 1995, and 1996) may be used in two different approaches. In the first approach the, the multipurpose limit equilibrium computer program can be used as a standalone computer program. Alternately, the

windows version of the computer program has been stored in the Kentucky Geotechnical Database (2004). This database is in an intranet system developed for engineers of the Kentucky Transportation Cabinet by Hopkins et al (2004). The computer program is stored on a Cabinet server in Frankfort, Kentucky. However, central offices and all twelve-highway district offices have access to the centrally located server. By using the server version, changes and updates can be made easily and conveniently. The main menu of the Kentucky Geotechnical database is shown in Figure 25. By clicking on "Engineering Applications" and "KTCSLOPE," the main menu of the computer program appears as shown in Figure 26. The same menu appears in the stand-alone version of the program. In addition to solving bearing capacity problems involving multilayered medium, which may be reinforced with tensile elements or unreinforced, the multipurpose program also handles the stability analyses of many different types earth structures.

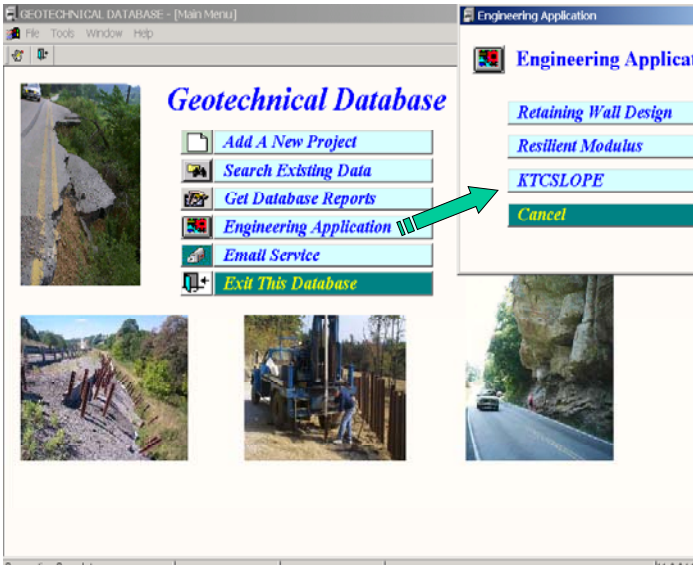

Figure 25. Method for accessing the Bearing Capacity program in the Kentucky Geotechnical Database.

The main menu of the stability program is divided into three parts that are labeled

- Stability Analysis
- Slope Design
- Wall design.

When the button, "Stability analysis" is clicked, the GUI screen in Figure 27 appears. This screen is divided into a menu that displays the following options:

- Get Input Data File
- Edit Input Data File
- Run Analysis
- Browse result File
- Go Back.

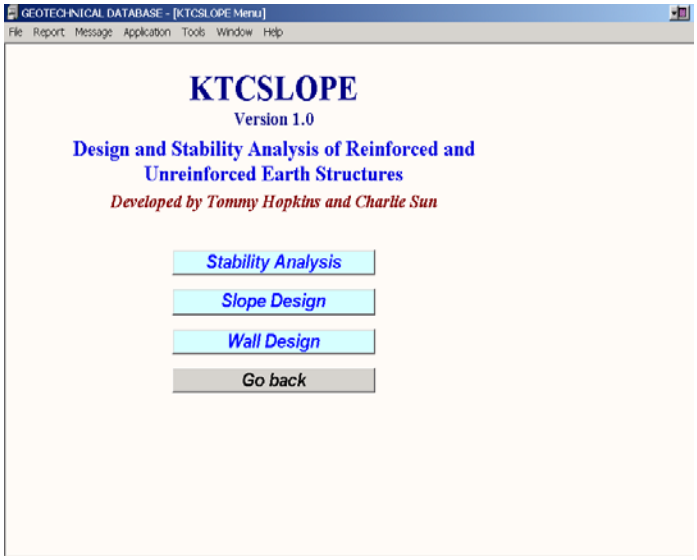

Figure 26. Main menu of the KTC computer software for calculating the stability of earth structures

If the button containing "Get Input Data File" is selected, then the GUI screen labeled "Select a File" appears. The user may select a previous file containing a stability problem. After a previous file is selected, the user may click the button "Edit Input Data File" and the GUI screen shown in Figure 27 appears. The data may be edited to

perform a new analysis or to run the stored problem. In this case, the stored problem is clicked from the file and the button "Edit Input Data File " is clicked. When this action is performed the GUI screen shown in Figure 27 appears, which contains data for the stored example. If the user prefers a blank screen for a new problem, then the button "Edit Input Data File" is clicked. A small screen appears asking the user if a file is to be retrieved. If the user clicks "no", then the screen in Figure 28 appears blank without any data. The user may enter a completely new set of data.

The "problem Control " screen In Figure 28 contains a main menu for entering data. This menu includes the following:

- Problem Control
- Ground Line
- Soil Property
- Boundary Lines
- Water
- Thrust Line
- Vertical Loads
- End Forces
- Failure Surface
- Reinforcement
- Save
- Save As
- Execute
- See Results
- Print section View
- Go Back.

Each graphical user interface associated with each item above is described in detail below.

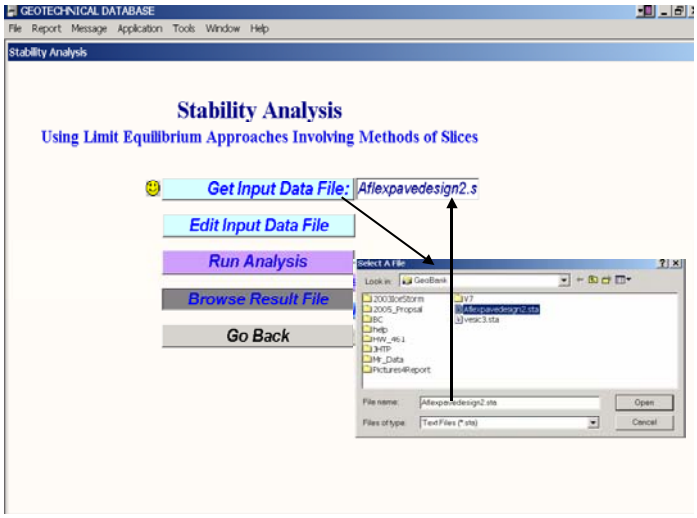

Figure 27. Selecting a stored stability problem.

Problem Control

The problem control graphical user interface, Figure 28, contains a number of boxes for entering information that must be provided by the user. Whenever a button on the main menu at the right of that figure is clicked an icon appears to the left of that button. This indicates that this GUI screen has been opened at least once. If the "folder" icon appears to the right of the clicked button, then the GUI screen associated with the clicked icon is presently appearing. Detailed descriptions of the boxes on the "Problem Control" screen are presented as follow:

- *Problem Identification*
  The user may enter a description of the particular type of stability problem and a date in this box.

- *Reinforcement*
  A drop down box is provided for the user to click either "Yes" or "No." *(Later the user will supply property attributes and locations of the tensile reinforcement elements. In some cases, the program will generate locations and other data.)*

- *Thrust Line*

  This imaginary line, which is defined by the user using x-and y-coordinates, locates the positions of the side forces on each slice. *(Normally, this feature is only used in rare cases and usually in most analyses is not required.)*

- *Thrust Ratio, O*

  See Figure 4, or 18. The thrust ratio is defined by Equation 131, or it is the ratio of the difference, y_t-y, to the height of the slice, h_t, where y_t is the y-coordinate of the thrust line and y is the y-coordinate of the ground line. Normally, a value of 0.33 is assumed in the analysis, although any value between 0 and 1 may be specified.

- *Method*

  Three limit equilibrium stability methods are available in this version of the computer program. These are as follows:

  - Modified Perturbation
  - Bishops
  - Hopkins

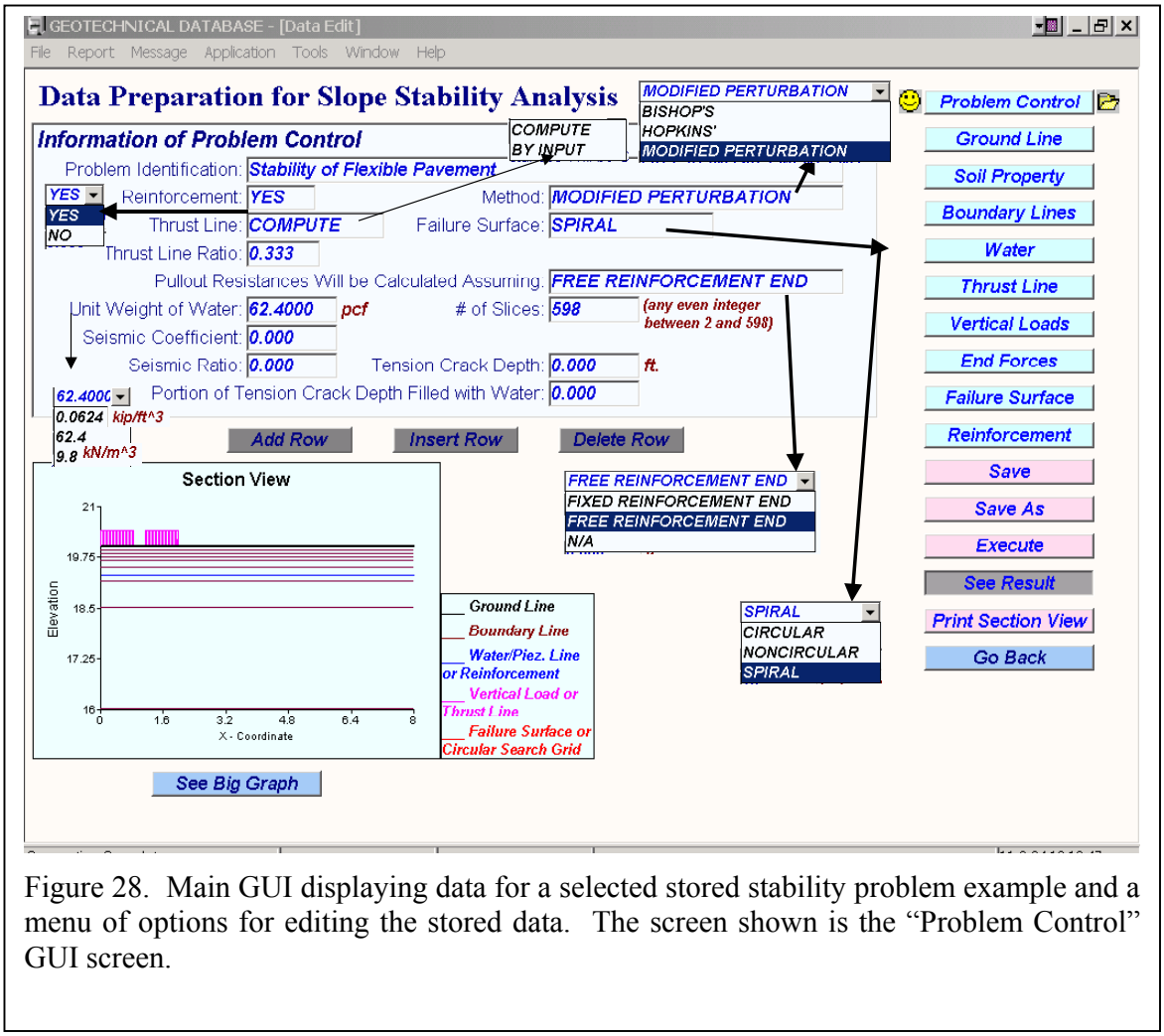

Figure 28. Main GUI displaying data for a selected stored stability problem example and a menu of options for editing the stored data. The screen shown is the "Problem Control" GUI screen.

- *Failure Surface*

  In this version of the computer program, the failure surface may be specified in three different ways. These include:

  - Circular

    A circular shear surface may be specified for each of the three stability methods—Modified Perturbation, Bishops, and Hopkins.

  - Noncircular

    The computer does not allow specifying a noncircular failure surface for the Bishop stability model since this method can be used only for circular failure surfaces.

  - Spiral

    The log spiral shape shown in Figure 14, or 16, can be specified with this option. However, this shape cannot be used with the Bishop model. The spiral shape can be used in the Perturbation and Hopkins' methods in all cases not involving tensile elements. When tensile element elements are involved in the stability problem, only the Perturbation method can be used. Moreover, both circular and noncircular failure surfaces may be used.

- *Pullout Resistance will be Calculated by Assuming*

  There are two options to calculate reinforcement forces in the program. These options are exercised by using the dropdown box shown in Figure xx. The options are:

  - Fixed Reinforcement End, or
  - Free Reinforcement End.

  If "Fixed Reinforcement End " is selected, then the reinforcement forces are calculated based on Equation 147, but reinforcement sheets are considered fixed at the right ends, i. e. $t_a = T_r$ in Equation 147, or the pullout resistance of a fabric in an active zone is equal to the long-term tensile strength of a fabric. When the option, "Free Reinforcement End," is selected the reinforcement force is calculated according to Equation 147.

- *Unit Weight of Water*

  The units of all data entered into the program must be consistent. The numerical value and units specified for the unit weight of water control the units of all other input data. If the user does not specify a value for the unit weight of water, then the computer program assumes a value of 62.4 pounds per cubic foot (pcf). Therefore, in this case, length must be in feet and force and weight must be in pounds to be consistent with the units of the unit weight of water. For example, all coordinate data must be in feet and such value, as the cohesion of a soil would have the units of pounds per square foot. If units other than those assumed by the computer program are used, then the user must specify a numerical value of the unit weight of water consistent with the intended units. For instance, if the unit weight of pore fluid is specified as 1.0, then the consistent set of metric units would be metric tons and meters, grams and centimeters (not kilograms and centimeters). If a value of the unit weight of the pore fluid other than fresh water is desired, than the desired unit weight of the pore fluid

should be specified. In the drop down box in Figure 28, the unit weight of water may be specified in four different ways, or

- 0.0624 Kips/ft^3
- 62.4 Lbs/ft^3
- 9.8 Kn/m^3
- Value and units supplied by user.

- *Seismic Coefficient*

  Earthquake loading is simulated using a pseudo-statical method. The seismic force is assumed to act horizontal on each slide in the direction of the failure (away from the slope or bearing capacity problem. The force on each slice is computed from

$$F_i = \frac{aW_i}{g} = \psi W_i) \tag{191}$$

  where F_i = horizontal seismic force acting on slice i,

  Wi = weight of slice i,
  g = acceleration of gravity,
  a = horizontal earthquake acceleration, and
  ψ = seismic coefficient in the region in which the earth structure is located.

- *Seismic Ratio*

  Seismic ratio (H_q) is the ratio of the distance S_q to the height of the slice Z_q , or

$$H_q = \frac{S_q}{Z_q} \tag{192}$$

  where

  S_q = the distance between the elevation of the point of application, Y_q, of the seismic force and the elevation of the shear surface, Y_f ($S_q = Y_q - Y_f$),
  Z_q = the distance between the elevation of the groundline surface, Y_s, and the Elevation of the shear surface ($Z_q = Y_s - Y_f$).

  Seismic loading is executed in the program by inserting values of the S***eismic Coefficient*** and ***Seismic Ratio***. By specifying a value of S***eismic Ratio*** (HQ), the user may locate the earthquake forces at any position of the slices. However, the earthquake forces are generally located at the midpoints of the slices; a value of 0.5 is usually inserted for the ***Seismic Ratio***.

- *Number of Slices*

  The maximum number of slices that may be specified by the user is 598. If the user fails to specify a number of slices, then the computer program assumes a value of 76. When the user specifies the number of slices, the specified value **MUST** be an **EVEN** integer. The computer program divides each trial mass into the number of slices specified by the user. It

is recommended that no fewer slices than 76 be used. It is good practice to check a given problem using different slices to determine the effect of the number of slices on the solution.

- *Tension Crack*

In cases where embankments are constructed on soft clay foundations, stresses in the upper reaches of the potential failure mass may be tensile. A problem arises in the design of embankments of soft foundations because it is uncertain as to what portions of the shear strength of the embankment is mobilized and may be relied on for stability. Uncertainties arise in the stability analysis because of differences in the stress-strain behaviors of the embankment and soft foundations soils. Embankments normally will be constructed of compacted soils that will be stiff and overconsolidated. The peak strength of the compacted embankment soils occurs at a relatively small strain. At this stage, only a small portion of the shear strength of the foundation soils may be mobilized. This situation leads to the development of tensile stresses in the upper zone of the embankment. Since soils cannot sustain tensile stresses, at least for a prolonged period of time, a tension crack may develop in the embankment. If the embankment cracks, a smaller portion of the shear strength of the embankment may contribute to overall stability. Therefore, the use of the peak strength of the embankment in the stability analysis may be under conservative if the embankment is prone to crack. Assuming no shear strength of the embankment soils may be over conservative since overturning moments are too large. For this later case, the safety factor is too low.

Two options are available for performing stability problems involving potential tension cracks. If the depth of tension crack is known, or estimated, then the user can input the tension crack depth.

In the second option, the user may allow the computer program to obtain a compatible value of tension crack and factor of safety. As shown elsewhere (Lambe, 1969; Chowdhury, 1978), the depth of tension crack may be expressed as (in terms of effective stress)

$$z = \left[\frac{2c'}{\gamma_t(1-\gamma_t)}\right]\left[\left(\frac{1+\sin\phi'}{1-\sin\phi'}\right)^{\frac{1}{2}}\right] \qquad \textbf{(193)}$$

where

z = depth of tension crack;
c' = effective stress parameter, cohesion;
γ_t = total unit weight;
r_u= pore pressure ratio; and
N' = effective stress parameter, angle of internal friction.

Equation 193 allows the maximum depth of the tension crack to be computed at failure (F=1.0) in terms of effective stress or total stress. However, for cases other than failure, that is, when the factor of safety of safety is greater than one, the tension crack depth may be computed using the mobilized strength parameters: N_f = tanN/F and c_f = c'/F. Substituting the mobilized strength parameters into equation 193, the depth of the tension crack may be expressed as

$$z = \left[\frac{2c_f'}{\gamma_t(1-\gamma_t)}\right]\left[\left(\frac{1+\sin\phi_f'}{1-\sin\phi_f'}\right)^{\frac{1}{2}}\right]. \quad (194)$$

According to Equation 194, the depth of the tension crack is a function of F, ($_{t,}$ c_f, r_u, and N_f. However, the factor of safety, and therefore, the mobilized depth of tension crack are unknown (except for the case of failure when F = 1.0). To solve this problem when the factor of safety is greater than one and for a given shear surface, that is, to obtain the depth of the crack compatible with the factor of safety, iteration may be performed using Equation 194. The iteration is performed on Z and F and ($_t$, c_f, r_u, and N_f are constant.

To start the iteration, an initial factor of safety must be assumed. A reasonable initial estimate of the factor safety (F_0) may be obtained by solving the problem assuming no tension crack. Substituting F_0 into Equation 194 and solving yields the first estimate of the depth of tension crack (Z_0). Using Z_0, a new value of the safety factor (F), is computed. The iteration is continued until

$$\left|Z_n - Z_{n-1}\right| < \varepsilon, \quad (195)$$

where ε = a selected numerical error. The numerical value of ε in the computer is 0.001. A detailed treatment of the tension crack problem, as used in the computer program, is given elsewhere (Hopkins, 1986) and is beyond the scope of this report. This tension crack scheme was not included in this version of the program. It will be included in future versions.

- *Tension Crack Depth Filled with Water*
  This value is the depth of water in the tension crack. In the program, this horizontal force is automatically computed and is treated as a boundary force.

Ground Line

The method used in the computer program to describe the geometry of a slope, bearing capacity problem, or wall and the arrangement of the soil types comprising the stability problem is illustrated below. The computer program can solve only two-dimensional problems. All geometry of a slope or bearing medium is defined by x- and y- coordinates and line segments. Customarily, the slope, or wall, faces to the right. However, they may face in either direction. The x-coordinate direction must be horizontal and, normally, increases positively from left to right. However, negative x-coordinates may be used. The y-coordinate direction is vertical and normally increases positively from bottom to top. However, negative y-coordinates may be used. Conventionally, the origin of the coordinate system is located to the left and below the slope.

Straight-line segments are used to approximate the entire cross section. This applies to the ground line surface, layer boundary interfaces, water table surface or piezometric lines, shear surface, and thrust lines. The line segments are defined by x- and y-coordinates. The uppermost line segments in the cross section are identified in the computer program as the ground line surface. Access to a graphical user interfaces for entering ground-line coordinates is executed by clicking the button

identified as "Ground Line" in Figure 28. The GUI shown in figure 29 appears. The menu appearing on the right-hand side of Figure 29 appears on each major GUI screen. The icon situated to the right of the menu in Figure 29 appears when a particular GUI screen is opened. This icon lets the user know which current screen is open. The icon on the left side of the menu lets the user know that data has been entered for a particular parameter. The x- and y-coordinates of the ground line are entered on this screen. As shown in this figure, when the button labeled "Add Row" is clicked new boxes appear for entering additional x- and y-coordinates. The user may also insert a row by clicking the button "Insert Row" or a row may be deleted by clicking "Delete Row." Those buttons facilitate the editing of data entries. As ground line and boundary line x-and y-coordinates are entered, a graphical view of the entered geometry appears in the lower left-hand corner of Figure 29.

Soil Property

Shear strength of each soil layer is defined in terms of the Mohr-Coulomb-Terzaghi strength criterion,

$$\tau = c' + (\sigma - u)\tan\phi$$

where c' = cohesion of the soil,
N' = angle of internal friction,F = total normal stress acting on the shear surface , and
u = pore water pressure acting on the shear surface.

When the strength of a particular layer is expressed in terms of total stress parameters, the values of N and c are total stress shear strength parameters. Pore pressures within the particular layers are specified as zero. The values, c', N,' (, and u, used for each slice are values applied at the midpoint

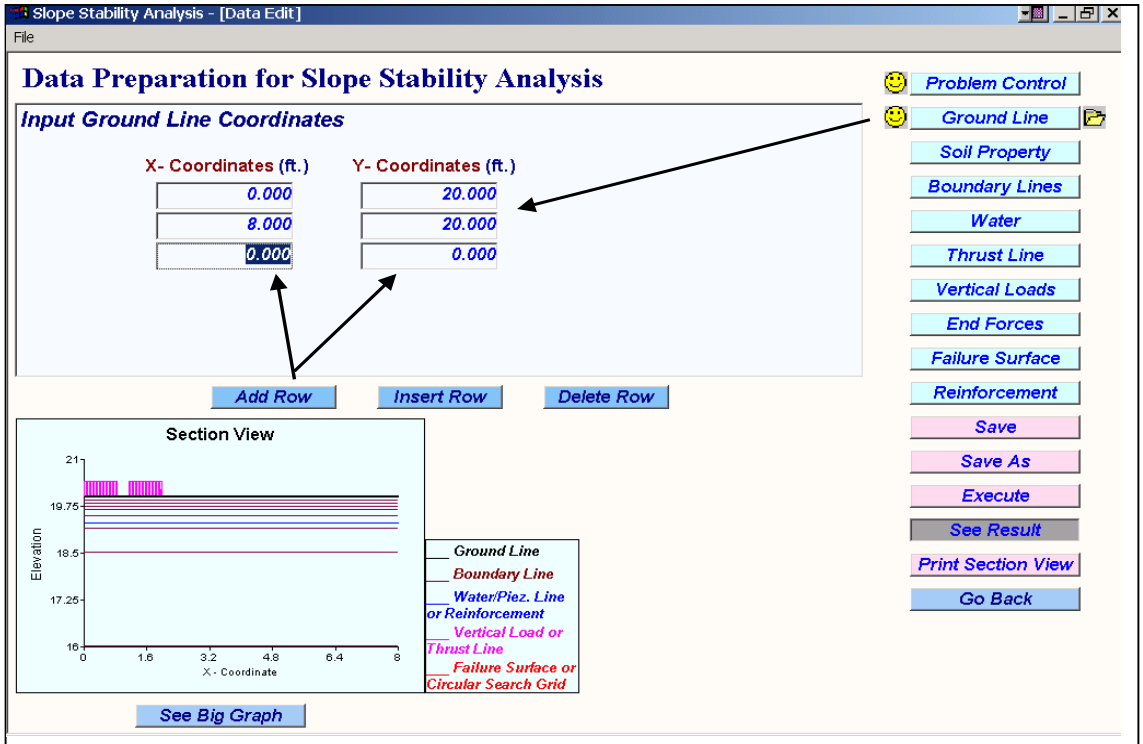

Figure 29. GUI for entering x- and y- ground-line coordinates.

of the base of each slice. If an effective stress analysis is specified, values of c' and N' are effective stress strength parameters and an appropriate method of representing the pore pressures is selected as described below.

Properties of each layer of soil are entered on the GUI screen shown in Figure 30. This GUI screen appears when the button labeled "Soil Property" is clicked. Properties are as follows:

- *Layer (Number)*
  The soil layer number increases with depth. In the example in Figure 30 (See also Figure 5), the topmost layer is number 1 while the bottom most layer is 8.

- *Cohesion*
  Cohesion is the effective or total stress parameter; c' of each soil layer or the undrained shear strength parameter, S_u.

- *Friction Angle*
  Effective or total stress parameter, angle of internal friction, N,' of each soil layer.

- *Unit Weight*
  Total unit weight of each soil layer, (;

- *Pore Pressure Factor*
  Pore pressures must be described for all soils in which the effective stress parameters, N' and c,' are used to obtain the effective normal stress acting at the bases of slices. Pore pressure problems, according to Bishop and Bjerrum (1969) may be divided into two main classes:

  CLASS 1. Pore pressure is an independent variable controlled by the magnitude of the stresses acting in the soil or tending to lead to instability. Problems of this type may involve the rapid construction in or excavation of low-permeability soils.

  CLASS 2. Pore pressure is an independent variable and does not depend on the magnitude of the total stresses acting on the soil. In this case, pore pressures are controlled by the groundwater level or by the flow pattern of the groundwater.

There are four methods, or options, in the computer program that handle the two classes of problems. Clicking inside the box (for any layer) labeled "Pore Pressure Type" opens a drop down box, as shown in Figure 30. The user has four choices, or options. These are

- By Pore Pressure Ratio (<1.0),
- By a Piezometric Line,
- By an a Infinitely Sloping Groundwater,
- By Assuming the Groundwater.

In the computer program, each soil type or layer may have only one value of r_u. When Method 1 is used to define the pore pressures in a given layer, the value of r_u must be some real number less than 1.0. This value is entered directly on the "Soil Properties" GUI screen, Figure 31. These methods are described as follows:

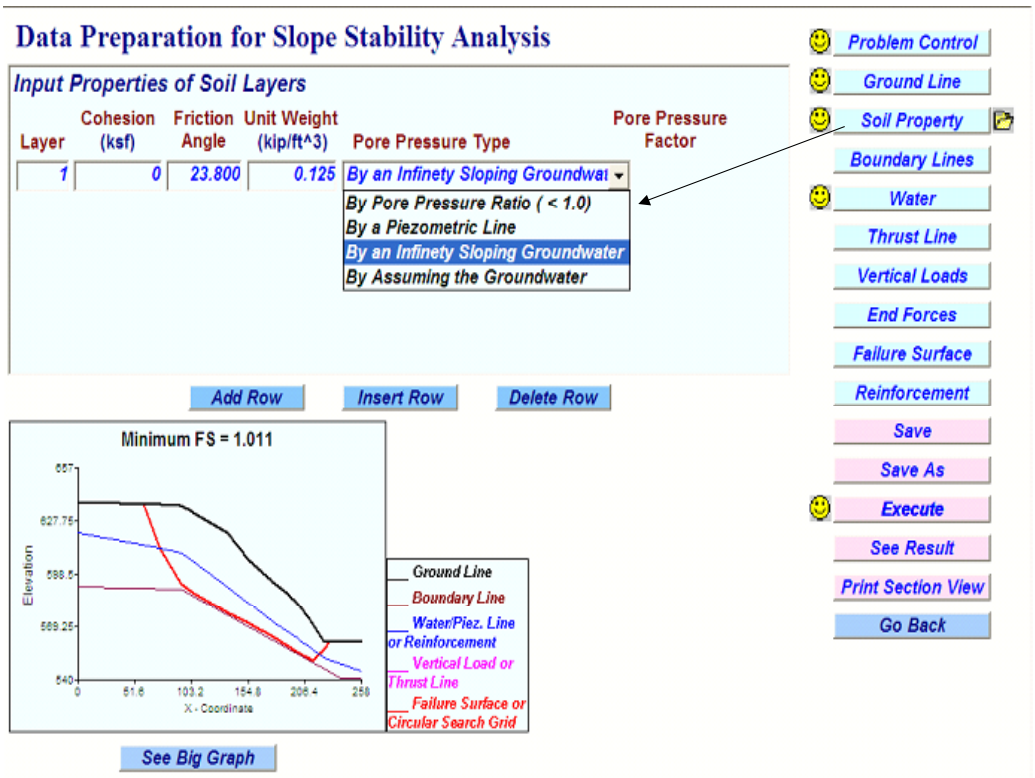

Figure 30. Data entry for defining cohesion, the friction angle, unit weight, and types of pore pressures in each soil layer.

Option 1.

Pore pressure in a given soil layer may be defined by a pore pressure ratio, r_u. This dimensionless parameter is the ratio of the pore pressure, u, to the vertical stress, F_v, of soil above the element considered, or

$$r_u = \frac{u}{\sigma_v} = \frac{u}{\gamma_t h_s} \tag{196}$$

where ($_t$ = total unit weight of soil above the element and
h_s = height of soil above the element.

The r_u ratio was first used by Daehn and Hilt (1951) as a means of expressing the results of the stability analysis of four earth dams. Bishop (1955) showed that, for both classes of problems, the pore-pressure ratio, the relationship between the factor of safety and r_u is almost linear. Later work, by Bishop and Morgenstern (1960) showed that both classes of problems, the pore pressure ratio is a very consistent means of expressing the influence of pore pressure on stability.

For Class 1 problems, the r_u ratio is obtained either from field measurements of pore pressures or estimates from triaxial tests and consolidation theory as described by Bishop and Bjerrum (1969) and

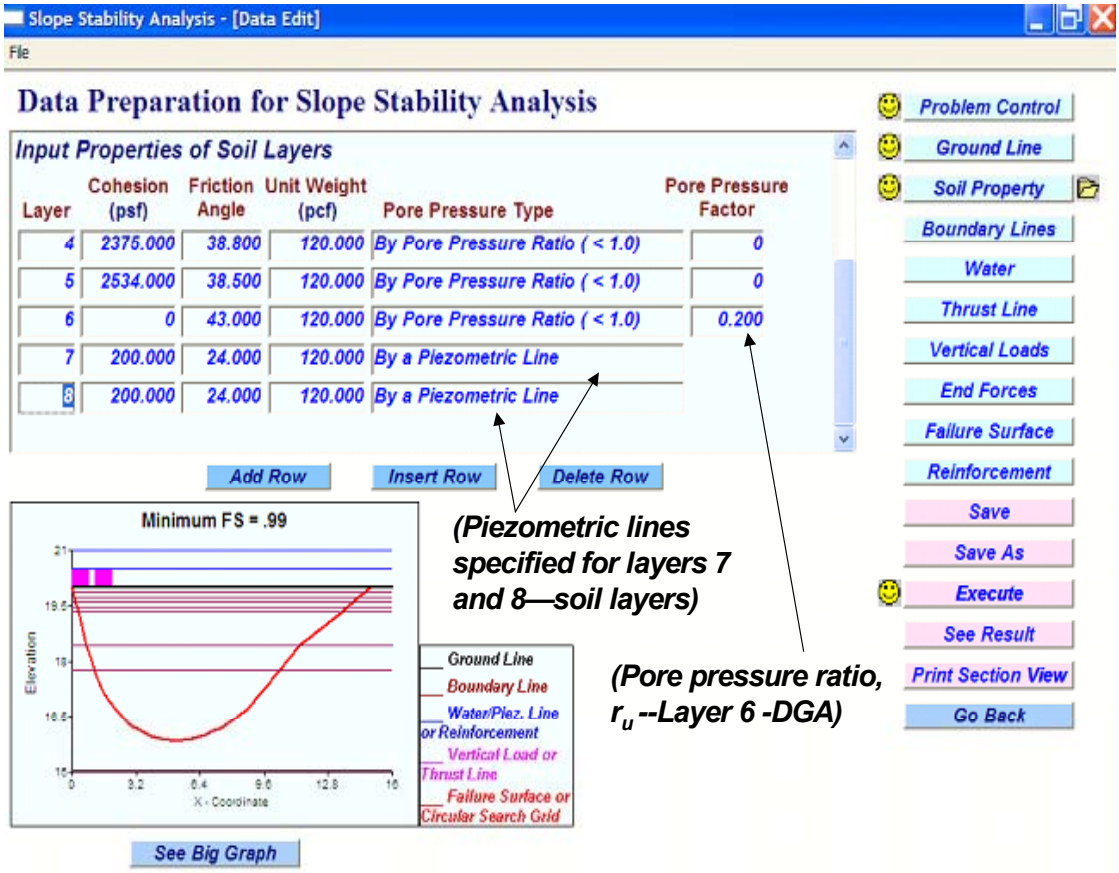

Figure 31. Data entry for defining cohesion, the friction angle, unit weight, and type of pore pressure in each soil layer.

Bishop and Henkel (1957). In the latter case, an estimate of the stress distribution within the soil must be made. In Class 2 problems, the r_u value is obtained from a flow net; it is expressed as an average value. Bishop and Morgenstern (1960) have given details of this technique.

Option 2.

Pore pressure in a given layer may be defined by piezometric lines. This method is convenient to use when piezometers are used to obtain pore pressures. However, both Class 1 and 2 problems maybe solved using this method. Pore pressures are obtained as described in Method 1. Each soil layer may have only one piezometric line. Straight-line segments and x- and y-coordinates approximate each piezometric level. See Figure 5 and associated discussion.

When the trial shear surface passes through a soil layer where the pore pressures are defined by piezometric coordinates, the pore pressure foe each slice of the unstable mass is calculated by multiplying the vertical distance between the shear surface of the slice and the appropriate piezometric line by the unit weight of water. The pore pressure (u_i) at the base of slice i is equal to the vertical distance (h_w) times the unit weight of water (($_w$), or

$$u_i = \gamma_w h_w. \tag{197}$$

Both Options 1 and 2 may be intermixed. For example, pore pressures in one soil layer may be defined by a r_u-value while pore pressures in another layer may be defined using x- and y-coordinates

Option 3.
Pore pressures may be defined using an infinitely sloping groundwater table or phreatic surface. In this option, the groundwater level is approximated by x- and y-coordinates defining straight- line segments. Pore pressure (u_i), at the base of each slice, is computed from

$$u_i = h_p \gamma_w = h_i \gamma_w \cos^2 j \tag{198}$$

where h_p = pressure head;
γ_w = unit weight of water;
j = gradient, or angle between a horizontal line and the groundwater line, and
h_i = vertical distance between the surface of the ground-water table and the shear surface.

Pore pressures for the flow net may be computed using Option 3. This method applies to class 2 problems where pore pressures are independent of the magnitude of the total stresses acting in the soil. To execute this option, it is only necessary to click the button, "By an Infinitely Sloping Groundwater," of the first soil layer. All other values of r_u are left blank, or set equal to zero. The coordinates of the water table are entered under the button labeled "Water." When Option 3 is used, Options 1 and 2 cannot be used.

Option 4.
Pore pressures may be defined by assuming or specifying a groundwater table. This method primarily applies to Class 2 problems. This method is executed by clicking on the button labeled "By Assuming the Groundwater" of the first soil layer. The groundwater table is described by x- and y-coordinates defining straight-line segments. All other values of r_u are left blank, or set equal to zero. Pore pressures (u_i) acting at a point on the base of each slice are computed from the equation

$$u_i = h_i \gamma_w \tag{199}$$

where h_i = vertical head of water between the base of slice and groundwater table at the center of the slice. When option 4 is used, options 1 and 2 cannot be used.

Figure 31 illustrates using a mix of Options 1 and 2. A pore pressure ratio of 0.20 was specified for layer 6, which is the dense graded aggregate base (DGA) of the flexible pavement. Material of this type may have sufficient fine materials to cause a buildup of pore pressure under large wheel loadings. In layers 7 and 8–soil layers—piezometric lines were used to define the pore pressures in those layers. Effective stress parameters were used to define the shear strength in layers 6, 7, and 8. The factor of safety for this particular problem was 0.99 or failure.

Boundary Lines

After the shear strength parameters, unit weight, and the pore pressure types have been entered for each layer, the x- and y- coordinates of the boundary lines, or the layer interfaces, are entered as

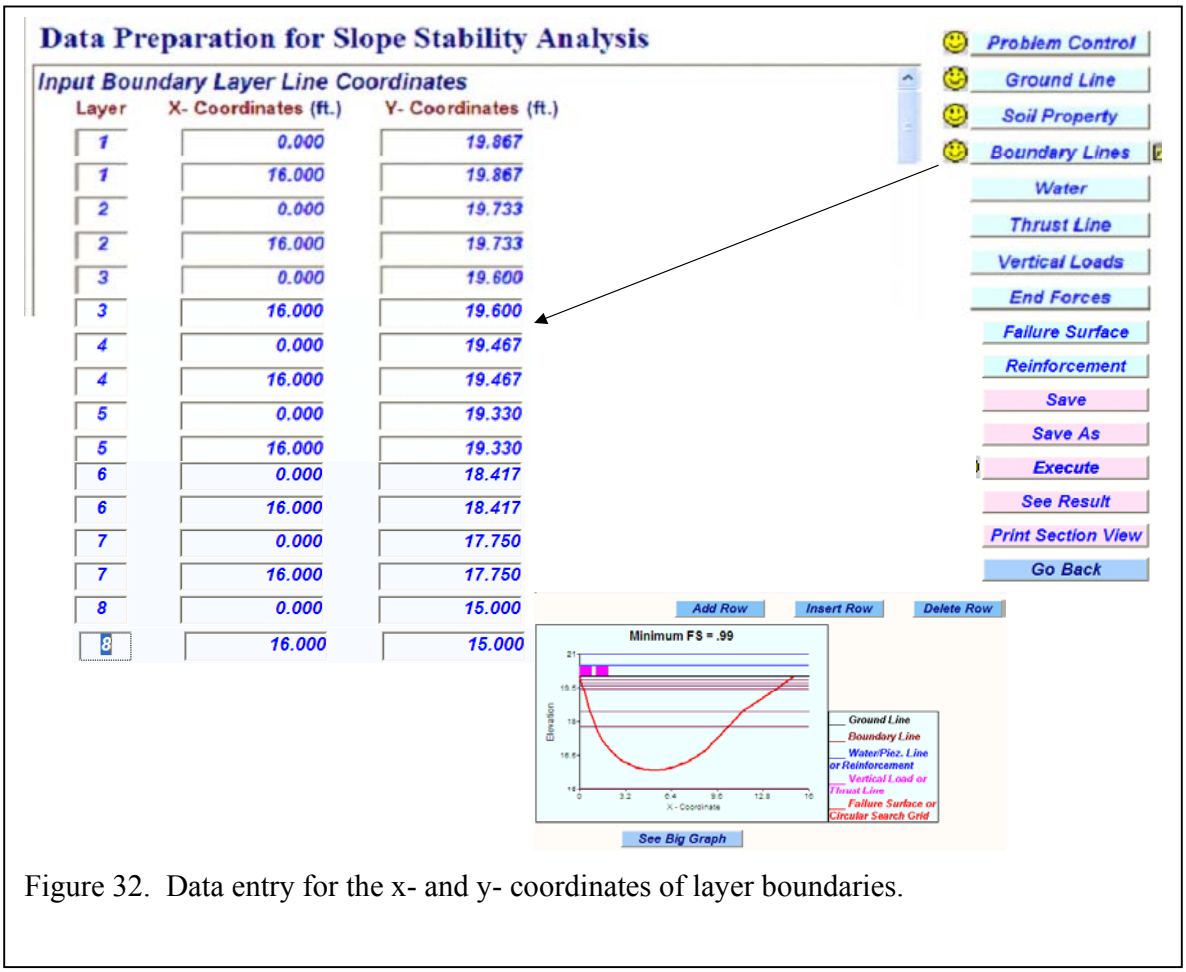

Figure 32. Data entry for the x- and y- coordinates of layer boundaries.

shown in Figure 32. The ground line segments and all layer line segments must be horizontal for bearing capacity problems. However, in all other stability problems this condition does not apply. In all stability problems, the starting x-coordinates of the ground line, all interfaces, groundwater table, all piezometric coordinates, and thrust line must be equal. Also, the ending x-coordinates of those lines must be equal. As x- and y- coordinates of the ground line, layer interfaces, thrust line (when specified manually), groundwater table, or piezometric lines, and external point and distributed loads are entered, a graph of the points is created as shown in the bottom left of each GUI screen. By creating the graph as the user enters geometric data entry errors are viewed and immediately can be corrected. If the user needs to view a larger plot of the cross section, then the button labeled "See Big Graph" is clicked. All geometric data is exhibited in a large view. To return to the main menu, the user clicks the button "Go Back."

Water

As shown by the example in Figure 31, the user specified piezometric coordinates as a means of defining the pore pressures in layers 7 and 8. To enter the x- and y- coordinates of the piezometric lines, the button labeled "Water" is clicked and the GUI screen shown in Figure 33 appears. The x- and y-coordinates of the piezometric lines are entered in the appropriate boxes created by clicking the button "Add Row." Other editing buttons include "Insert Row" and Delete Row."

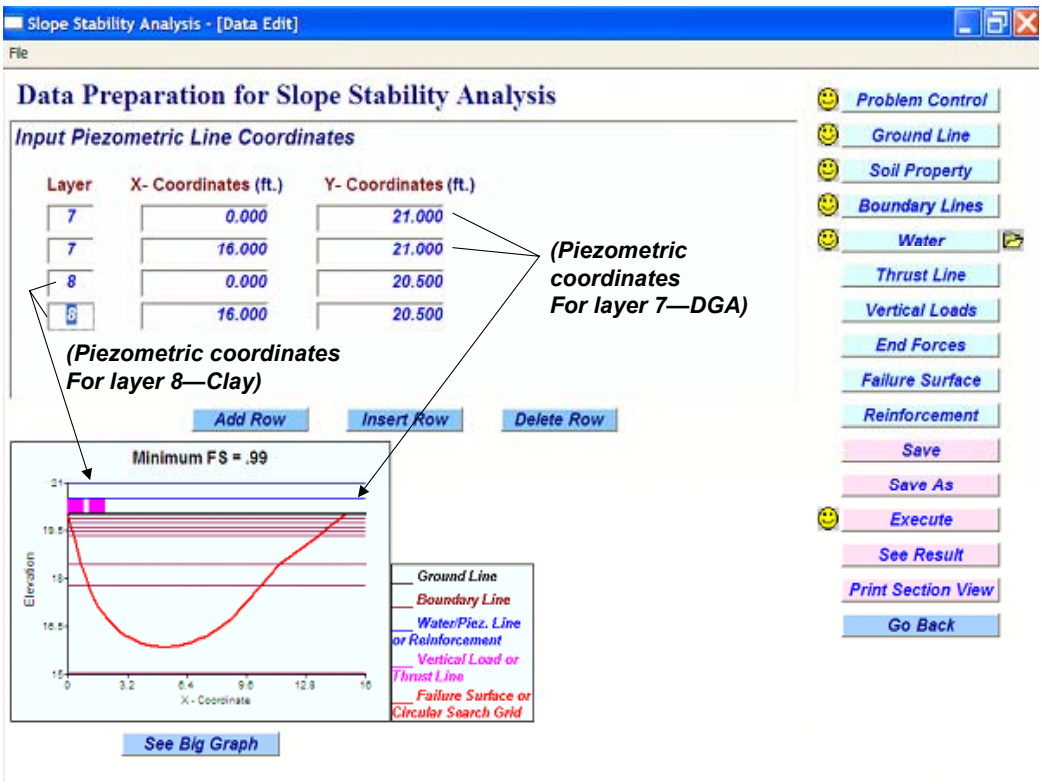

Figure 33. Entering x-and y-coordinates of piezometric coordinates.

Thrust Line

When the user selects "Compute" in the dropdown box identified as "Thrust Line" in the Problem Control GUI screen (Figure 28) the computer program automatically computes the locations of the interslice forces, or the x- and y-coordinates of the trust line. To activate this case, a value of thrust ratio (usually 0.33) must be entered, as shown in Figure 28. However, if "By Input" is selected then the user must enter all x- and y- thrust line coordinates for all slices. The x-and y-coordinates of the interslice force locations are entered in the GUI screen shown in figure 34.

Vertical Loads

Vertical Loads are entered as shown in Figure 35. The tire stress used in this example was 100 psi. Dual wheel tires were assumed in the example. Because the unit weight of water used in the example was specified as 62.4 lb/ft^3 length measurements are in feet. The external vertical tire stress is converted to an external distributed load, or

$$q_{yi}\Delta x = \frac{100lb}{in^2}\Delta x\ ft\left(\frac{144in^2}{ft^2}\right) = \frac{14,400lb}{ft}. \qquad (200)$$

where q_{yi} is equal to the distributed vertical external forces (psi). In the computer program, the loads are assumed constant between two consequent x-coordinates, x_i and x_{i+1} and equal to q_{yi}. The

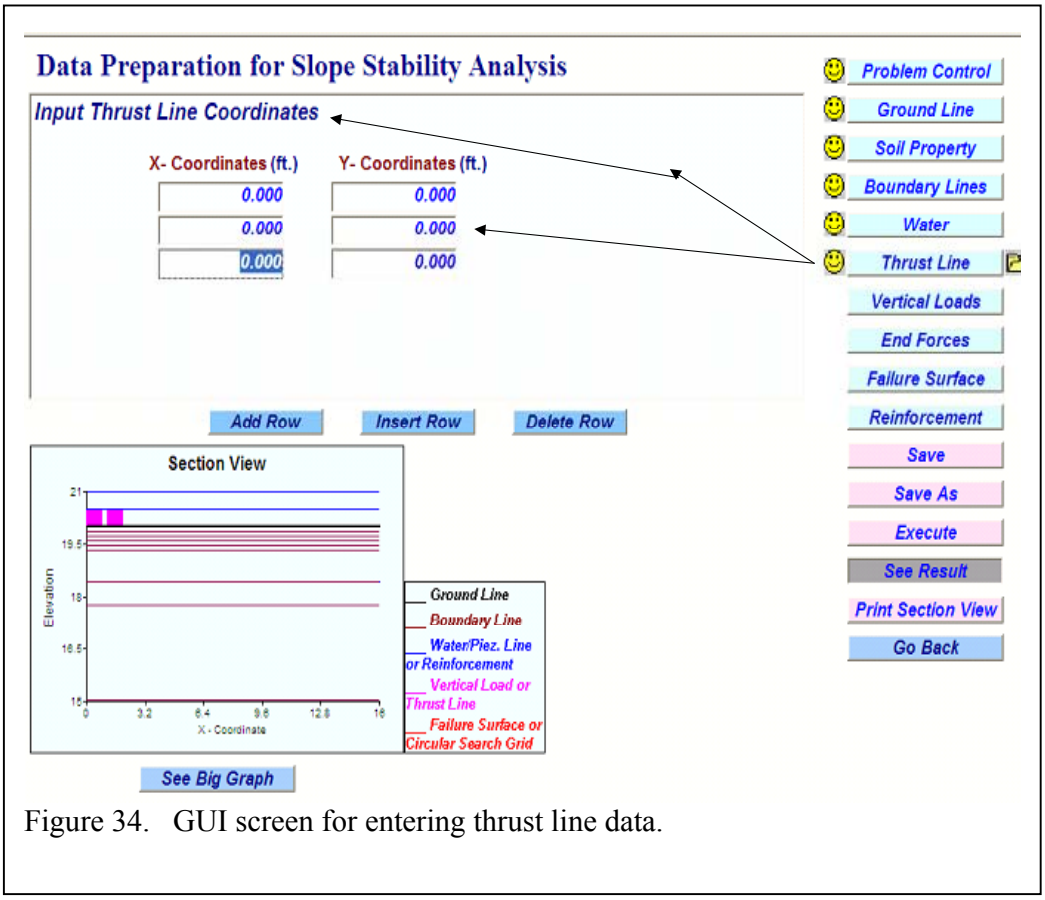

Figure 34. GUI screen for entering thrust line data.

sequence of entering the x-and q-coordinates, for this example, is illustrated in Figure 35 and in a graphical display of the coordinates in Figure 36. Also, the reader is referred to Figures 10 and 11 and the associated discussion. As shown in this example, the factor of safety (without reinforcement) is 1.137. A graphical display of the coordinates is shown in Figure 36.

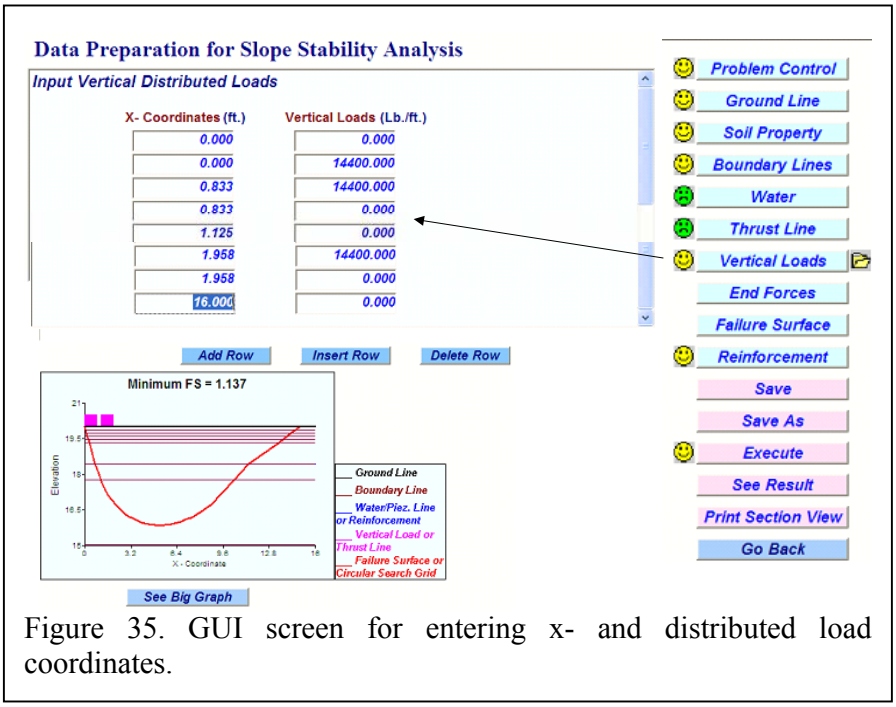

Figure 35. GUI screen for entering x- and distributed load coordinates.

End Boundary Loads

This data entry screen is obtained by clicking "End Forces" on the main menu. End boundary forces are illustrated in Figure 37. These forces, designated as E_a, E_b, T_a,

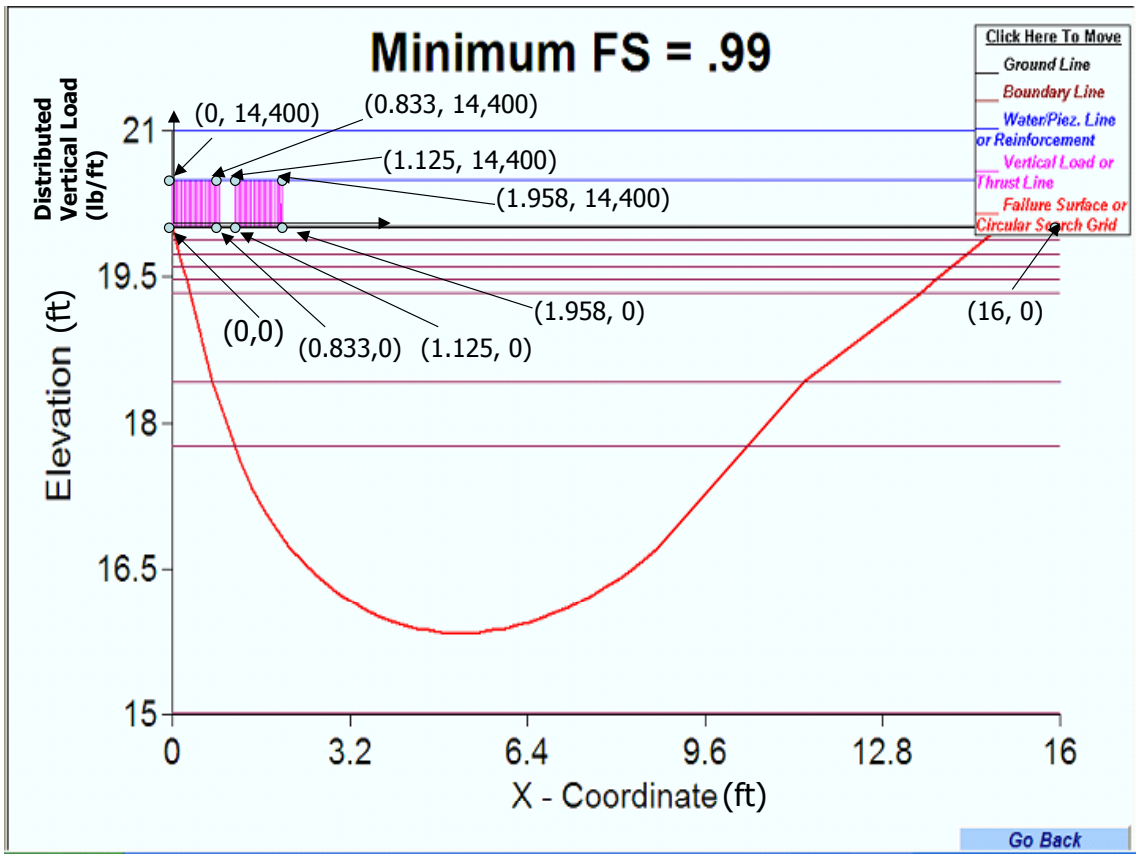

Figure 36. View of enlarged cross section and coordinates of external distributed load.

and T_b. E_a and T_a are the horizontal and vertical forces, respectively, acting on the boundary of the uphill side of the potentially unstable soil mass. E_b and T_b are the horizontal and vertical forces, respectively, acting on the boundary of the downhill side of the potentially unstable soil mass.

An example of an end boundary load would be the hydrostatic force exerted by a body of water resting against the slope or the hydrostatic thrust (E_a) exerted by a water-filled crack located at the top of the slope. In this case, the depth of tension crack is fixed and the height of water in the tension crack may entered be as shown in the "Problem Control" screen, Figure 28. In that example, the tension crack depth of 3.6 ft was specified by the user and it was completely filled with water. When this data (special case) is entered in Figure 28, the program automatically calculates the end boundary force due to water in the crack. Alternately, the end boundary forces may be entered manually in the GUI screen in Figure 38. The factor of safety obtained from the Perturbation Method for the example shown was 1.639.

Failure Surface

Search Grid-Predetermined Trial Centers

When the type of failure surface on the "Problem Control Screen" is clicked "Circular" the user must specify a grid for centers of trial shear surfaces (see Figures 39 and 40). The grid is rectangular in shape. The rectangular grid is specified by two coordinate points, as shown in Figure 40. The x-and y-coordinates, XSTART and YSTART, of the upper left-hand corner of the grid and the x-and y-

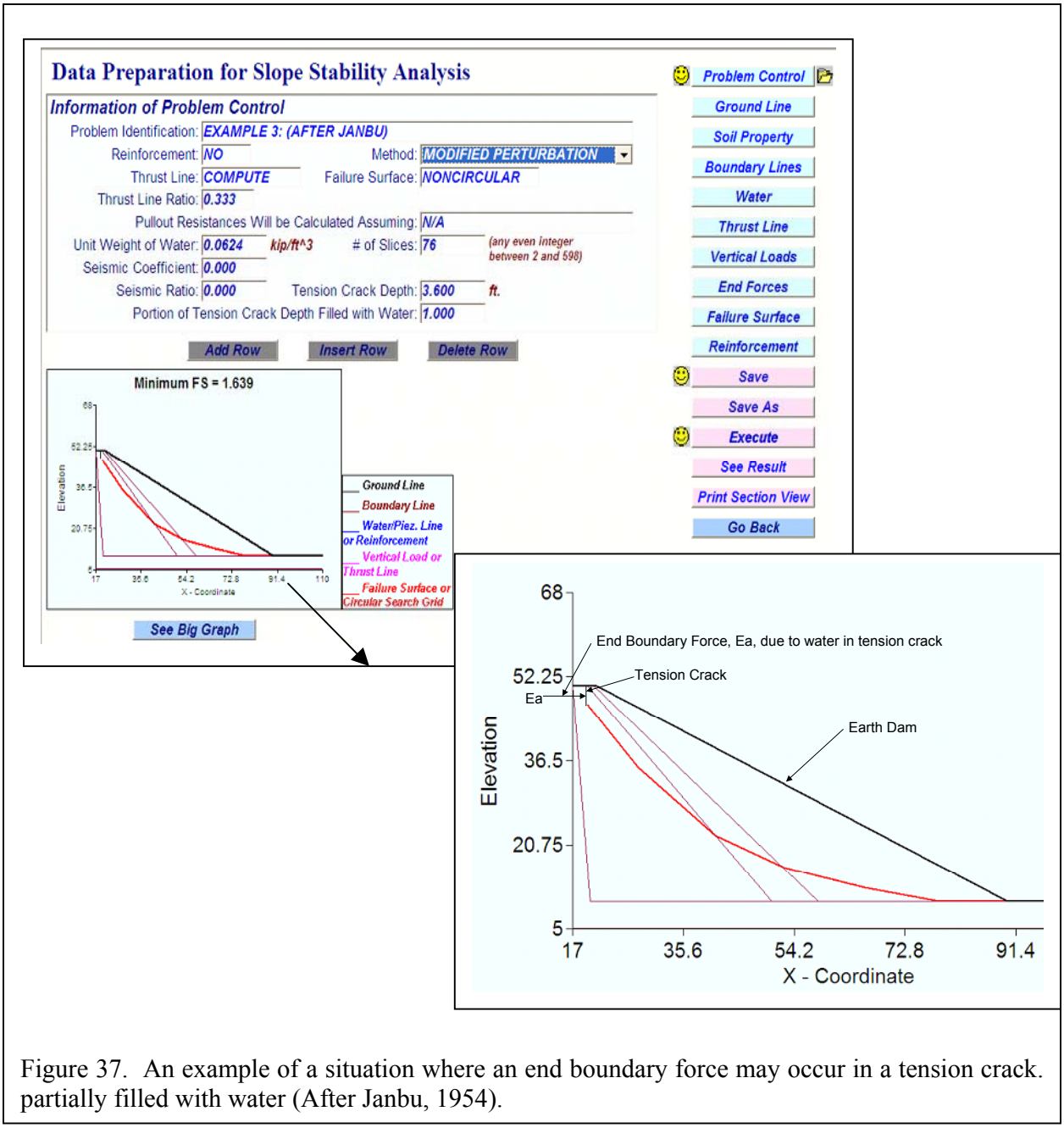

Figure 37. An example of a situation where an end boundary force may occur in a tension crack. partially filled with water (After Janbu, 1954).

coordinates, XFIN AND YFIN, of the lower right-hand corner of the grid must be specified. To establish the number of trial centers of the grid in the horizontal direction each increment, the user must specify the width, XDEL, of each increment. The value selected for the increment, XDEL, must be such that

$$\frac{XFIN - XSTART}{XFIN} = m \ (int\,eger\,value). \tag{201}$$

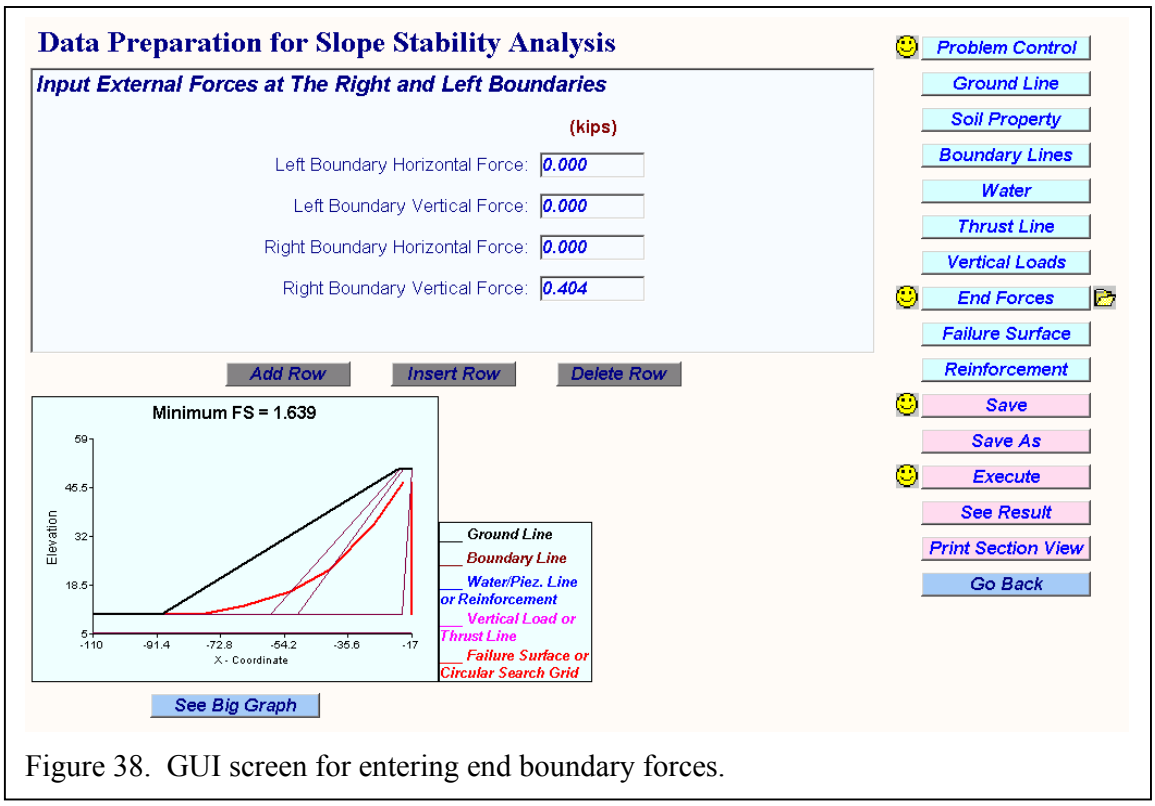

Figure 38. GUI screen for entering end boundary forces.

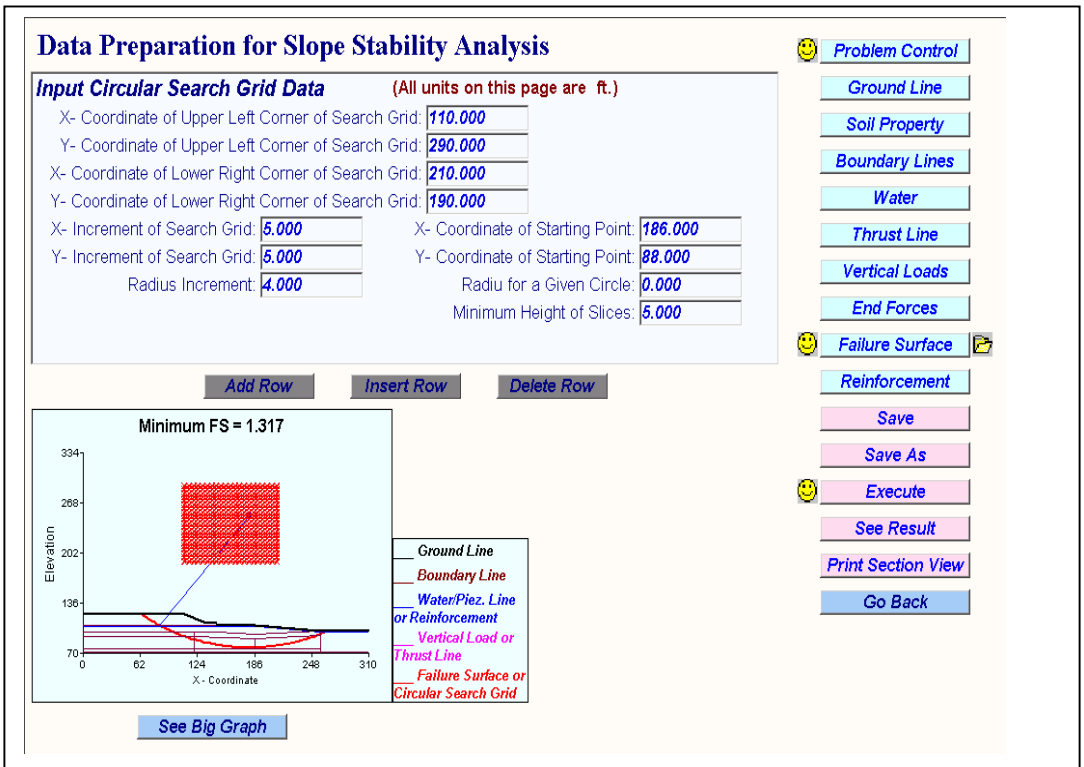

Figure 39. Data input required in performing a circular search analysis using a grid of trial centers (example after Bailey and Christian, 1969).

The number of trial centers of the grid in the vertical direction is established by specifying the width, YDEL, of each increment. The value selected for YDEL must be such that

$$\frac{YSTART - YFIN}{YDEL} = n \ (int egervalue). \tag{202}$$

The grid of trial centers, as specified above, may be reduced to a single point by setting

$$XSTART = XFIN \ and \ YSTART = XFIN.$$

Generation of trial centers starts from the top, left-hand corner (XSTART, YSTART) of the grid and proceeds to the right in the x-direction until

$$XSTART + (m-1)XDEL = XFIN. \tag{203}$$

The integer m is defined by Equation 201. After generating the top row of the trial centers and solving for the factors of safety, the program selects the trial centers for the next lower row. Each time a row of trial centers is computed, the program starts at XSTART and moves downward an amount YDEL. This operation proceeds until

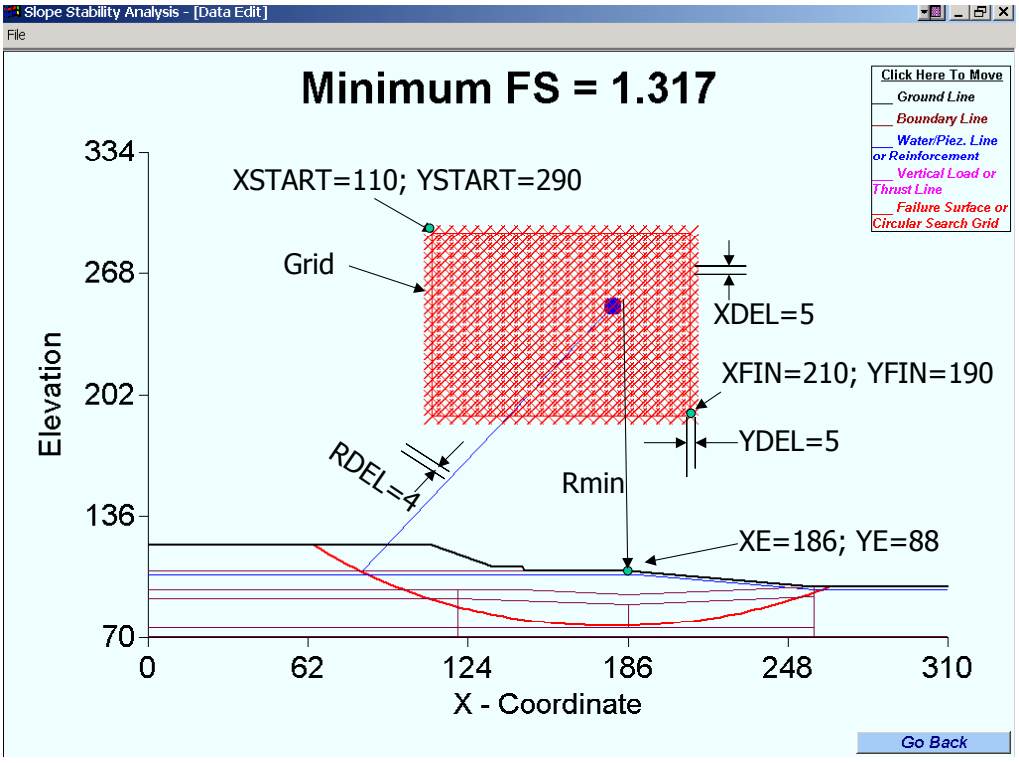

Figure 40. Parameters for defining search grid and trial circles.

$$YSTART - (n-1) * YDEL = YFIN, \quad (204)$$

where n is defined by Equation 202.

When Equation 204 is satisfied, all trial centers (and safety factors) have been solved. For each trial center, the computer program stores the minimum factor of safety and later prints these factors of safety in the form of a grid of minimum factors of safety. However, factors of safety for all trial circles as well as other geometric data are printed. Additionally, the program selects and prints the minimum factor of safety of all trial circles obtained from the search-grid operation.

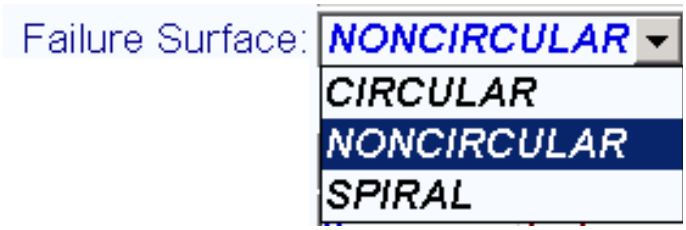

Figure 41. Specifiying a noncircular shear surface using the dropdown box on the Problem Control screen.

The radius of each trial shear surface is generated by specifying the length of the radius increment, RDEL:

$$RO = RMIN + RDEL \quad (205)$$

where RO= radius at the trial center,

RMIN = the initial radius, and
RDEL = the radius increment.

If XDEL, YDEL, and RDEL remain blank, then the default values for each of those increments is 5.0.

Initial Radius Coordinates and Analysis of Individual Shear Surfaces

To establish an initial radius, RMIN, at a given center, the user must specify a point on the cross section by the coordinates XE and YE, as shown in Figure 41. The initial radius, RMIN, at each trial center is computed as the distance from the center of the circle and the specified point. Additional radii are generated from Equation xx. When circular shear surfaces are generated, the starting coordinate point XED, YE must never be placed above the ground line. By placing the starting radius coordinated point below the ground line, the user can control the depth of shear surfaces and avoid the analysis of shallow shear surfaces.

The radius RMIN at trial center is incremented until a trial center intersects the bottom layer boundary. When this occurs, the computer program determines a circle (and corresponding radius) that is tangent to the bottom layer boundary. After computing the factor of safety for the tangent circle, the computer program proceeds to the next trial center of the grid. The minimum factor of safety at each trial center is determined and stored.

If the factor of safety of a single circle is required, then only values of XSTART, YSTART, and RO (the value of the known radius) need be supplied. Values of XFIN, YFIN, XDEL YDEL, RDEL, and XE and YE are not needed.

There is a special opportunity in the computer program for analyzing retaining walls. In this case, in performing a search analysis, the user need not supply the x-coordinate of an initial point but

rather XE is input as zero. The computer program calculates XE as an x-coordinate of a point of intersection of a vertical wall face and a horizontal line, y=YE.

Noncircular Failure Shear Surface

The user may specify a noncircular shear surface by clicking "NONCIRCULAR" in the drop down box (Figure 42) under "Failure Surface" in the Problem Control Screen Figure 28. When this shear surface is specified, the user must supply x-and y-coordinates of the individual shear surface in the screen shown in Figure 42. To access this screen, the "Failure Surface" on the main menu in Figure 28 is clicked. Although the -type surface is noncircular, the user does not have to supply x-and y-coordinates in this specific case because the program automatically generates the coordinates.

In performing bearing capacity analysis, a Prandtl-type shear surface is recommended. A full discussion of this type of shear surface was fully described in the report section entitled, "Shear Surface Used in Bearing Capacity Analysis." Figure 14 illustrated the shape of the this shear surface for a one-layered problem while Figures 16 and 17 illustrated the shear surface for a multilayered bearing media. This type of "shear is obtained when "SPIRAL" is clicked in the dropdown box in Figure 27 under "Failure Surface." The x-and y-coordinates of this type of shear surface are automatically generated by the computer. However, the user must define the left-hand and right-hand x- and y-coordinates of the "active Zone", as illustrated in Figure 43.

Reinforcement Geometry and Strength Properties

When tensile reinforcing elements are involved in the stability problem and the user answered "YES" in the box labelled "Reinforcement" in the "Problem Control Screen," information regarding the

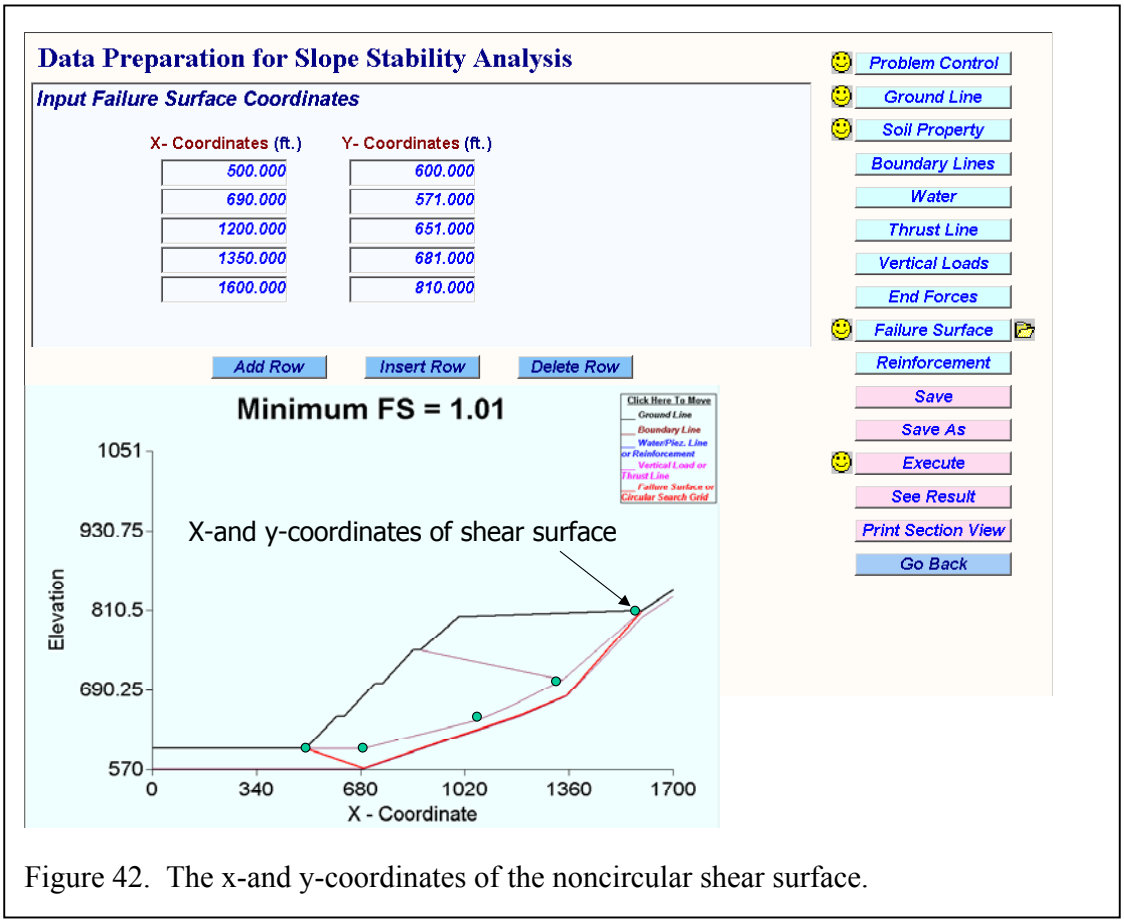

Figure 42. The x-and y-coordinates of the noncircular shear surface.

tensile element must be supplied. This information is supplied on a screen that appears when the button labelled "Reinforcement" on the menu in the right-hand side of the "Problem control Screen" is clicked. The screen is shown in Figure 44. The length, end point (x-coordinate at the end of the layer), elevation, the interaction coefficients (see at the top and bottom tensile element reinforcement sheet are entered as shown in the figure. Any number of reinforcement sheets and properties may be entered using the "Add Row" or "Insert Row." Any row of data may be deleted using the "Delete Row" command. In the example shown in the Figure 44, the initial factor of safety without reinforcement was 1.15. Assuming a strength of 1350 lb/ft and interaction coefficients of 0.9 and placing the reinforcement layer at 2 inches from the bottom of the base aggregate, the factor of safety increases to 1.25. This is based on the assumption, of course, that sufficient strain has occurred in the reinforcement layer to mobilize a strength of 1350 lbs/ft. The soil-fabric interaction coefficients for soils above and below the reinforcement sheet are the coefficients k_1 and k_2 in Equations 150 and 151.

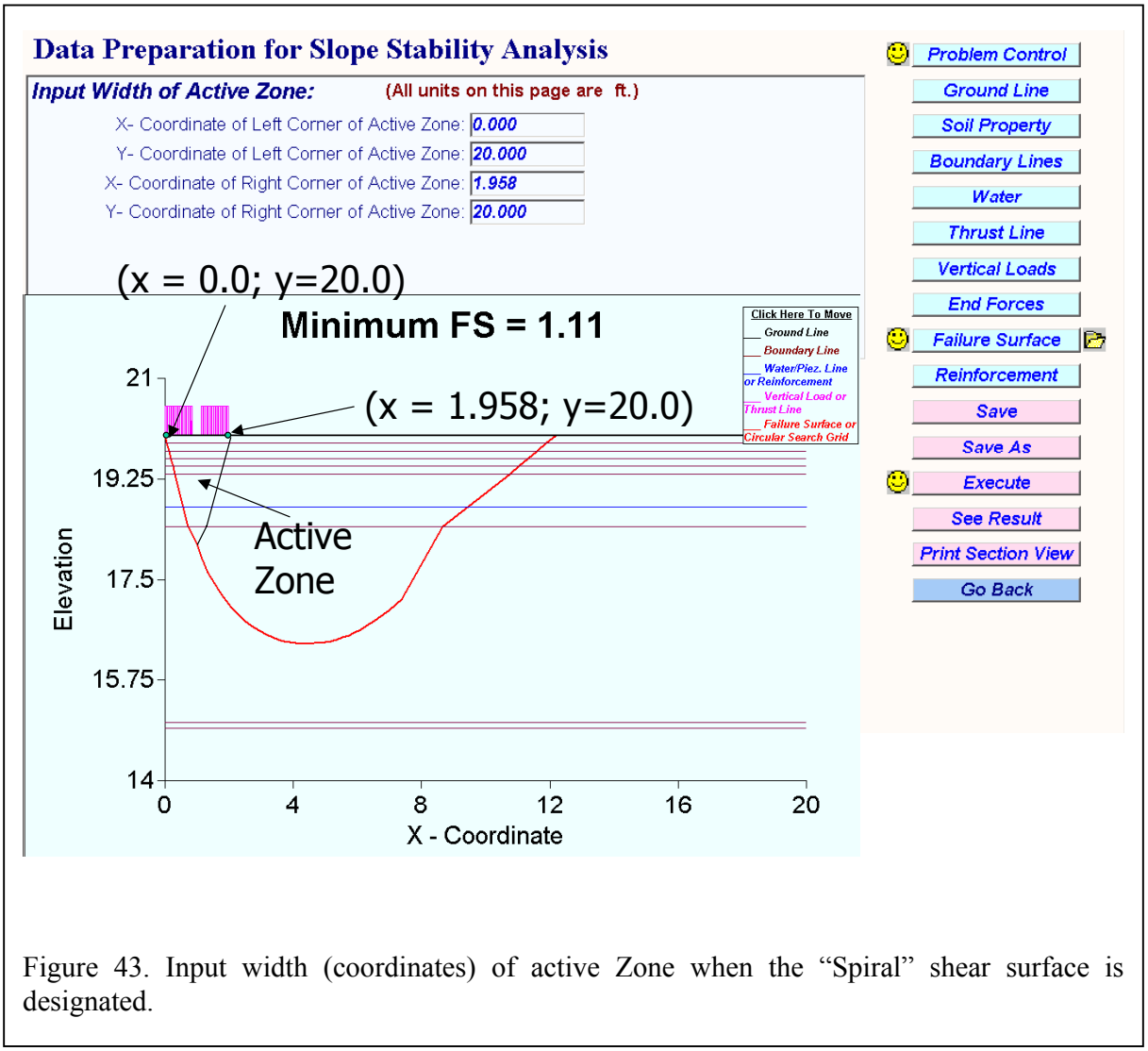

Figure 43. Input width (coordinates) of active Zone when the "Spiral" shear surface is designated.

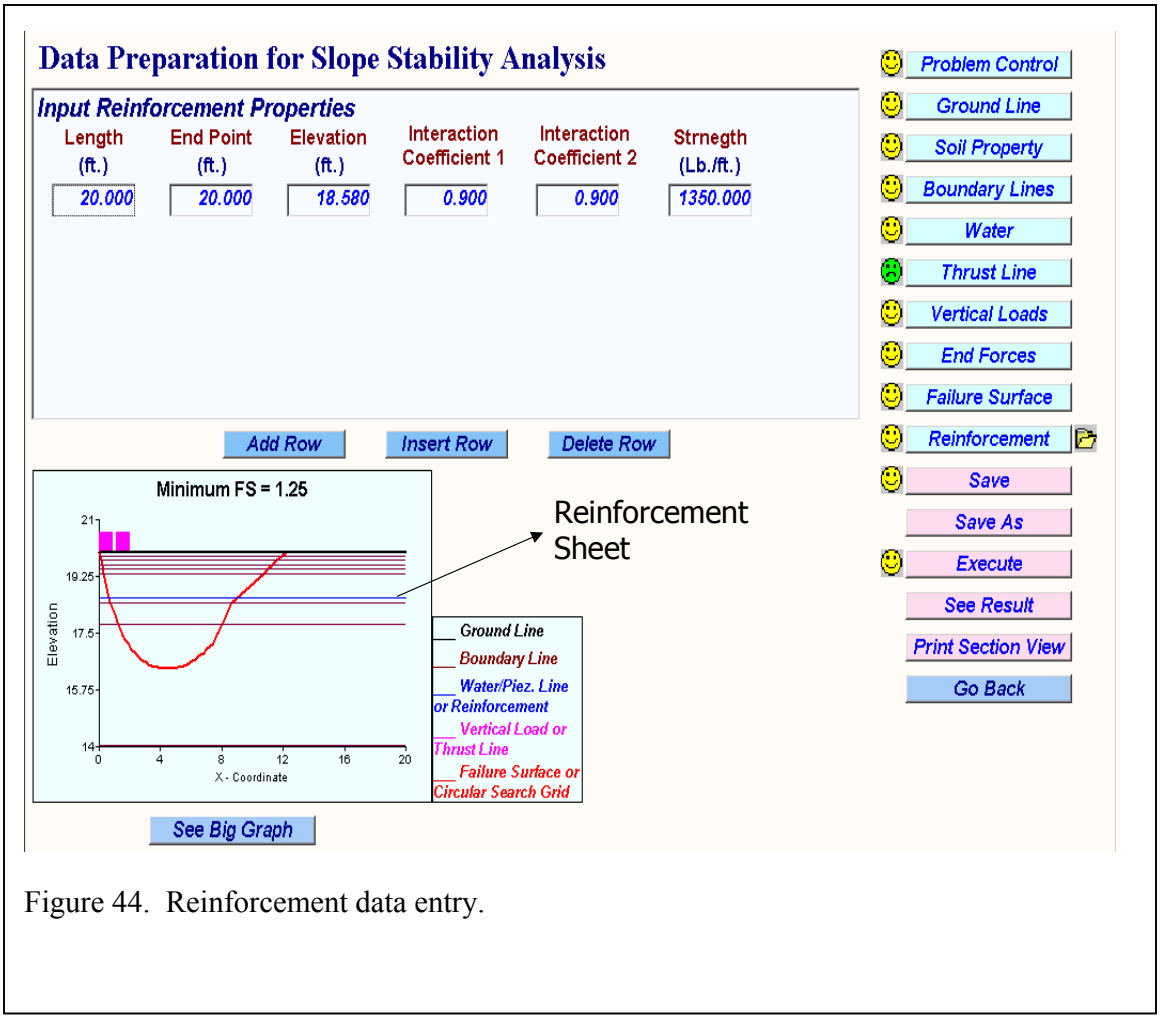

Figure 44. Reinforcement data entry.

Printout of Results

As shown on the main menu on the right-hand portion of each screen (Figure 28 for example) the user can "Save," "Save As," "Execute" (the problem), "See Result," "Print Section View," and "Go Back" (to previous screen). The printout includes problem control data such as the type of analysis, the method used, coordinates of the ground line, number of slices used, and etc, as shown in Figure 45. Example output pertaining to each layer is illustrated in Figure 46. In Figure 47, example output data includes the thrust ratio ($(\eta = 0.33)$ used in the analysis, the x-coordinates of external vertical distributed loads (for an 80 psi tire contact stress—dual wheels), end boundary forces, and x- and y-coordinates of the Prandtl-type shear surface (see Figures 13-15 and 16 and 17). Cross section data computed according to number of slices entered is illustrated in Figure 48. Output example showing computed values of pullout resistance in the active and passive zones is illustrated in Figure 49. In this output, the pullout resistant forces are compared to the input strength of the fabric. The input strength of the fabric is compared to the pullout resistant forces; the force selected for calculations satisfies Equation 147. The output also includes the number of iterations required for convergence of the factor of safety, the value of the factor of safety (for a noncircular analysis), as shown in Figure 50, and a check of the factor of safety to determine if it satisfies determine if horizontal, vertical, and moment equilibriums are satisfied.

When the user specifies a grid of safety factors (for circular analyses—see Figures 39 and 40) a printout is obtained as shown in Figure 51. The grid printout contains the minimum factor of safety at each specified trial center. The program searches automatically the factors of safety at trial circle coordinates and printout out the minimum value of factor of safety. Finally, all factors of safety generated at each trial circle center are searched; the minimum value of factor of safety is determined and printed.

```
        GENERALIZED SLOPE STABILITY ANALYSIS


Stability of Flexible Pavement

DATE   6/ 8/2005


-----------------------------------------------------------------
               PROBLEM CONTROL DATA


TYPE OF ANALYSIS - REINFORCED

FREE REINFORCEMENT END  WAS SPECIFIED

LIMITING EQUILIBRIUM METHOD USED - MODIFIED PERTURBATION

THRUST LINE - BY CALCULATION

TYPE OF FAILURE SURFACE - SPIRAL

UNIT WEIGHT OF WATER   =   62.4000   (FORCE /CUBIC LENGTH)
     UNITS OF ALL INPUT-OUTPUT DATA IN THE STABILITY ANALYSIS
     PROGRAM ARE THOSE IMPLIED BY THE NUMERICAL VALUE USED
     FOR THE UNIT WEIGHT OF THE PORE WATER

NUMBER OF SLICES       =598

MAX. NO. OF ITERATIONS = 15

NUMBER OF SLICES FOR
COMPUTING PULLOUT
RESISTANCE             = 10


-----------------------------------------------------------------
           COORDINATES OF GROUND LINE

                X             Y

              0.000        20.000
             20.000        20.000

-----------------------------------------------------------------
```

Figure 45. View of problem control data and ground line coordinates output.

```
-------------------------------------------------------------
          LAYER NUMBER                1
          COHESION,                1234.00000
          PHI (DEGREES)              42.20000
          UNIT WEIGHT,              100.00000
          RU FACTOR                   0.00000

          TOTAL STRESS ANALYSIS USED IN THIS LAYER
          NO PORE PRESSURES COMPUTED

          COORDINATES OF LAYER BOUNDARY LINE

               X             Y

               0.000        19.867
              20.000        19.867

        -----------------------------------------------------
          LAYER NUMBER                2
          COHESION,                1574.00000
          PHI (DEGREES)              41.00000
          UNIT WEIGHT,              120.00000
          RU FACTOR                   0.00000

          TOTAL STRESS ANALYSIS USED IN THIS LAYER
          NO PORE PRESSURES COMPUTED

          COORDINATES OF LAYER BOUNDARY LINE

               X             Y

               0.000        19.733
              20.000        19.733

        -----------------------------------------------------
```

Figure 46. Example output showing properties of layers and coordinates of boundary line.

```
          -----------------------------------------------------
            THRUST LINE PARAMETER USED---ETA=  0.333


                 X-COORDINATES AND VALUES
              OF EXTERNAL VERTICAL DISTRIBUTED LOADS

                       0.000     0.000
                       0.000 11520.000
                       0.833 11520.000
                       0.833     0.000
                       1.125     0.000
                       1.125 11520.000
                       1.958 11520.000
                       1.958     0.000
                      20.000     0.000

        -------------------------------------------------------------
                       END BOUNDARY FORCES

            LEFT  BOUNDARY HORIZONTAL FORCE =      0.00
            RIGHT BOUNDARY HORIZONTAL FORCE =      0.00
            LEFT  BOUNDARY VERTICAL   FORCE =      0.00
            RIGHT BOUNDARY VERTICAL   FORCE =      0.00

        -------------------------------------------------------------
              COORDINATES OF SPIRAL FAILURE SURFACE

                       X             Y

                       0.000        20.000
                       0.059        19.867
                       0.120        19.733
                       0.182        19.600
                       0.246        19.467
                       0.312        19.330
                       0.709        18.417
                       0.979        18.147
                       1.167        17.843
                       1.355        17.608
                       1.543        17.414
                       1.731
```

Figure 47. Example output of values of external vertical distributed loads, end boundary forces, and coordinates of log spiral shear surface.

TOTAL HORIZONTAL END BOUNDARY FORCES

LEFT END: - 0.000
RIGHT END: - 0.000

CROSS SECTION DATA
WIDTH OF SLICES = 0.020

SLICE NO.	SLICE LAYER	REINF FORCE	SLICE HEIGHT AT SLICE CENTER	WEIGHT OF SLICE	EXTERNAL VERTICAL LOAD ON TOP OF SLICE	PORE PRESS	X-COORD AT SLICE CENTER	Y-COORD OF GRDLINE AT SLICE CENTER	Y-COORD OF FAILURE SURFACE AT SLICE CENTER
1	1	0.00	0.02	0.05	234.74	0.00	0.01	20.00	19.98
2	1	0.00	0.07	0.14	234.74	0.00	0.03	20.00	19.93
3	1	0.00	0.11	0.23	234.74	0.00	0.05	20.00	19.89
4	2	0.00	0.16	0.34	234.74	0.00	0.07	20.00	19.84
5	2	0.00	0.20	0.45	234.74	0.00	0.09	20.00	19.80
6	2	0.00	0.25	0.56	234.74	0.00	0.11	20.00	19.75
7	3	0.00	0.29	0.66	234.74	0.00	0.13	20.00	19.71
8	3	0.00	0.34	0.77	234.74	0.00	0.15	20.00	19.66
9	3	0.00	0.38	0.88	234.74	0.00	0.17	20.00	19.62
10	4	0.00	0.42	0.98	234.74	0.00	0.19	20.00	19.58
11	4	0.00	0.47	1.09	234.74	0.00	0.21	20.00	19.53
[illegible]	4	0.00	0.51	1.19	234.74	0.00	[illegible]	20.00	19.4[illegible]
[illegible]	[illegible]	0.00	0.55	1.29	234.74	[illegible]	[illegible]	[illegible]	[illegible]
[illegible]	[illegible]	[illegible]	0.59	[illegible]	[illegible]	[illegible]	[illegible]	[illegible]	[illegible]

SLICE NO.	X-COORD AT SLICE SIDE	Y-COORD OF GRDLINE AT SLICE SIDE	Y-COORD OF FAILURE SURFACE AT SLICE SIDE	SLICE HEIGHT AT SLICE SIDE	TANGENT OF FAILURE SURFACE ANGLE
1	0.000	20.000	20.000	0.000	-2.257
2	0.020	20.000	19.954	0.046	-2.257
3	0.041	20.000	19.908	0.092	-2.250
4	0.061	20.000	19.862	0.138	-2.194
5	0.082	20.000	19.817	0.183	-2.194
6	0.102	20.000	19.773	0.227	-2.188
7	0.122	20.000	19.728	0.272	-2.140
[illegible]	0.143	20.000	19.685	0.315	-2.140
[illegible]	0.163	20.000	19.64[illegible]	[illegible]	[illegible]
[illegible]	0.183	20.000	[illegible]	[illegible]	[illegible]

Figure 48. Example output of cross section data.

```
Slice number:           30
Slice number:           31
Slice number:           32
Delta X =   6.3807815E-02,  XA =   0.0000000E+00,  XB =   0.6380782
Accumulated reinf. force on slice:            1   1251.794
Accumulated reinf. force on slice:            2   2503.588
Accumulated reinf. force on slice:            3   3755.382
Accumulated reinf. force on slice:            4   5007.175
Accumulated reinf. force on slice:            5   6258.969
Accumulated reinf. force on slice:            6   7510.763
Accumulated reinf. force on slice:            7   8762.557
Accumulated reinf. force on slice:            8   10014.35
Accumulated reinf. force on slice:            9   11266.14
Accumulated reinf. force on slice:           10   12517.94
Pull out Force before consider free/fix:    12517.94
Delta X =    1.936192    ,  XA =   0.6380782    ,  XB =    20.00000
Accumulated reinf. force on slice:            1   37984.59
Accumulated reinf. force on slice:            2   38529.73
Accumulated reinf. force on slice:            3   39074.88
Accumulated reinf. force on slice:            4   39620.03
Accumulated reinf. force on slice:            5   40165.18
Accumulated reinf. force on slice:            6   40710.33
Accumulated reinf. force on slice:            7   41255.48
Accumulated reinf. force on slice:            8   41800.63
Accumulated reinf. force on slice:            9   42345.77
Accumulated reinf. force on slice:           10   42890.92
Pull out Force after  consider free/fix:    42890.92
Reinf. force on slice:    1350.000
Slice number:           33
Slice number:           34
```

Figure 49. Output example showing computed values of pullout resistance in the active and passive zones.

```
 ITERATION   FACTOR OF SAFETY

    1           1.098
    2           1.101
    3           1.101


          FACTORS OF SAFETY DERIVED FROM

  HORIZONTAL EQUILIBRIUM -  1.101
  VERTICAL   EQUILIBRIUM -  1.101
  MOMENT     EQUILIBRIUM -  1.101


-----------------------------------------------------------------------

          FACTOR OF SAFETY IN NONCIRCULAR ANALYSIS:

                      F =      1.101

***********************************************************************
END OF PROGRAM
```

Figure 50. Output example showing the number of iterations required for convergence of the factor of safety, a check of the horizontal, vertical, and moment equilibrium, and final factor of safety.

TRIAL CIRCLE CENTER GRID SYSTEM
COORDINATES NOT TO SCALE
MINIMUM SAFETY FACTOR AT EACH GRID POINT

	110.0	115.0	120.0	125.0	130.0	135.0	140.0	145.0	150.0	155.0	160.0	165.0	170.0	175.0	180.0	185.0	190.0	195.0	200.0	205.0	210.0
290.0	*	*	*	2.04	1.85	1.83	1.73	1.63	1.62	1.57	1.55	1.45	1.38	1.37	1.37	1.41	1.47	1.51	1.61	1.67	1.74
285.0	*	*	*	2.03	1.85	1.82	1.72	1.62	1.61	1.56	1.56	1.45	1.38	1.36	1.37	1.41	1.44	1.51	1.61	1.66	1.74
280.0	*	*	*	2.01	1.84	1.81	1.74	1.62	1.61	1.56	1.53	1.47	1.38	1.35	1.37	1.38	1.43	1.51	1.57	1.63	1.71
275.0	*	*	*	2.01	1.84	1.79	1.74	1.61	1.56	1.55	1.52	1.47	1.37	1.35	1.34	1.38	1.43	1.51	1.57	1.62	1.71
270.0	*	*	*	1.99	1.83	1.76	1.74	1.62	1.55	1.55	1.52	1.46	1.37	1.34	1.34	1.38	1.40	1.48	1.57	1.61	1.67
265.0	*	*	*	1.91	1.82	1.75	1.74	1.61	1.55	1.55	1.52	1.46	1.37	1.34	1.34	1.35	1.40	1.48	1.53	1.61	1.67
260.0	*	*	1.99	1.89	1.78	1.75	1.74	1.60	1.55	1.55	1.50	1.46	1.37	1.33	1.33	1.35	1.40	1.47	1.53	1.58	1.65
255.0	*	*	1.95	1.92	1.83	1.74	1.74	1.60	1.56	1.55	1.50	1.46	1.37	1.34	1.33	1.35	1.38	1.45	1.53	1.58	1.66
250.0	*	*	1.95	1.89	1.84	1.75	1.74	1.60	1.57	1.52	1.51	1.47	1.37	1.34	1.32	1.33	1.38	1.45	1.52	1.58	1.62
245.0	*	*	1.97	1.85	1.82	1.74	1.69	1.63	1.56	1.51	1.51	1.45	1.37	1.34	1.32	1.33	1.38	1.45	1.50	1.56	1.64
240.0	*	*	1.91	1.86	1.81	1.74	1.69	1.65	1.56	1.51	1.52	1.45	1.36	1.34	1.32	1.32	1.36	1.42	1.50	1.54	1.65
235.0	*	*	1.91	1.86	1.81	1.70	1.69	1.67	1.55	1.51	1.52	1.46	1.37	1.35	1.33	1.33	1.37	1.43	1.47	1.55	1.67
230.0	*	2.04	1.91	1.85	1.81	1.70	1.69	1.67	1.51	1.51	1.52	1.47	1.37	1.35	1.33	1.32	1.35	1.43	1.47	1.54	1.64
225.0	*	1.98	1.92	1.85	1.81	1.76	1.68	1.63	1.51	1.51	1.48	1.49	1.34	1.36	1.34	1.33	1.36	1.41	1.48	1.51	1.65
220.0	*	1.99	1.93	1.85	1.80	1.77	1.67	1.62	1.52	1.52	1.47	1.50	1.36	1.36	1.35	1.34	1.35	1.42	1.45	1.52	1.67
215.0	*	*	1.95	1.87	1.77	1.74	1.62	1.62	1.52	1.51	1.48	1.50	1.37	1.37	1.36	1.36	1.36	1.40	1.46	1.51	1.65
210.0	*	*	1.94	1.88	1.77	1.74	1.63	1.62	1.59	1.48	1.49	1.51	1.40	1.36	1.37	1.37	1.36	1.41	1.43	1.53	1.61
205.0	*	*	1.94	1.88	1.75	1.73	1.63	1.63	1.61	1.49	1.50	1.48	1.43	1.37	1.39	1.39	1.38	1.40	1.45	1.57	1.59
200.0	*	*	1.95	1.90	1.82	1.69	1.66	1.58	1.60	1.50	1.50	1.50	1.46	1.39	1.37	1.41	1.39	1.38	1.45	1.54	1.59
195.0	*	*	*	1.87	1.82	1.69	1.69	1.59	1.59	1.51	1.52	1.51	1.47	1.41	1.41	1.41	1.38	1.39	1.44	1.56	1.55
190.0	*	*	*	1.89	1.83	1.69	1.69	1.60	1.60	1.51	1.49	1.54	1.50	1.44	1.43	1.44	1.42	1.40	1.46	1.54	1.52

MINIMUM SAFETY FACTOR FROM GRID SEARCH = 1.317
X-COORDINATE OF CRITICAL CIRCLE, XO = 180.000
Y-COORDINATE OF CRITICAL CIRCLE, YO = 250.000
RADIUS OF CRITICAL CIRCLE, RO = 174.111

Figure 51. Example output for grid search (circular analysis).

REASONABLENESS OF SOLUTIONS

Creditability and reasonableness of results obtained from the Hopkins and Slepak-Hopkins models and the newly developed software were established by solving and comparing solutions from the proposed bearing capacity model to solutions from other theoretical, or empirical, mathematical models for different classes of bearing capacity problems. The classes of problems are as follows:

- a homogeneous layer of bearing medium,
- a bearing medium composed of two different layers of material, and
- a multilayered, bearing medium -- case studies.

Bearing capacity solutions of the various classes of selected bearing capacity problems are discussed as follows.

Homogeneous Bearing Medium

As one approach to establishing the reasonableness of solutions obtained from the Hopkins and Slepak models, classical bearing capacity factors, which historically have been used for several decades by geotechnical and structural engineers to design structural footers resting on a soil foundation, are compared to bearing capacity factors obtained from the Slepak-Hopkins and Hopkins models. Basically, the classical bearing capacity factors, N_c, Nq, and $N_($ were obtained using the Slepak-Hopkins limit equilibrium model. Formerly, the factors had been derived using the Hopkins limit equilibrium model. Those factors have been compared to classical bearing capacity factors in a previous publication (Hopkins 1986). Since the factors of safety obtained from the Hopkins model are within "3 percent of the factors of safety obtained from the Slepak-Hopkins model, the comparisons are not repeated here. In deriving the factors, iteration is used until a factor of safety equal to 1.00 is obtained. The assumed shear surface used in the iteration is a type (non-circular) as depicted in the Figures 13 through 17. Detailed discussions of the comparisons of classical bearing capacity factors and bearing capacity factors derived from the Slepak-Hopkins model are presented below.

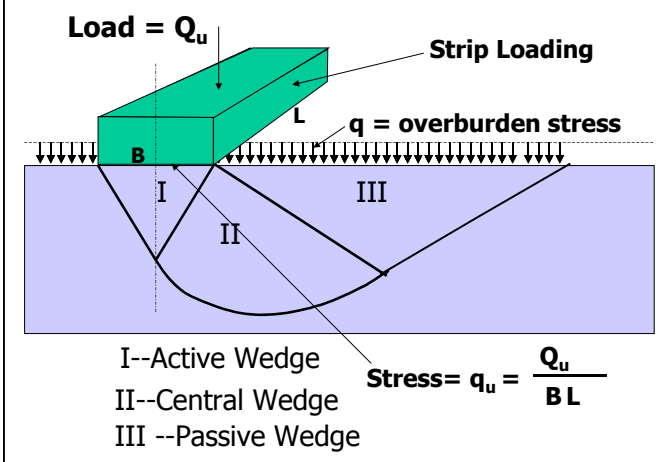

Figure 52. Bearing capacity of a shallow footer.

Classical Bearing Capacity Equations and Factors

Although a closed analytical solution has not been found for determining the maximum unit load, q_u, that a foundation can support, Prandtl (1921) and Reissner (1924 -- Vesic', c.f. Winterhorn and Fang), using methods of the Theory of Plasticity, found that for weightless soils (γ = o):

$$q_u = \frac{Q_u}{BL} = cN_c + qN_q \tag{206}$$

where (see Figure 52)

q_u = ultimate stress which the footing can withstand without failure,
Q_u = ultimate load which the footing can withstand without failure,
B = width of footing,
L = length of footing,
γ = unit weight of the bearing medium,
c = cohesion,
D = depth of footing below the surface,
q= uniformly distributed surcharge due to the overburden stress = γ.D, and
N_c, Nq = dimensionless bearing capacity factors.

From solutions provided by Prandtl (1921) and Reissner (1924),

$$N_q = e^{\pi \tan\phi} \tan^2\left(\frac{\pi}{4} + \frac{\phi}{2}\right) \tag{207}$$

and

$$N_c = (N_q - 1)\cot\phi. \tag{208}$$

According to Vesic' (c.f. Winterhorn and Fang 1975), it can be shown that for a cohesionless soil (c = o; q = o):

$$q_u = \frac{1}{2}\gamma B N_\gamma \tag{209}$$

where N_γ is a dimensionless bearing capacity factor that must be evaluated numerically (see Caquot and Kerisel, 1953). Also, Vesic' presents an analytical expression,

$$N\gamma \approx 2(N_q + 1)\tan\phi \tag{210}$$

for approximating this bearing capacity factor.

Based on superposition, which is not strictly correct, the ultimate bearing capacity of a footing may be approximated by the expression

$$q_u = cN_c + qN_q + (0.5)B\gamma N_\gamma \tag{211}$$

This expression may be referred to as the classical bearing capacity equation and is often referred to as the Buismann-Terzaghi equation (Buismann 1940; Terzaghi 1943). This equation in this form applies strictly to footings of an infinite length (strip loading). Bearing capacity factors given by

Equations 96,97 and 99 were developed from theoretical considerations for the shear surface shown in Figure 21. Terzaghi (1943) also developed values of the bearing capacity factors, N_c, N_q, and $N\gamma$ assuming a different failure pattern, or shear surface, than that shown in Figure 21. According to Vesic' (c.f. Winterhorn and Fang 1975), the Terzaghi bearing capacity factors, although numerically there are substantially small differences, are being abandoned and the trend among engineers is to retain the Prandtl-Reissner and Caquot-Kerisel factors.

The ultimate bearing capacity obtained from Equation 100 may be applied only for solving problems involving a single, homogeneous bearing medium and in footings that are infinitely long (strip loading)--plane strain problems. The problem, from a theoretical viewpoint, becomes exceedingly complex when the foundation shape is something other than a long rectangular shape. The expression generally used in practice, which is semi-empirical and based on comparative loading tests with footings of different shapes, is

$$q_u = cN_cS_c + qN_qS_q + (0.5)\gamma BN_\gamma S_c \tag{212}$$

where S_c, S_q, and S_γ are dimensionless shape factors, or parameters. These values change with foundation shape; they may be obtained from DeBeer, 1967 and Vesic', 1975 (c.f. Winterhorn and Fang).

Bearing Capacity Factors Derived from the Slepak-Hopkins Limit Equilibrium Model

The bearing capacity factors, N_c, N_q, and $N\gamma$, may be calculated from the Slepak-Hopkins and Hopkins limit equilibrium bearing capacity computer models and the mathematical algorithms. Bearing capacity factors computed from the Slepak-Hopkins model may then be compared to factors obtained from classical bearing capacity theory—Equations 207, 208, and 209. By deriving bearing capacity factors from the Slepak-Hopkins model to classical bearing capacity factor, the reasonableness of solutions-- at least for a single, homogeneous bearing medium—obtained from the Slepak-Hopkins model may be judged. Consequently, such a procedure is useful in establishing the creditability of the Slepak-Hopkins pavement bearing capacity model and computer program. For example, to determine the value of N_c when φ equals zero, the following procedure may be used:

Scenario 1 -- N_q - bearing capacity factor

Let

$q = 0$,
$\gamma = 0$, and
$S_c = 1$,

then Equation 212 becomes:

$$q_u = cN_c \tag{213}$$

Also, let c equal to 1.00, then

$$q_u = N_c \tag{214}$$

that is, the ultimate bearing stress is equal to the bearing capacity factor, N_c. Values inserted into the bearing capacity computer program for this example are as follows (see Figure 52):

q_u = an initial value is assumed,
γ = unit weight of the bearing medium = 0,
c = 1
B = width of footing (an assumed value; independent variable) = 10,
S_c = 1 (an infinite strip is assumed),
q = 0 (no overburden stress is used; D = 0),
y_g = elevation of ground surface is assumed
φ = an assumed value -- varied in the analyses.

A trial and error procedure is used to satisfy Equation 214 (F=1.0). For example, let φ equal zero and q_u equal 5.14 (from Equation 208). Values of other parameters are shown above. The factor of safety is 0.996. Varying q_u, and iterating, a factor of safety of 1.000 is obtained when q_u equals 4.91. This routine is continued using different values of N. Selecting another value of N equal 43 degrees, Equation 206 yields a value of 105.11 for N_c. Inserting this value for q_u, a factor of safety of 0.981 is obtained from the perturbation method. Iterating on F, a factor of safety of 1.000 is obtained when

$$q_u = N_c = 97.7.$$

Values of N_c obtained from the perturbation method are compared to values of N_c obtained from Equation 208 in Figure 53 and in Table 3. Differences in the classical values of N_c bearing capacity factors and those obtained from the (Modified) Perturbation Method only range from about 1 to 10 percent for values of N ranging from 0 to 45 degrees.

Scenario 2 -- N_q - bearing capacity factor
Let

c = 0,
q = 1,
γ = 0, and
$S_c = S_q = S_\gamma = 1$,

Then Equation 212 becomes

$$q_u = N_q . \tag{215}$$

and a trial-and error-procedure is used to determine the bearing capacity factor, N_q. A value of N is assumed and iteration is performed until a factor of safety of 1.00 is obtained. When this condition is obtained Equation 215 is satisfied. Comparison of values of N_q obtained from the Slepak-Hopkins model are compared to those obtained from the -Reissner Equation in Figure 54 and Table 3. The differences only range between 1 to 3 percent.

Scenario 3 -- N_γ - bearing capacity factor
Several methods have been proposed for determining the values of the bearing capacity factor, N_γ (Terzaghi, 1943; Caquot and Kerisel, 1953; deMello 1969; Feda, 1961; and Vesic', 1970). Many

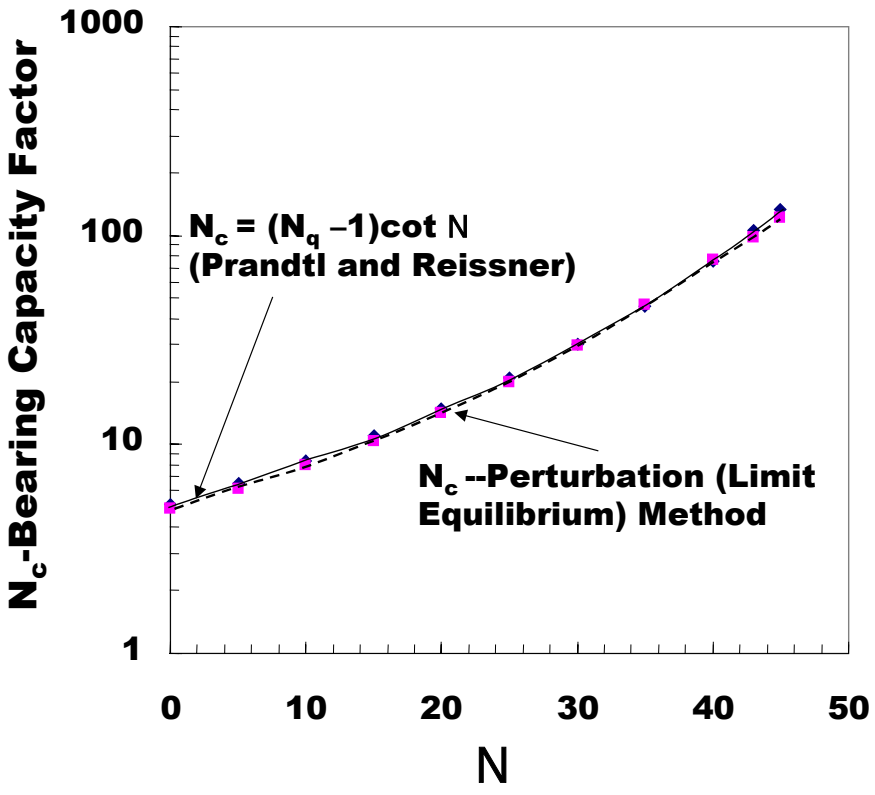

Figure 53. N_c-bearing capacity factor as a function of N.

different values of N_γ have been proposed and correct values of this bearing capacity factor remain very much unsettled.

Values of N_γ for different values of φ were estimated by Caquot and Kerisel (1953)--Vesic', 1975; c f Winterhorn and Fang) based on the assumption that θ_a is equal to 45 ^{o} + φ/2, and

$$N_\gamma \approx 2(N_q + 1)\tan\phi \tag{216}$$

where N_q is defined by Equation 207 (Prandtl, 1921). Those values are based on the assumption that the base of the footing is frictionless.

Myerhof (1951, 1963)) estimated values of $N_($ from the expression

$$N_\gamma \approx (N_q - 1)\tan(1.4\phi) \tag{217}$$

where N_q is defined by Equation 207 (Prandtl 1921).

An expression by Brinch Hansen (1970) defines values of $N_($ as

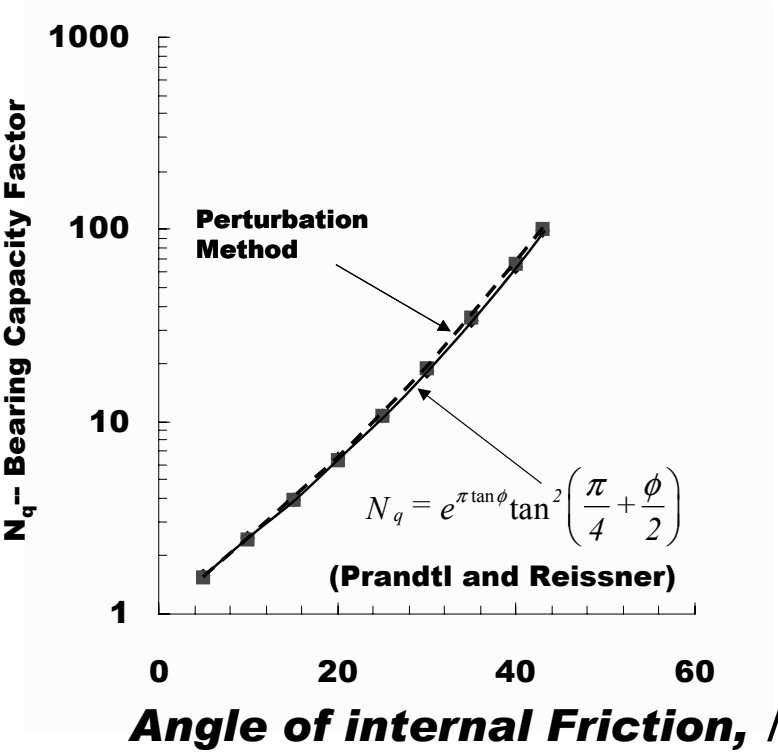

Figure 54. N_q-bearing capacity factor as a function of N.

$$N_\gamma \approx 1.8(N_q - 1)\tan\phi\,. \tag{218}$$

Values of N_γ may also be computed from the Slepak-Hopkins mathematical bearing capacity computer model. These calculations are based on the assumed failure pattern in Figure 14.

Let

c = 0
q = 0
γ = 1
B = 2
$S_c = S_q = S_\gamma = 1$,

Then Equation 212 becomes:

$$q_u = N_\gamma\,. \tag{219}$$

Again, a trial and error procedure is used to determine the bearing capacity factor, $N_($. A value of N is assumed and iteration is performed until a factor of safety of 1.00 is obtained. When this condition is obtained Equation 219 is satisfied. Values of $N_($ obtained from the Slepak-Hopkins model are compared to those obtained from the various proposed methods by others in Figure 55 and Table 3.

Table 3. comparisons of bearing capacity factors computed from different proposed methods.

Angle of Internal Friction (Degrees)	Bearing Capacity Factors										
	Prandtl and Reissner[1] N_c	Slepak-Hopkins N_c	Prandtl and Reissner[1] N_q	Slepak-Hopkins N_q	Caquot and Kerisel N_γ	Brinch and Hansen N_γ	Meyerhof N_γ	Slepak and Hopkins N_γ	Hopkins (1991) N_γ	Experimental Test Results (Model Footing Tests)	
										DeBeer/ Ladanyi (1961) N_γ	**Feda (1961)**
0	5.14	4.92	1		0.0	0	0	0	0		
5	6.49	6.17	1.57	1.557	0.45	0.09	0.07	0.512	0.52		
10	8.35	7.95	2.47	2.443	1.22	0.47	0.37	1.504	1.524		
15	10.98	10.38	3.94	3.92	2.65	1.42	1.13	3.43	3.47		
20	14.83	14.1	6.4	6.34	5.39	3.54	2.87	7.28	7.38		
25	20.72	20	10.66	10.66	10.88	8.11	6.77	15.5	15.40	14	
30	30.14	29.75	18.4	18.9	22.40	18.08	15.67	34.15	32.50	33	
35	46.12	46.3	33.3	34.5	48.03	40.71	37.15	75	70.20	83	
40	75.31	76	64.2	66.2	109.41	95.45	93.69	177	157.00	210	170
43	105.11	97.7	99.2	101.5	186.53	164.52	171.14		255.83		
45	133.88	121.5	134.88		271.75	240.97	262.74	463	371.00		

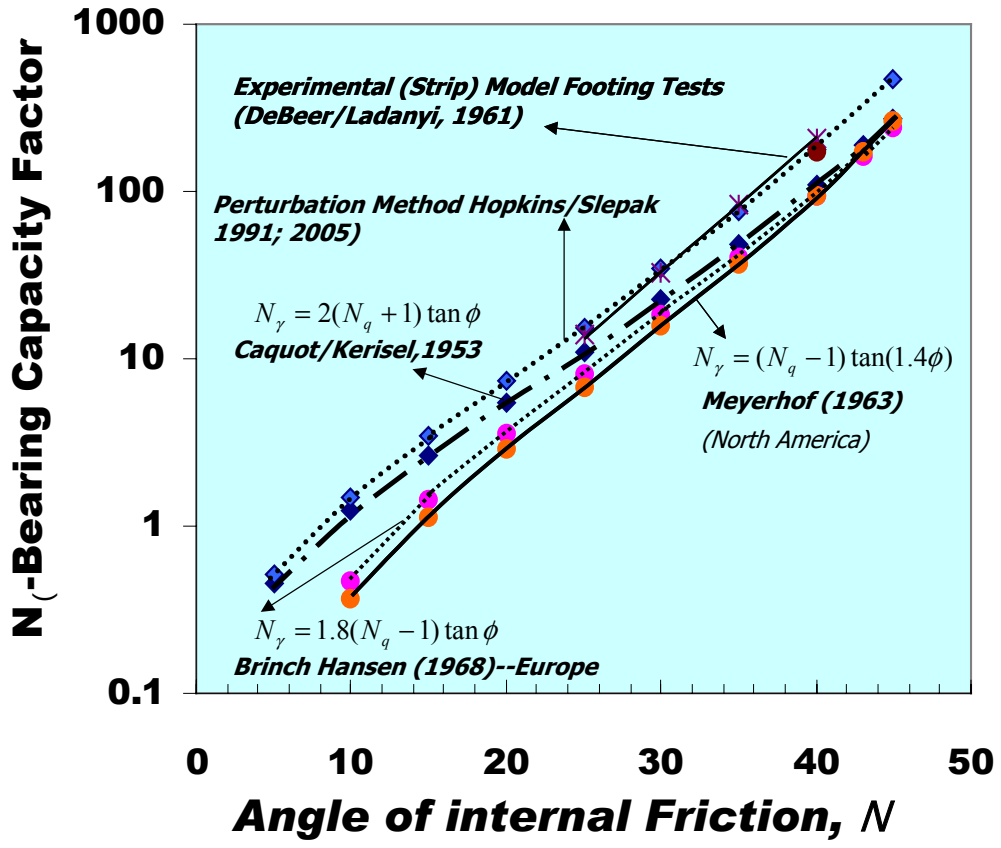

Figure 55. Proposed values of the $N_($-bearing capacity factor as a function of N.

As shown by the comparisons in Figure 55 and Table 3, the Slepak-Hopkins $N_($-bearing capacity factors range from about 12 to 38 percent larger than the $N_($-values estimated by the Caquot-Kerisel equation. However, when the Slepak-Hopkins $N_($-bearing capacity factors are compared to $N_($-bearing capacity factors from experimental model footing tests (DeBeer and Ladanyi, 1961; Feda, 1961) the differences are much smaller. The $N_($-bearing capacity factors from the Slepak-Hopkins approach are some 3 to 11 percent larger than $N_($-bearing capacity factors from the experimental tests for N-values of 25 and 30 degrees and about 10 to 16 percent lower than the experimental results for N-values of 35 and 40 degrees, respectively. For the same values of N, the Caquot-Kerisel $N_($-bearing capacity factors are some 22 to 42 percent smaller than the experimental values of $N_(.$ $N_($-bearing capacity factors obtained from the Hopkins bearing capacity model (1991) are very similar to those obtained from the Slepak-Hopkins Perturbation Model. Comparisons of the various bearing capacity factors obtained from the Slepak-Hopkins model (and the Hopkins model, 1991) with published values, the Slepak-Hopkins model yields reasonable results, at least for one layer of bearing material.

Minimum Subgrade Strength

In the scenarios described, the values of bearing capacity factors, N_c and N_q, derived from the Slepak-Hopkins bearing capacity perturbation model (and the Hopkins model, 1991) were shown to be close to values obtained from the Prandtl-Reissner equations. Futhermore, values of N_γ-values from the perturbation method were larger than N_γ-values proposed by others. However, the N_γ-values from

the perturbation approach were shown to be closer to N_γ-values obtained from experimental model footing tests. Consequently, the perturbation approach is a viable model.

The Slepak-Hopkins perturbation model may be may be used to develop some practical aspects concerning pavement subgrades during construction. For example, the model may be used to estimate the minimum strength required to avoid failure of the subgrade subjected to construction traffic. The minimum CBR strength of the subgrade necessary to avoid failure under construction traffic and the minimum bearing strength to control a pavement may be found. These aspects are discussed as follows.

Minimum undrained shear strength of subgrade

The minimum undrained shear strength, c, or S_u, of the subgrade required to withstand failure may be determined from the perturbation bearing capacity model. Similar analysis using the Hopkins model were presented previously elsewhere (1991). The assumed failure pattern of the subgrade when subjected to an assumed dual-wheel loading is shown in Figure 14. In this construction scenario, only one layer of material is involved for this stage of construction. The relationship between undrained shear strength of the subgrade and tire contact stress, T_c, of the dual-wheel loading is shown in Figure 56. The two curves were developed assuming factors of safety of 1.0 (a failure condition) and 1.5. A -type shear surface is assumed in the analysis. Also, the problem is considered a plane strain situation, that is, the footing (of the tire in motion) acts like an infinite footing. Assuming factors of safety of 1.0 and 1.5, the relationships may be expressed, respectively, as:

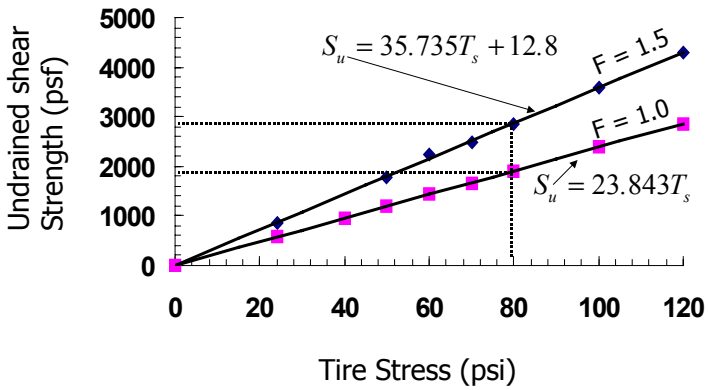

Figure 56. Undrained shear strength as a function tire contact stress.

$$S_u \approx 23.84T_s \text{ (psf)} \quad \text{and} \tag{220}$$

$$S_u \approx 35.74T_s + 12.8 \text{ (psf)} \tag{221}$$

where S_u = undrained shear strength (in lbs/ft^2, or psf) and
T_c = tire contact stress (in psi).

For tire contact stress of 80 psi, the minimum undrained subgrade strength required to maintain a factor of safety of 1.0 is about 1907 psf. When the tire contact stress is 80 psi the minimum undrained subgrade strength required to maintain a factor of safety of 1.5 is about 2872 psf. Based on this analysis, the required undrained shear strength of the subgrade must be greater than about 1907 psf (or 13.2 psi). However, as the strength of the subgrade approaches a factor of safety of 1.0, settlement (and rutting) under the wheels loads begin to occur according to model analysis. To prevent this situation, the factor of safety against failure must be some value above 1.0. Moreover, as the tire stress increases above 80 psi, the minimum undrained strength required to maintain stability must increase above 1907 psf.

Minimum value of CBR of the subgrade--theoretical

The minimum CBR value of the subgrade required to withstand failure may be determined from the Perturbation Bearing Capacity Model. Similar analysis using the Hopkins model were presented previously elsewhere (1991). To perform the analysis requires establishing some type of relationship between the undrained shear strength, S_u and CBR. In a previous study, Hopkins (1991) developed the following relationship:

$$CBR = 0.465 S_u^{1.014} \text{ (psi)} \tag{222}$$

Using the expression given by Equation 222, a relationship between CBR and tire contact stress may be developed using the Perturbation Model.

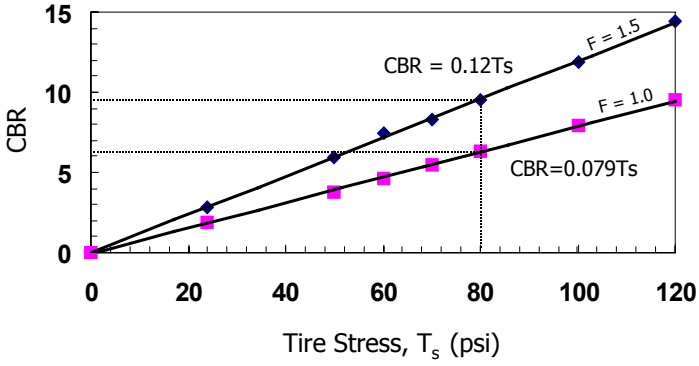

Figure 57. CBR as a function of tire contact stress.

As in the previous analysis, the assumed failure pattern of the subgrade when subjected to an assumed dual-wheel loading is shown in Figure 14. In this construction scenario, only one layer of material is involved for this stage of construction. Using Equations 220 and 221 (Figure 56) and the expression given by Equation 222, CBR may be expressed as a function of tire contact stress. Selecting values of tire contact stress and factor of safety, the undrained shear strength may be computed from the equations in Figure 56. Using Equation 222, the undrained shear strength may be converted to CBR. Selecting several values of tire contact stress, the expressions in Figure 57 may be developed. For a factor of safety of 1.0, the minimum CBR strength at failure is:

$$CBR = 0.079 T_s \text{ (\%)}. \tag{223}$$

To maintain a factor of safety of 1.5, the minimum subgrade CBR may be obtained from the relationship:

$$CBR = 0.12 T_s \text{ (\%)}. \tag{224}$$

Assuming a contact tire stress of 80 psi, the minimum subgrade CBR value must be about 6.3 to maintain a factor of safety of 1.0. However, to prevent failure and gross tire sinkage the factor of safety must be greater than 1.0. For example, the minimum subgrade CBR strength must be 9.6 to maintain a factor of safety against failure of 1.5.

Minimum CBR bearing strength--field studies

Thompson (1988) cited two field subgrade studies that show the relationships among tire contact stresses, field CBR values, and tire sinkage (or rutting). Relationships between tire pressures and sinkage values for tire inflation pressures ranging from 50 to 80 psi are shown in Figure 58. For this range in tire pressures, the minimum CBR strength of the subgrade required for limiting tire sinkage

to 0.25 inches, or less, must be between about 5.3 (50 psi tire inflation pressure) and 8.5 (80 psi), respectively. Data, labeled as "Kraft" in Thompson's paper (1988), were re-analyzed to obtain an equation that relates tire pressure (T_c), CBR, and tire sinkage(s). Graphical results of these re-analyses are shown in Figure 58 and may be expressed in the approximate form as:

$$CBR = \frac{1}{\frac{6.04}{T_c}(1+S) + 0.2S - 0.034} \quad . \tag{225}$$

For an inflation pressure of 80 psi (and assuming the tire pressure is approximately equal to the tire contact stress, T_c,) and limiting tire sinkage to 0.25 inch, the required CBR bearing strength is about 9.1, as determined from Equation 225 (for Kraft data at 0.25 inches of sinkage)). This CBR-value is nearly equal to the theoretical CBR-value of 9.6 obtained from the Slepak-Hopkins perturbation model at a factor of safety of 1.5. This value is slightly higher than the field value of 8.5 shown in Figure 58.

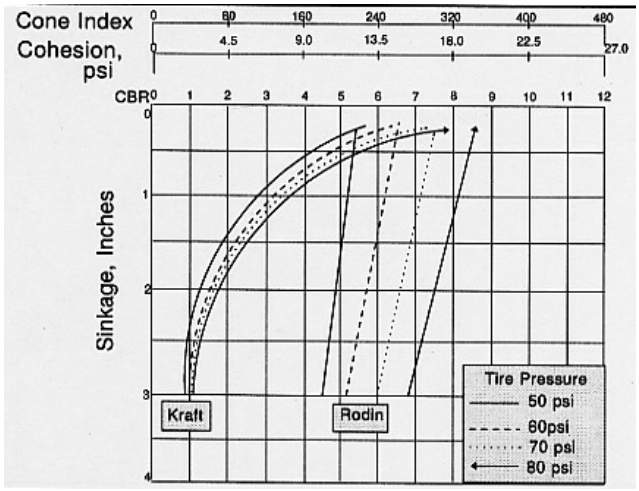

Figure 58. Tire sinkage as a function of subgrade strength (after Thompson 1988).

As shown in Figure 58, and for tire pressures ranging from 50 psi to 80 psi, the CBR values required for limiting tire sinkage to a value of 0.25-inch ranges from 5.3 to 8.5, respectively (Rodin data). Using these tire pressures and corresponding CBR values--which correspond to a tire sinkage of 0.25 inches--and converting the CBR values to undrained shear strength (Equation 190), the average factor of safety obtained from the Perturbation Bearing Capacity Model for each combination of tire pressure and CBR value is about 1.37. Performing a similar analysis using a tire sinkage of 3.0 inches, CBR-values of 5.3, 6.4, 7.5, and 8.5 that correspond to tire stresses of 50, 60, 70, and 80 psi respectively, and converting the CBR-values to undrained shear strength using Equation 190, the average factor of safety obtained Perturbation Model was about 1.12—a state near failure. The relationship obtained for this analysis is shown in Figure 59.

A similar analysis was performed using CBR-values from the data labeled “Kraft” in Figure 58. The analyses were performed using CBR values that occurred at a sinkage value of 0.25 inches and tire pressures of 50, 60, 70, and 80 psi. The average factor of safety for the sinkage value of 0.25 was about 1.47. This relationship is shown in Figure 59.

Finally, analyses were performed holding the factor of safety constant. Tire pressures were varied and values of 50, 60, 70, and 80 psi were used in the analyses. In the first scenario, a factor of safety of 1.0 was assumed. For each selected value of tire stress, the undrained shear strength of the subgrade was varied until the factor of safety was equal to 1.0. Similar analyses were performed using a factor of safety of 1.5. Relationships obtained from the model analyses performed in that fashion are shown in Figure 59 and compared to the curves obtained from the field data. As the tire sinkage increases, the factor of safety against failure decreases. When the sinkage value approaches about 3 to 4 inches, the factor of safety approaches a value of 1.0. As tire sinkage decreases and approaches a value of 0.25 inches or less, the factor of safety approaches a value of 1.5.

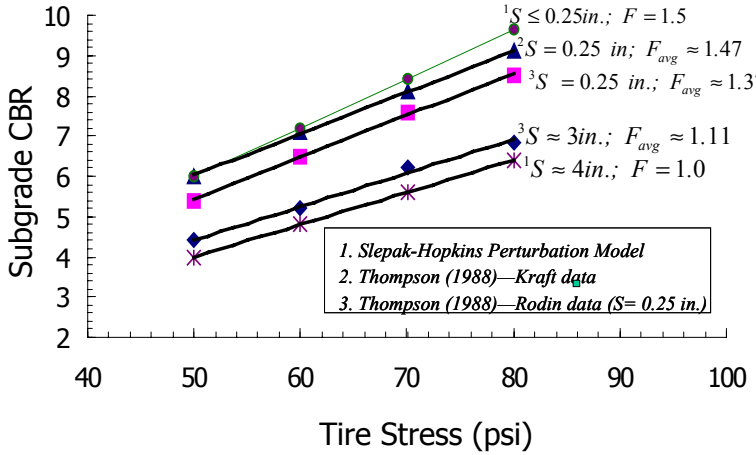

Figure 59. Relationship among factor of safety from the Slepak-Hopkins Perturbation model, tire sinkage (S), and tire stress (sinkage data from Thompson, 1988).

Both theoretical analyses using the Perturbation Model and field data indicate that the CBR strength required to insure good stability and low tire sinkage values of the subgrade during construction is about 9. A safety factor of 1.5 or greater is a reasonable value to maintain this condition and is a good working value. This condition corresponds to a tire contact stress (dual-wheelps) of 80 psi. When tire stresses larger than 80 psi are encountered than a larger value of CBR of the subgrade must be determined from the relationships above. Results obtained from the field experiments confirm the results obtained from the Slepak-Hopkins and Hopkins models for subgrades during construction (one homogenous layer).

Bearing Medium Composed of Two Different Layers of Materials

Application of classical bearing capacity theory to highway problems involving non-homogenous soil conditions has been limited because classical theory is limited to only one layer of material and highway construction problems usually, at some stage, involve more than one layer of material. Two common types of very typical situations encountered during roadway construction involving two different layers of materials are illustrated in Figures 60 and 61. In the most common situation, a granular base of the pavement is constructed on a compacted soil subgrade. Alternately, the soil subgrade is stabilized, or modified, using some type of chemical admixture, such as hydrated lime or Portland cement, as illustrated in Figure 61. If the soil subgrade remains unsoaked during construction, then bearing capacity problems do not normally develop. CBR-values of compacted, unsoaked clayey soils typically, range from 10 to 40 (Hopkins, 1991). For example, assume that an 8-inch layer of base aggregate has been placed on the unsoaked, compacted soil subgrade. Assume also that the CBR-value of the soil subgrade is 10. Converting that value of CBR to undrained shear strength using Equation 190 yields

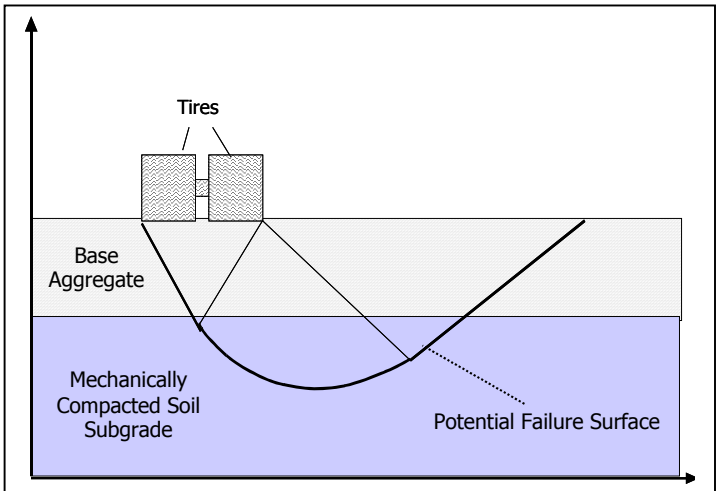

Figure 60. A common type of two-layered problem occurring during early construction of the pavement.

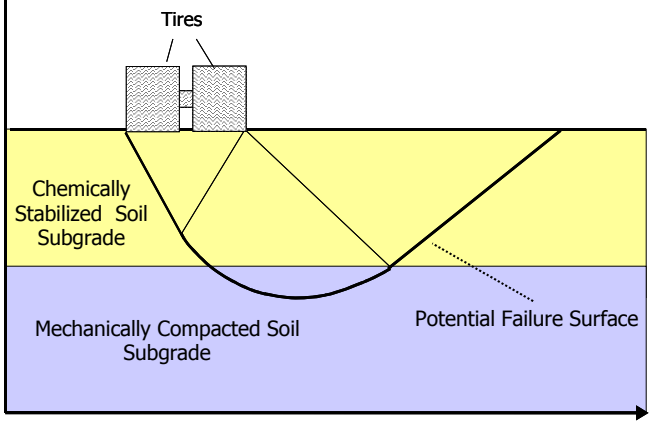

Figure 61. Construction of chemically stabilized subgrade on a mechanically compacted soil subgrade.

a value of 2719 lbs/ft^2. Using a ϕ-value of 43 degrees for the aggregate and assuming a dual-wheel tire of 80 lbs/ft^2, a factor of safety against failure of 1.74 is obtained from the Perturbation Method.

Similarly, assume that an 8-inch layer of soil subgrade is stabilized with hydrated lime and rests on the soil subgrade. Assuming an undrained strength of 3456 lbs/ft^2 (seven-day strength at the 85th percentile test value; Hopkins and Beckham 1997), the factor of safety is 1.79.

Stability and constructability of the base aggregate, or the chemically treated layer, depends on the shear strength of the subgrade. The relationship between the required thickness of granular base or stabilized layer as a function of the subgrade strength may be developed using the perturbation approach, as shown in Figure 62. In those analyses, factors of safety of 1.0 and 1.5 and a tire contact stress (dual wheels) of 80 psi are assumed. If the subgrade CBR value equals 3 (an undrained strength of 6.4 psi, or 917 psf), then thicknesses of 22.5 and 42.7 inches would be required to maintain factors of safety of 1.0 and 1.5, respectively. However, thicknesses of this magnitude may have to be constructed in lifts. Reduced loading of gravel trucks may have to be used to reduce contact tire pressures to avoid deep rutting, or failure of the subgrade. Alternately, if the subgrade is very weak, then the soft material may have to be undercut to firmer material and replaced with stone to avoid failure, or deep rutting and shoving and pushing of the subgrade during construction.

To avoid failure, or deep rutting, the subgrade must contain some minimum strength and aggregate thickness to maintain stability. As shown in Figures 56 and 57, the untreated subgrade beneath the aggregate base, or chemically treated base, must have a certain minimum strength. For a tire contact stress of 80 psi, the minimum strength ranges from about a CBR of 8 to 10, as shown in Figure 62, for factors of safety ranging from 1.0 to 1.5.

In some instances, the aggregate base is reinforced with a geotextile tensile element, as depicted in Figure 2. Depending on the degree of strain mobilization, Perturbation Model analyses show that the factor of safety increases when tensile elements are used to reinforce the base. In figure 63, the thickness of aggregate base, with and without tensile elements, required to maintain a factor of safety of 1.5 under a dual wheel contact stress of 80 psi is shown. In those analyses, it was assumed that sufficient strain occurs to mobilize the ultimate strength of the tensile element. A tensile element force of 1350 lb/ft was used. The estimated trend, as shown in Figure 64, indicated

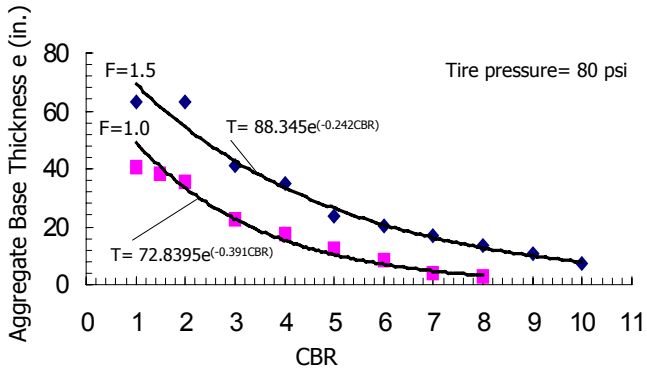

Figure 62. Aggregate thickness as a function of the CBR-value of the soil subgrade for factors of safety of 1.0 and 1.5.

that, for this situation, the thickness required for the reinforced case ranges from about 7 inches to 2 inches for CBR strengths of the subgrade ranging from 1 to 10. However, the differences would be much less when the mobilized strains are less.

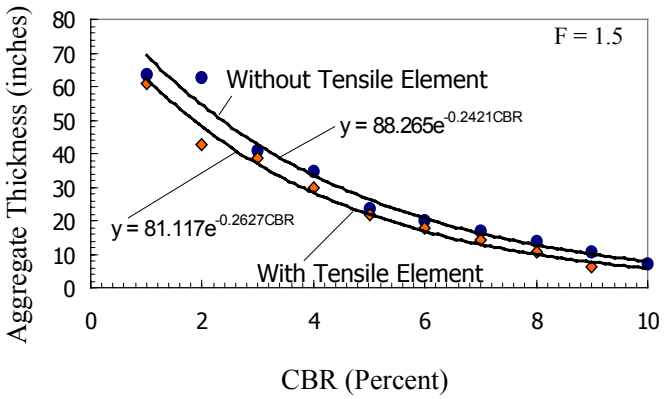

Figure 63. Thickness of aggregate base with and without tensile element required to maintain a factor of safety of 1.5. Reinforced base aggregate subjected to a dual tire contact stress of 80 lbs/ft^2.

Multilayered Bearing Medium

The Slepak and Hopkins Perturbation approach was extended to analyze foundations containing multiple layers of soils, or materials, which have different, shear strengths. In this study, the Hopkins and the Slepak-Hopkins stability models were extended to analyze flexible pavements containing different materials and tensile element forces.

Analyses of the 1959-1960 AASHO Road Test

In 1962, the American Association of State Highway Officials (AASHO -- currently identified as AASHTO, or the American Association of Highway Transportation Officials) published the results of an extensive road test conducted at Urbana, Illinois during 1959 and 1960. Many trucks having various axle configurations and loads were driven continuously for several months over pavement sections of various thicknesses. Several pavement loops were constructed. Several loops contained sections of various combinations and thicknesses of asphalt concrete, base material (crushed stone), and a subbase material (a sand-gravel mixture). In 1991, the Hopkins Model was used to analyze 237 pavement sections occurring on loops 3, 4, 5, and six (lanes 1 and 2) of the AASHO Roadway Test. Since the Slepak-Hopkins Perturbation Model yields essentially the same factor of safety as the Hopkins model, results obtained from the Hopkins model (for the unreinforced case) would apply to the Slepak-Hopkins model.

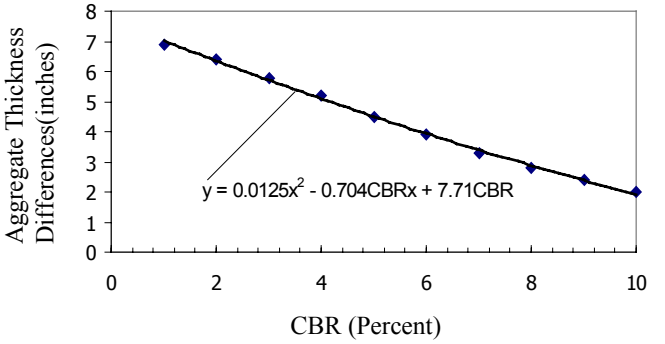

Figure 64. Estimated difference in thickness of an aggregate base with and without a tensile element.

The performances of the roadway sections at any given time were judged in terms of a present serviceability index. This index, defined as a measure of the pavement condition, depends on the surface roughness, cracking, and patching. The index ranges on an arbitrarily selected scale from zero to five. Asphalt pavements generally had an initial index of about 4.2. When a pavement section reached a value of 1.5, the section was considered to be in a failure condition. Most often when the index decreased to 2.0, it decreased immediately to 1.5; the section was either taken out of the test, or an overlay pavement was constructed, and the testing of the section continued. The purposes of the Hopkins model analyses were to gain an overview of the magnitudes of the factors of safety obtained for the various

pavement sections and to determine the reasonableness of results obtained from the analyses. Most of the pavement sections essentially failed; that is, the serviceability index reached a value of 1.5. The exact nature of the failures was not described. About 89 percent of the sections analyzed reached a serviceability index of 1.5.

Assumed Shear Strengths of Flexible Pavement Layer, Aggregate Base, and Soil Subgrade

Because shear strength of asphalt materials varies with temperature and temperatures within the asphalt concrete materials vary with pavement depth, the shear strength varies with pavement depth (Hopkins, 1991; Hopkins and Beckham 1995). To examine the variation of shear strength with temperature, unconsolidated-undrained triaxial compression tests were performed on asphalt core specimens obtained from an asphalt concrete pavement site in Kentucky. The testing procedure and apparatus were described previously in the section entitled "DEFINING SHEAR STRENGTH PARAMETERS OF FLEXIBLE PAVMENT LAYERS." Relationships of the angle of internal friction, ϕ, and cohesion, c, and temperature were shown in Figures 22 and 23. A temperature-depth model developed by Southgate et al, 1969,1975,1981, and 1982) was used to define the temperature at any selected depth. The assumption was made that the relationships in Figures 22 and 23 represented the strengths of the flexible pavement at the AASHO Road Test.

Table 4. Conversion of CBR-value of AASHO Road test loop to undrained shear strength.

1959-60 AASHO Road Test Loop Number	Soil Subgrade CBR-Value of Loop	Undrained Shear Strength, $S_u = 2.173CBR^{0.979}$
3	2.7	827
4	3.7	1,126
5	3.0	917
6	3.9	1,186

Shear strength parameters, ϕ and c, of the base material (crushed stone) were estimated to be 43 degrees and zero, respectively. This assumption was based on actual triaxial test results obtained from testing similar compacted aggregates. Since CBR-values of each loop were given in publications by the AASHO Road Test, the relationship given by Equation 188 was used to convert the "CBR-values to undrained shear strength, S_u. Converted values are shown in Table 4.

Typical Data Set-Up and Illustrations of the Analysis of Unreinforced Flexible Pavement and Results

Typical data setup is shown in Figure 65. To illustrate the stability analysis of unreinforced flexible pavement using the method by Hopkins (1986,1991, 1994a, 1994b, 1995; Slepak and Hopkins, 1998), flexible pavement sections of loops 3, 4, 5, and 6 (lanes 1 and 2) of the 1960 AASHO Road Test (1962) were made using two different temperature assumptions (Hopkins, 1991). In the first analysis, the surface temperature, (T_s), and the average air temperature, (T_a), were assumed to be 60^o and 27.3^o C, respectively. Surface temperatures of pavements in that part of the country (Ottawa, Illinois—study site) can reach values of 60^o C. To account for temperature variation (and variation of shear strength) with depth in the asphalt pavement, relationships given by Southgate, et al (1982) were used. For assumed surface and air temperatures of 60^o and 27.3^o C, the temperature, T, for any depth, D (in cm) may be determined from their relationships.

Each pavement section was divided into 2.54-cm layers (Figure 65, pavement section 599, loop 4, lane 1). The temperature at each mid-point of each layer was calculated from equations given elsewhere (Southgate et al, 1969,1975,1981, and 1982). Using those equations and the data in Figures in 22 and 23, strength parameters, ϕ and c, of each finite layer were determined. A second set of analyses was performed using a surface temperature of 25^o C. Temperatures were assumed to be 25^o C throughout the full depths of the asphalt concrete pavements.

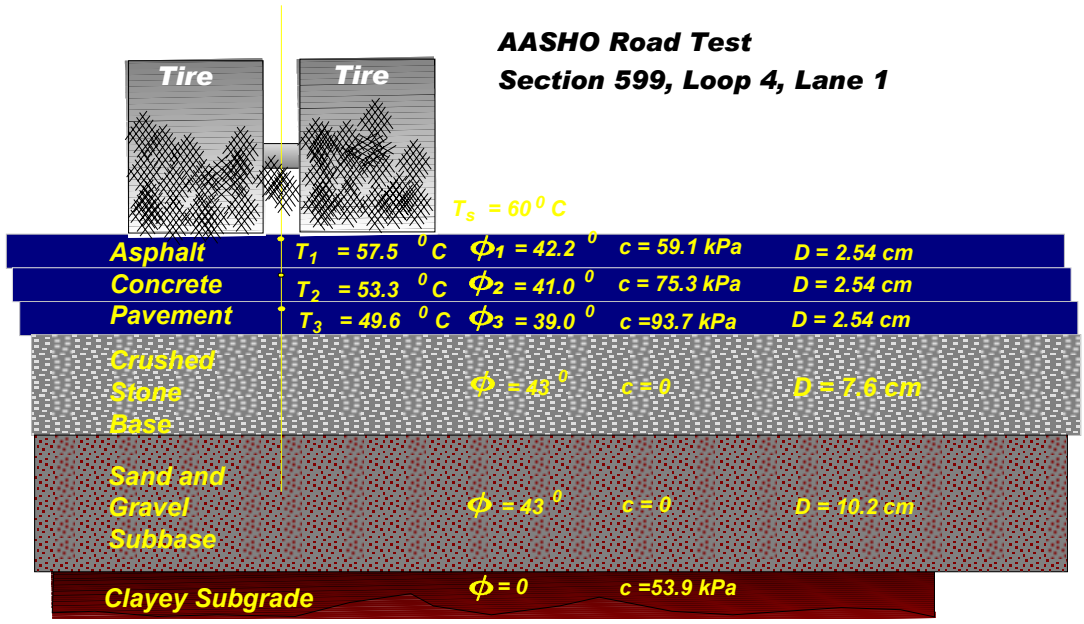

Figure 65. Typical model design setup.

Results

In Figure 66, the factors of safety of the pavement sections (T_s equal 60^o C) are shown as a function of weighted, 18-kip, equivalent single-axle loads (ESAL). Factors of safety of some 29 sections of a total of 215 pavement sections are not shown in this figure because the present serviceability index never reached a value of 2.5 during the road test. The factors of safety of those 29 sections ranged from 1.19 to 2.00 and averaged 1.51. ESAL values were greater than eight million. Factors of safety of all sections ranged from 0.63 to 1.8. As shown in Figure 64, the slope of the factor of safety-ESAL curve increases rapidly up to a factor of safety of about 1.3 and an ESAL value of one million. When the factor of safety is greater than 1.3, or the ESAL value is greater than about one million, the slope of the curve tends to decrease, become flatten, and approach a safety factor of about 1.5. At that stage, the ESAL value approaches eight million. When the factor of safety exceeds a value of 1.5, the ESAL values are greater than eight million.

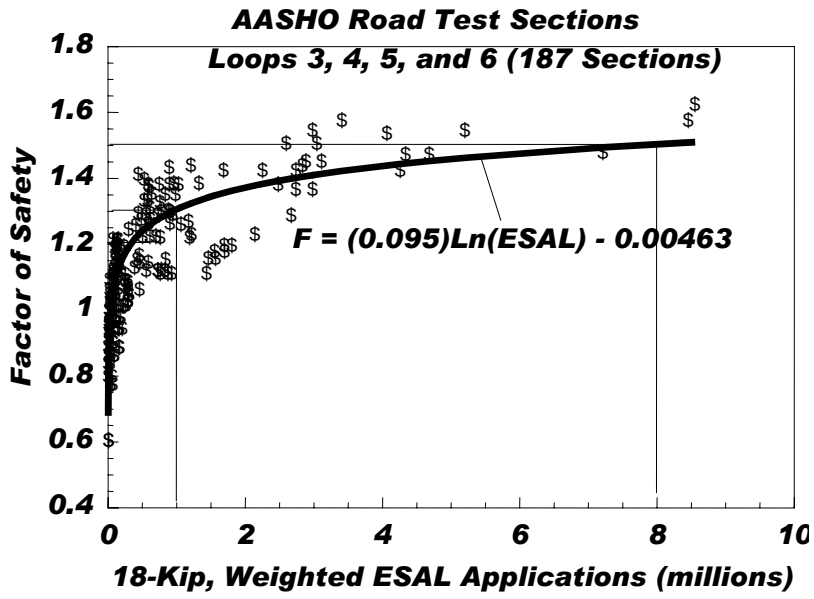

Figure 66. Factor of Safety of 1962 AASHO pavement sections as a function of values of ESAL (After Hopkins, 1991; Hopkins and Slepak, 1998).

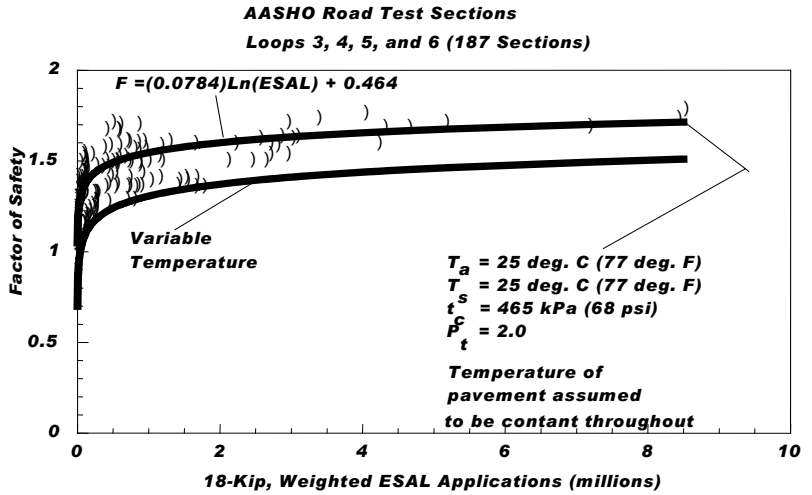

Figure 67. Effect of temperature on the factor of safety of AASHO flexible pavement sections.

The curve in Figure 66 was based on a surface temperature of 60° C and an average air temperature of 27.3 ° C. As a means of examining the effect of temperature on the factor of safety (Figure 67), the analyses were repeated using a surface temperature of 25° C and assuming that the temperature of the asphalt pavement of each section was equal to a constant value of 25°C throughout. Decreasing the surface temperature of the asphalt pavement from a value of 60° to 25° C causes a slight increase in the factor of safety. For ESAL values ranging from 1 to eight million, the differences in factors of safety of the two curves range from about 0.23 to 0.27, as shown in Figure 67.

Data shown in Figure 66 may be illustrated in another form. Values of ESAL were sorted in ascending order, grouped (arbitrarily), and the average factor of safety of each group was computed. As the average factor of safety increases, the value of ESAL for each group increases, as shown in Table 1. The average factor of safety of 53 percent of all sections ranged from only 0.95 to 1.14 and ESAL values were less than only 0.5 million (P_t equal 2.0). The serviceability index of some 13.5 percent of the sections did reach a value of 2.0 during the duration of the road test and the ESAL values exceeded 8 million. The average factor of safety of this group generally exceeded 1.5. These data show that reasonable solutions can be obtained using limit equilibrium methods, as proposed herein. A more in depth analysis of the 1959-60 Road Test has been given elsewhere (Hopkins, 1991)

Table 5. Average factors of safety of ESAL groups

ESAL Group (Pt = 2.0)	Average Factor of Safety, F	Percentage of Total Pavement Sections
<50,000	0.95	14.9
50,000 - 200,000	1.08	26.0
200,000 – 500,000	1.14	12.1
500,000 – 1 million	1.30	17.2
1 million – 8 million	1.40	16.3
>8 million	1.51	13.5

CASE STUDY—KY ROUTE 842

Flexible Pavement Design Sections

As another means of validating results obtained from the Slepak and Hopkins Perturbation Model, a roadway section located in Northern Kentucky was analyzed. During construction of a flexible pavement section on a portion of KY Route 842 in Boone County, problems were encountered at a few locations. In some areas, additional aggregate was added during construction while in other areas patching was required shortly after construction. Six sites were selected for a detailed study.

Two design alternates for this roadway section are shown in Figure 68. In the first section, the design involves using 8 inches of mechanically stabilized subgrade. This technique is seldom used in Kentucky and usually involves mixing large stone with the clayey subgrade. Hopkins and Beckham (1995, 2000) show that this technique is ineffective when the clay content in the stone-soil matrix equal or exceeds 10 percent. In this case, the strength of the stone-clay matrix becomes nearly equal to the strength of the clay.

Although design values of ESALs (Equivalent Single Axle Loads) and CBR were not available, values may be obtained from computer software developed by Sun, Hopkins, and Ni (2004-unpublished work). The Kentucky flexible design curves (Southgate et al, 1981) were programmed using a finite difference technique. PowerBuilder 8.0 was used to create a Windows' computer software that contained the 1981 design curves in a finite difference form. The main menu of the software is shown in Figure 69. The graphical user interface is shown in

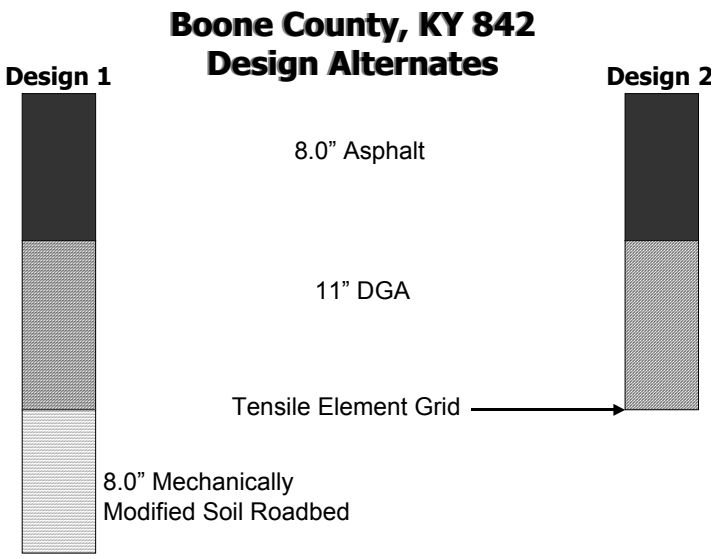

Figure 68. Original design alternates for KY Route 842.

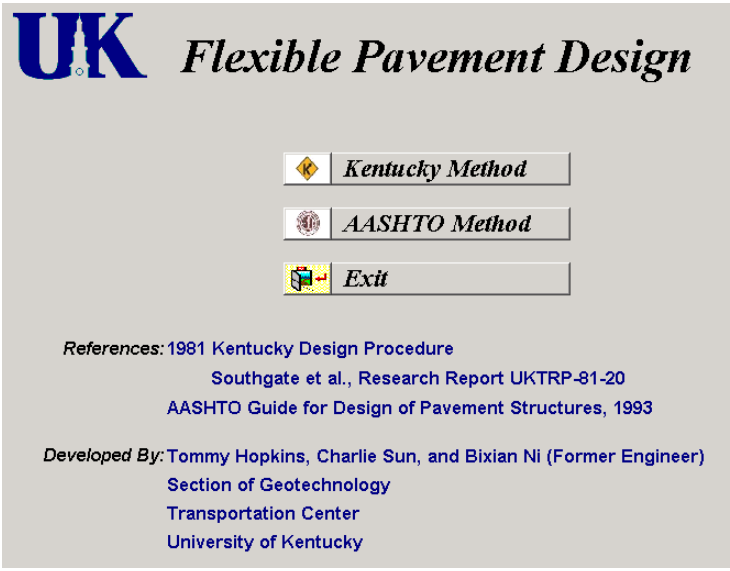

Figure 69. Main menu of 1981 flexible pavement design curves (after Southgate et al) and computer software (after Sun, Hopkins, and Ni, 2004).

Figure 70. By inserting different combinations of ESALs and CBR values, iterations are performed until the given design section was duplicated. In this case, when the ESAL value is equal to 0.55 million and the CBR value is equal to 3, the proposed design section (alternate 2) of 8 inches of asphalt and 11 inches of aggregate base is obtained. It also included a tensile element grid.

Stability of the design flexible pavement section is extremely sensitive to the selected value of the design shear strength or CBR value. For design 2, using a CBR- value of 3 and an ESAL value of 0.55 million, yields the section shown as Design 2 (Figure 68). As shown in Figure 71, the CBR value of an adjacent section is only 1.4 (85th percentile test value). Based on CBR data (50 samples) stored in the Kentucky Geotechnical Database (Hopkins, et al, 2004) for Boone County, the 85th percentile test value is 2.1 (Figure 72). Using the three different CBR values, the design thicknesses obtained from the 1981 flexible design curves, corresponding to each value of CBR, are shown in Figure 73. Analyses of those three sections using the Perturbation Method, and assuming no tensile element plastic grids, yield factors of safety that are much less than 1.0, 1.01, and 1.15, respectively—essentially a failure condition.

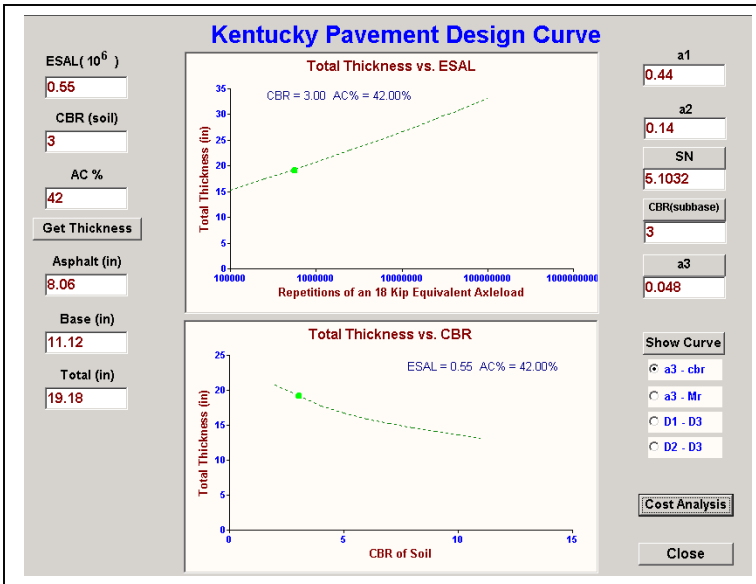

Figure 70. Computer software for using the 1981 Kentucky flexible pavement design curves.

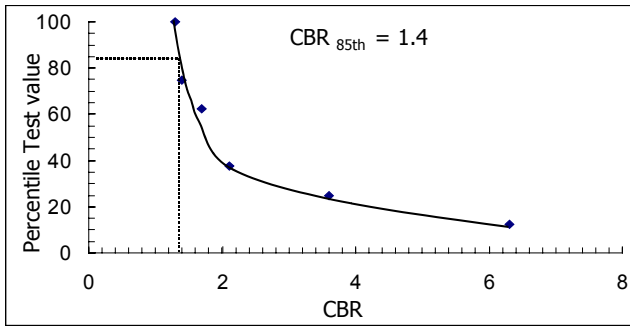

Figure 71. Percentile test value as function of CBR for an adjacent roadway section.

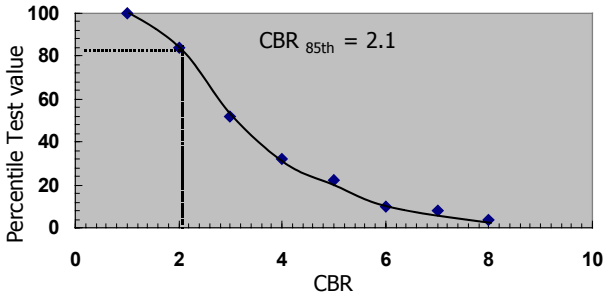

Figure 72. Percentile test value as function of CBR for an adjacent roadway section.

Assuming a CBR strength of 3.0 (or an undrained shear strength of S_u equal to 917 lbs/ft^2) of the soil subgrade and the strengths of the tensile element plastic grids equal to 450, 920, and 1340 lbs/ft, which correspond to strains (in percent) of 2, 5, and ultimate, respectively, factors of safety obtained were equal to 1.18, 1.22, and 1.25, respectively.

Assuming the same conditions but using a CBR value of the subgrade equal to 2.0 (S_u equal to 617 lbs/ft^2, or psf), the factors of safety obtained from the Perturbation method are 1.01 (no tensile elements), 1.04,

1.08, and 1.10, respectively. Stability of the subgrade is very sensitive to the strength of the subgrade and the choice of the design CBR, or undrained shear strength, is very critical in obtaining a stable situation during and after construction.

Problems were encountered in a portion of KY 842. In some instances, aggregate was added to certain areas during construction. Revised sections are depicted in Figure 74 and compared to the original design sections.

Coring Techniques and Field Testing Procedures

Core holes were drilled approximately every tenth of a mile within the study section. Special coring techniques were developed to avoid using water. Compressed air, instead of water, was used to advance the core barrel down to the top of the subgrade of each section. By using compressed air as the drilling media, soaking and softening of the top of the subgrade at each hole was prevented. Hence, the subgrade as it exists in its natural setting was preserved and undisturbed.

Typically, three or four holes were drilled at each location. The first core hole was drilled to measure the thicknesses of the asphalt and aggregate base layers of the flexible pavement section. After removing and measuring the thickness of the asphalt core, the base aggregate was removed by hand to expose the top of the stabilized subgrade (or in some cases the top of the untreated subgrade). The depth, or thickness, of the aggregate base was noted. Then a standard penetration test (SPT) was performed on the stabilized subgrade to obtain a split spoon specimen of the stabilized subgrade.

At the same location, a second hole was drilled. After augering through the flexible pavement and aggregate base and exposing the top of the stabilized subgrade, an in situ CBR test was performed, as shown in Figure 75. After completing the CBR test, a moisture content specimen was obtained at the top of the stabilized subgrade. A third hole was advanced through the asphalt layer and aggregate base and a thin-walled, undisturbed sample, or a core specimen was obtained of the stabilized subgrade. Latitudes and longitudes of each section and borings within each section were determined using mapping-grade, GPS (Global

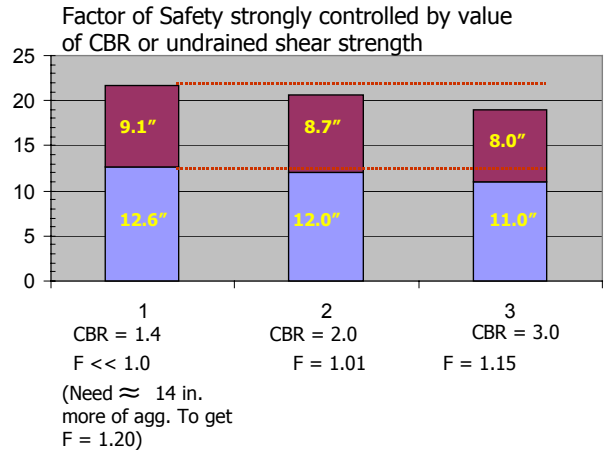

Figure 73. Different pavement sections from the 1981 flexible pavement curves (after Southgate et al).

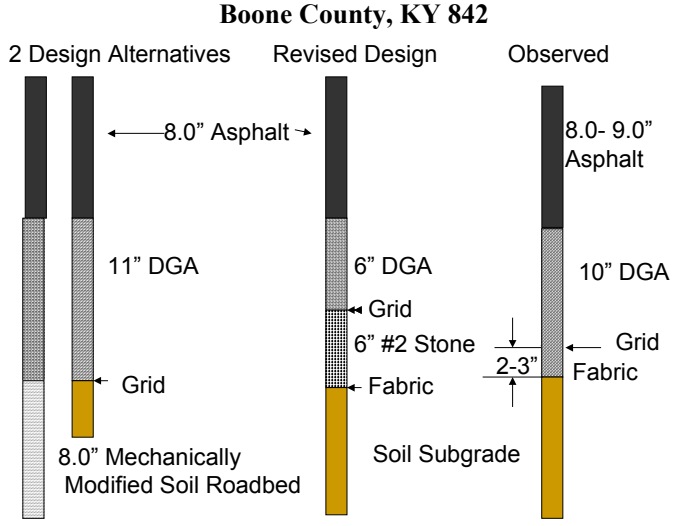

Figure 74. Revised and observed sections compared to the design alternative sections.

Positioning System) equipment. Accuracy of the locations of holes was within a submeter of the true location.

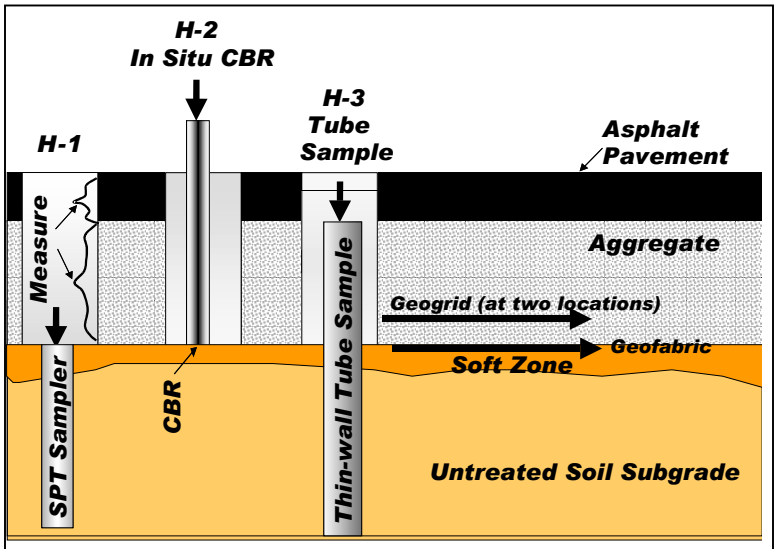

Figure 75. Field testing sequence and sample recovery

Bearing Capacity Analyses of Selected Sites

Site 1

Values of in situ CBR, a moisture content profile of the upper reaches of the soil subgrade, and measured thicknesses of asphalt pavement and DGA (Dense Graded Aggregate) base are shown for Site 1 in Figure 76. At site 1, no tensile elements were found during drilling. Using the temperature model by Southgate (1981), the asphalt layer was divided into four layers and equations appearing in Figures 23 and 24 were used to define the shear strength parameters, ϕ, and c, for each layer of the asphalt pavement. Values of ϕ and c, of the DGA base were (assumed) 43 degrees and zero, respectively. The in situ CBR value for this site was 6.4. Tire contact pressure of 80 psi was assumed in the analyses (and subsequent analyses described below). A dual wheel arrangement illustrated in Figure 65 was used also. Using Equation 190, the undrained shear of the soil subgrade was 1926 lbs/ft^2. The factor of safety against failure obtained from the Perturbation Method for this site was 1.90. No tensile element was found during drilling at this site. Pavement problems were not observed at this site.

Site 2

Conditions found at site 2 are displayed in Figure 77. Moisture content of the top few inches of the subgrade was larger in value than the moisture content of the subgrade located below the top portion. A dry shale zone was located in the subgrade as shown in Figure 77. The CBR value of the subgrade was 1.5—an extremely soft subgrade. The flexible pavement and DGA thicknesses were 8.5 and 12 inches, respectively. Bearing capacity analysis of the flexible pavement section yielded a factor of safety much less than 1.0. Even using a slightly larger value of CBR (equal to 2.0) yielded a factor of safety of only 0.98. As noted in Figure 76,

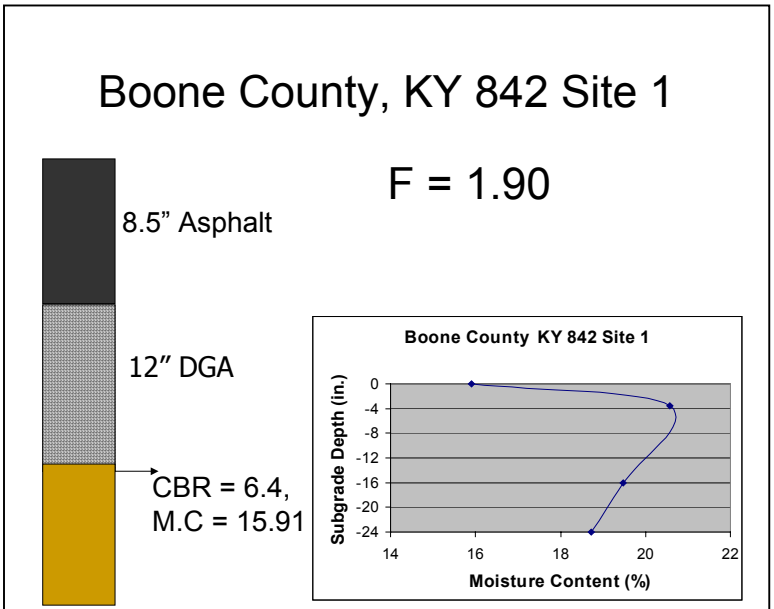

Figure 76. Measured thicknesses of asphalt pavement and DGA (Dense Graded Aggregate), a moisture content profile of the top inches of subgrade, and in situ value of CBR

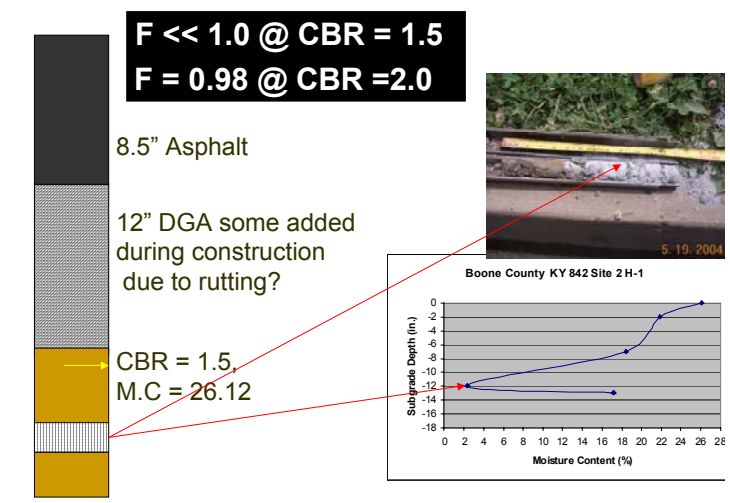

Figure 77. Measured thicknesses of asphalt pavement and DGA (Dense Graded Aggregate), a moisture content profile of the top inches of subgrade, and in situ value of CBR.

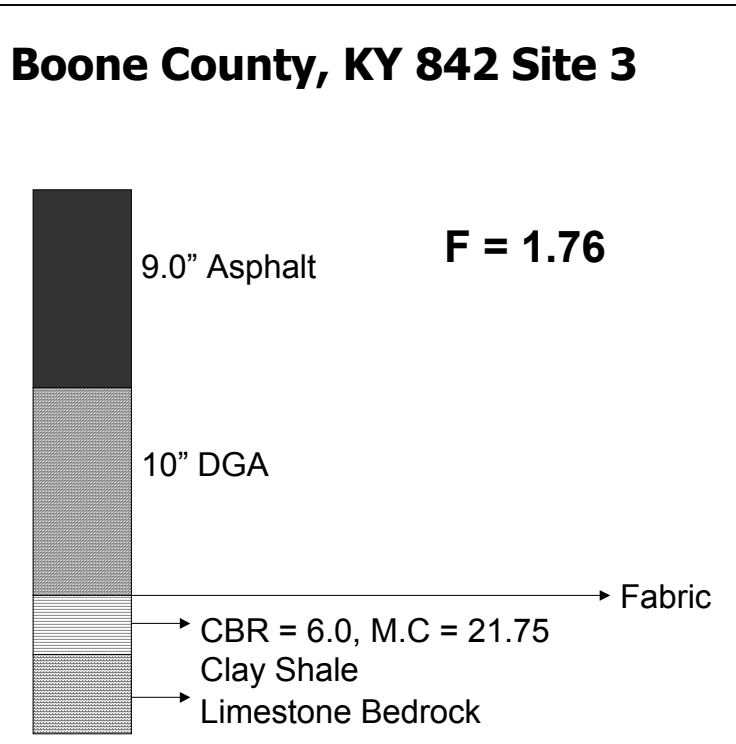

Figure 78. Measured thicknesses of asphalt pavement and DGA (Dense Graded Aggregate) and in situ value of CBR.

some DGA had to be added during construction at this location. Pavement problems were very visible at this site. No tensile elements were found at this location.

Site 3

Figure 78 shows the conditions encountered at site 3. The in situ CBR was 6.0. Converting this value to undrained shear strength using Equation 190, the factor of safety against failure obtained from the Perturbation bearing capacity model was 1.75. No pavement problems were observed at this location. Tensile elements were not observed during the drilling problem. However, a fabric (separator) was located at the top of the subgrade. Inserting a small strength of 200 lbs/ft into the analyses increases the factor of safety to 1.76. However, analyses of the flexible pavement at this location show that the stability should be very adequate unless the subgrade CBR starts to decrease substantially.

Site 4.

At site 4, Figure 79**,** a tensile element layer was located about 2 inches above the bottom of the aggregate base. Additionally, a fabric separator was located at the bottom of the aggregate base to prevent intrusion of clay particles into the base. Thickness of the flexible pavement was about 7 inches. This thickness was slightly less then the thickness observed at other locations. The aggregate base measured some 12 inches. Value of the in situ CBR of the subgrade was 3.9. Analyses of the flexible pavement section at this location yielded a factor of safety against failure of 1.28. Using published strength values of one brand of tensile elements, at 2, 5, and

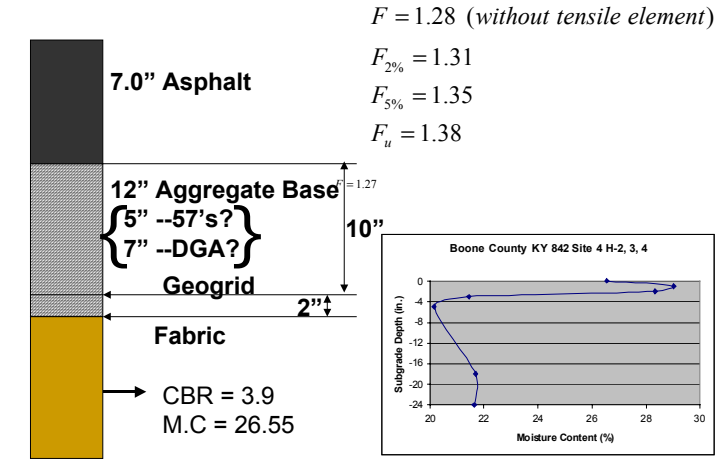

Figure 79. Measured thicknesses of asphalt pavement and DGA (Dense Graded Aggregate), a moisture content profile of the top inches of subgrade, and in situ value of CBR.

ultimate strains (in percent), factors of safety, denoted $F_{2\%}$, $F_{5\%}$, and F_u, of 1.31, 1.35, and 1.38, respectively, were obtained from the Perturbation model. Strength values used in the analyses were 450, 940, and 1320 lbs/ft, respectively. In those analyses, no strength was assigned to the fabric separator. Adding a small strength of 200 lbs/ft for the fabric separator, values of factors of safety of 1.32, 1.36, and 1.39, respectively. Using published strengths of one type of tensile element (690, 1370, and 2,050 corresponding to strains-- in percent-- of 2, 5, and ultimate strains), factors of safety were 1.34, 1.39, and 1.45 were obtained. The layer of tensile elements was positioned at a location that was 2 inches above the bottom of the base. However, the high-strength tensile elements were not used in this case and the analyses were shown for comparative purposes only. Some pavement problems were visible at this site.

Site 5

The In situ value of CBR at Site 5 could not be obtained. However, a value of moisture content of the upper portion of the subgrade was obtained. Using the relationship between in situ CBR and moisture content measured at other CBR sites, a value of 5.4 was estimated (Figure 80). Based on that CBR, the undrained shear strength was estimated to be 1631 lb/ft^2. Using the estimated value of CBR, the factor of safety (Figure 82) was estimated to be 1.58 (without tensile elements). Using values of 450, 920, and 1320 lbs/ft, which corresponds to strains of 2 percent, 5 percent, and ultimate strain, factors of safety were, respectively, 1.62, 1.66, and 1.70 were obtained from the Perturbation Method. If stronger tensile elements had been used, then larger values of factors of safety could have been obtained. For example, if tensile strengths of 690, 1,370, and 2,050 lbs/ft, corresponding to mobilized strains of 2 percent, 5 percent, and ultimate strain and ultimate, respectively, ad been used, then factors of safety of 1.62, 1.66, and 1.70, respectively, would be obtained from the Perturbation Method.

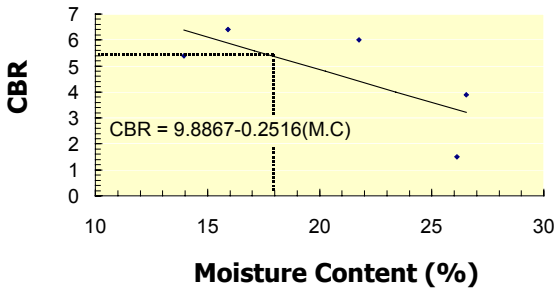

Figure 80. In situ CBR as a function of in place moisture content.

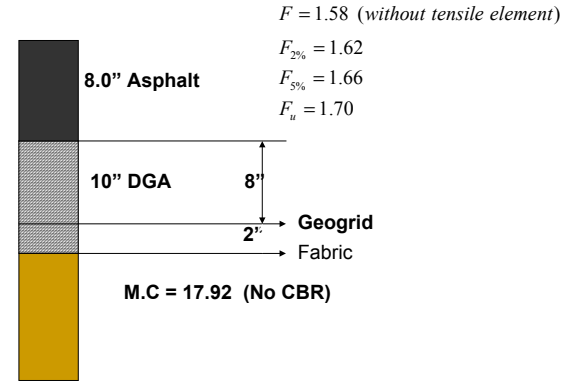

Figure 81. Measured thicknesses of asphalt pavement and DGA (Dense Graded Aggregate), a moisture content profile of the top inches of subgrade, and in situ value of CBR.

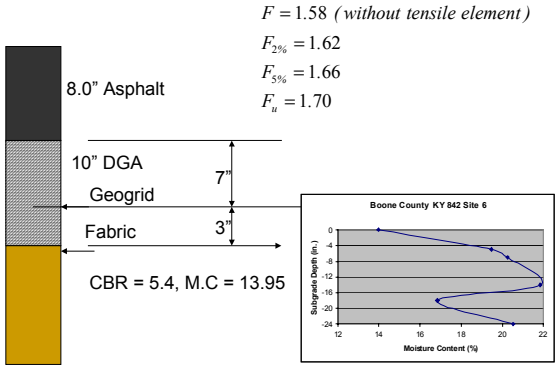

Figure 82. Measured thicknesses of asphalt pavement and DGA (Dense Graded Aggregate), a moisture content profile of the top inches of subgrade, and in situ value of CBR.

Site 6

Conditions encountered at Site 6 are shown in figure 82. The in situ value of CBR was 5.4, or an undrained shear strength of 1631 lbs/ft^2. An estimated factor of safety without tensile elements was 1.58. Using values of 450, 920, and 1320 lbs/ft, which corresponds to strains of 2 percent, 5 percent, and ultimate strain, factors of safety were, respectively, 1.62, 1.66, and 1.70 were obtained from the Perturbation method. No serious problems were observed at this site at the time of the study.

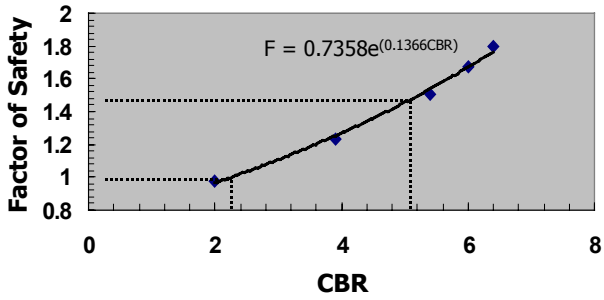

Figure 83. Factor of Safety as a function of in situ CBR, KY Route 842, Boone County.

In Figure 83, the relationship between factor of safety and in situ CBR is shown for this roadway. As the CBR drops below a value of about 2.2, the factor of safety decreases to a value of 1.0, or less—a failure condition. To maintain adequate stability, the CBR needs to be equal to about 5, or a safety factor equal to, or greater than about 1.5.

SUMMARY AND CONCLUSIONS

Mathematical bearing capacity models proposed and developed by Hopkins in 1991 and Slepak and Hopkins in 1993 were extended to analyzing flexible pavements reinforced with tensile elements embedded in earthen structures. Major portions These advanced models, which are based on limit equilibrium and are operated together, can be used to analyze the bearing capacity, or stability, of early construction of loads on a single layer of material, two-layered problems involving a layer of base aggregate and subgrade, and a foundation involving multiple layers of different materials, such

as a flexible asphalt pavement. A -type shear surface is used in the model analyses of layered foundations. The approach developed by Slepak and Hopkins, referred to as the Perturbation Method, is recommended when reinforcement is used. Either the Perturbation method, or the Hopkins method, may be used in stability problems that do not involve reinforcement, or tensile elements. The Perturbation method can be used to analyze all classes of stability problems involving circular or noncircular shear surfaces. Both effective and total stress analyses may be performed. Effective stress analyses may be performed in the stability analyses of flexible pavements if pore water pressures are known (or estimated) using the Perturbation Method.

Although the current model does not account for strain compatibility, the strength of the tensile elements may be input for assumed strain levels. Pullout resistance forces are computed for both active and passive zones. Those forces are compared to the strength entered by the user and the smaller value is used in the analyses. Any number of tensile elements may be analyzed in a given problem. In the limit equilibrium approach, shear strengths, the angle of internal friction, N, and cohesion, c, are entered for each layer of material. Triaxial testing of the asphalt material is performed in a manner that the shear strength parameters, N and c, are developed as a function of temperature. Hence, if the temperature of the asphalt layer is known (or assumed) at a site, then values of N, and, c, may be calculated from the relationships between the shear strength parameters and temperature. Moreover, to facilitate and provide an efficient means of analyzing early construction cases and flexible pavements reinforced with geosynthetics, "Windows" software was developed. The report includes a "user guide" for operating the computer software. Since N and c vary with depth of asphalt and temperature in the case of the asphalt layer, the entire asphalt layer is divided into finite layers. When the surface temperature of the asphalt is known (or assumed), a temperature distribution model is used to estimate the temperature at any depth below the asphalt layer surface. Consequently, the shear strength parameters are known at any depth (of each finite layer) below the surface.

To establish the validity and reasonableness of the newly developed limit equilibrium models, bearing capacity factors are derived from the limit equilibrium methods and compared to classical bearing capacity factors, N_c and N_q, developed by and Reissner in 1921. Differences range from 1 to 10 and 1 to 3 percent, respectively. The Slepak-Hopkins model yield values of $N_($ that are 12 to 38 larger than values published by Caquot and Kerisel. However, values of $N_($ from the Slepak-Hopkins model are only 3 to 11 percent larger than back-calculated values obtained by Debeer and Ladanyi from experimental footing tests. The Slepak-Hopkins model was also used to analyze 237 flexible pavement sections of the 1959-1960 AASHO Road Test. Factors of safety from the model analyses showed that very reasonable results were obtained and were in line with failures recorded at the test site. Factors of safety of pavement sections that in the Road Test that survived the 2-year testing program ($\geq$8 million equivalent single axle loads –ESAL) generally exceeded 1.5.

Finally, actual analyses of a stretch of roadway where failures occurred were analyzed. Three sites included sections involving tensile elements. At three locations where tensile elements were used, and assuming tensile element mobilized strains of 2 percent, 5 percent, and ultimate strain, the factor of safety increased some 2-5 percent, 2. –5 percent, and 6 to 12 percent, as shown by Perturbation analyses. Fabrics with larger strengths than those used at this site could produce larger factors of safety.

RECOMMENDATIONS AND IMPLEMENTATION

To advance the use and implementation of limit equilibrium bearing capacity models described herein, the following recommendations are proposed:

- The Perturbation Method proposed herein is recommended for general use in all classes of stability problems. In particular, the method is suitable for analyzing bearing capacity problems involving early pavement construction situations involving base aggregates reinforced with tensile elements. The approach, however, is suitable for analyzing completed flexible pavements reinforced with tensile elements. The method is also suitable for analyzing those situations where tensile elements are not used.

- To further validate the model, additional field research studies need to be made that involve flexible pavements reinforced with tensile elements. Additional flexible pavement sites, however, where obvious pavement failures have occurred, need to be analyzed that do not involve tensile elements. In cases involving failures, the Perturbation model should show low factors of safety. The examples described herein appear to indicate that low factors of safety were obtained in areas where the flexible pavement showed distress.

- As deformation occurs under wheel loadings—bearing capacity problems--the strains of pavement layers and the strains of geofabrics are not necessarily the same, that is, there is incompatibility of strains. To mobilize the strength of the geofabric, sufficient strains must occur in the geofabric—and the pavement layers. Although the forces should be derived from the principle of strain compatibility, in this study, a simple assumption with respect to reinforcement forces was made, that is, the external forces of the geofabric act horizontal. Development of a strain compatibility model was much beyond the scope of this study and a new research proposal should be considered in the future to develop a model. The assumption made in the Perturbation Model still allows the user to determine the factor of safety against failure if it assumed that a certain percentage of strain is mobilized in the geofabrics.

- To fully implement the Perturbation computer software it is recommended that a one- or two-day workshop be developed and taught to interested parties. The workshop should be geared toward teaching and explaining, in detail, the necessary parameters for performing bearing capacity analysis. This workshop would be developed for practicing geotechnical engineers.

- For practicing engineers who are not versed in geotechnical engineering and are mainly interested in performing bearing capacity analyses of early construction and completed flexible pavements cases involving tensile element forces, it recommended that simplified data entry screens be devised. In this case, the workshop could be shortened to one half-or one-day.

REFERENCES

Baker, R., and Garber, M., (1977a). *Discussion of On Slip Surface and Slope Stability Analysis by Chen, and Snitbhan,* N. S. Soils and Foundations, 17, No. 1, p. 65-68.

Baker, R., and Garber, M., (1977b). *Variational Approach to Slope Stability*, Proc. 9th ICSMFE, 2, p. 9-12.

Baker, R., and Garber, M., (1978). *Theoretical Analysis of the Stability of Slopes,* Geotechnique, 28, No. 4, p. 395-411.

Bailey, W.A. and Christian, J.T., (1969). *A Problem-Oriented Language for Slope Stability Analysis—User's Manual*, Soil Mechanics publication 1969, Department of Civil Engineering, (ICES LEASE-1, Slope Stability Analysis (for Computer)), Massachusetts Institute of Technology.

Bathurst, R.J., Benjamin, D.J., and Jarret, P.M.(1988). *Laboratory Study of Geogrid Reinforced Walls,* Royal Military College of Canada, Kingston, Ontario, Proceedings, Symposium on Geosynthetics for Soil Improvement, ASCE Geotechnical Special Publication No.18, p. 178-192.

Bishop, A.W., (1955). *The Use of the Slip Circle in the Stability Analysis of Slopes*, Geotechnique, Vol. 5.

Beech, J.F. (1987); *Importance of Stress-Strain Relationships in Reinforced Soil System Designs,* Proceedings of Geosynthetic '87 Conference, USA, p.133-44.

Berg, R.R., Chouery-Curtis, V.E. and Watson, C. H. (1989). *Critical Failure Planes in Analysis of Reinforced Slopes*, Proceedings of Geosynthetic '89 Conference, USA, p. 269-278.

Billiard, J.W. and Wu, J.T.H. (1991). *Load Test of a Large-Scale Geotextile-Reinforced Retaining Wall*, Geosynthetics '91 Conference, Proceedings, Vol. 2, p. 537-548.

Bishop, A.W. and Morgenstern, N. R (1960). *Stability Coefficients for Earth Slopes*, Geotechnique, Vol. 10.

Bishop, A.W. and Bjerrum, L.(1969). The Relevance of The Triaxial Test to the Solution of Stability Problems, Proceedings, Research Conference on Shear Strength of Cohesive Soils, Boulder Colorado, ASCE, June 1969.

Bonaparte, R., Holtz, R. D. and Giroud, J. P. (1987). *Soil Reinforcement Design Using Geotextiles and Geogrids, Geotextile Testing and the Design Engineer*, ASTM, STP No. 952, p. 69-116.

Bishop, A.W. and Henkel, D.J., (1957). *The Measurement of Soil Properties in the Triaxial Test,* Edward Arnold (Publishers) LTD., London, England.

Brinch Hansen, J. (1970). *A Revised Extended Formula for Bearing Capacity*, Danish geotechnical Institute bullentin, No. 11, Copenhagen.

Busiman, A.S.K. (1943). *Groundmechanica,* Waltman, Deft.

Castillo, R. and Luceno, A., (1983). *Variational Methods and Upper Bound Theorem, Journal of Engineering Mechanics*, ASCE, 109(5), p. 1157-1174.

Caquot, A. and Kerisel, J., (1953). *Ultimate Bearing Capacity of a Foundation on the Surface of a Cohesionless Soil,* Proceedings of the Third international Conference on Soils Mechanics and foundation Engineering, Switzerland.

Chen, W. F., (1975). *Limit Analysis and Soil Plasticity, Developments in Geotechnical Engineering,* Vol. 7

Chen, Z. U. and Morgenstern, N. R., (1983). *Extensions to the Generalized Method of Slices for Stability Analysis*, Canadian geotechnical Journal, 20, p. 104-119.

Ching, R.K.H. and Fredlund, D.G., (1983). *Some Difficulties Associated with the Limit Equilibrium Method of Slices*, Canadian Geotechnical Journal, Vol. 10, No. 4, National Research Council Canada.

Chowdhury, R. N. (1978). *Slope Analysis,* Developments in Geotechnical Engineering, Vol. 22.

Coulomb, C., (1773). Application Des Regles De Maximis Et Minimis a Quelques Problemes De Statique relatifs a L'Architecture, Memories De Savants Etrangers De L'Academic Des Sciences De Paris.

Claybourn, A.F. and Wu, J.T.H., (1991). *Case History Comparison of Geosynthetic-Reinforced Soil Walls*, Geosynthetics '91 Conference, Proceedings, Vol.2, p. 549-559.

DeBeer, E. E. and Ladanyi, B., (1961). *Etude Experimentwale de Ja Capacite Portante du sable sous des Foundations Etablies en Surface,* Proceedings of the 5th International Conference on Soil Mechanics and Foundation Engineering.

Daehn, W.W. and Hilf, J.W., (1951), *Implications of Pore Pressure in Design and Construction of Rolled Earth Dams*, International Congress on Large Dams, 4, Transactions, Vol. 1, New Delhi.

DeJong De Josselin, G. (1980). *Application of the Calculus of Variations to the Vertical Cut-off in Cohesive Frictionless Soil,* Geotechnique, 30(1), p. 1-16.

DeJong De Josselin, G. (1981). *Variational Fallacy*, Geotechnique, 31(4), p. 289-290.

De Mello, V. F. B., (1969). *Foundations of Buildings in Clay,* Proceedings of the 5th International Conference on Soil Mechanics and Foundation Engineering.

Delmas, Ph.; Berche, J. C. and Gourc, J. P., (1986). *Le Dimensionement Des Ouvrages Renforces Par Geotextile*, Programme CARTAGE. Bulletin Liaison Laboratoire Des Ponts et Chaussees, 142, p.33-44.

Duncan, J. M. and Wright, S. G. (1980). *The Accuracy of Equilibrium Methods of Slope Stability Analysis,* Engineering Geology, 16, p.5-17.

Feda, J., (1961). *Research on the Bearing Capacity of Loose Soil,* Proceedings of the 5th International Conference on Soil Mechanics and foundation Engineering.

Fellenius, W. (1927). Erdstatische Berechnungen Mit Reibung and Kohaesion, Erust, Berlin.

Fellenius, W. (1936). *Calculation of Stability of Earth Dams*, Transactions, 2nd Congress Large Dams, 4, p. 445.

Fredlund, D.G., (August 1985). *Soil Mechanics Principles that Embrace Unsaturated Soils,"* Proceedings of the Eleventh International Conference on Soil Mechanics and Foundation Engineering, San Francisco, California.

Fredlund, D.G. and Rahardji, H., (February 1985). *Theoretical Context for Understanding Unsaturated Residual Soil,* First International Conference on Geomechanics in Tropical Lateritic and Saprolitie Soils, Brazilian Society for Soil Mechanics, Vol. 1.

Fr`hlich, O. K., (1953). *The Factor of Safety with Respect to Sliding of a Mass of Soil Along the Arc of a Logarithmic Spiral.* Proceedings 3d ICSMFE, Switzerland, 2, p. 230-233.

Gourc, J. P.; Ratel, A., Delmas, Ph. (1986); *Design of Fabric Retaining Walls: The Displacement Method,* Proceedings 3rd ICG, 4, p. 1067-1072.

Gourc, J. P., Gotteland, P. H. and Delmas, Ph., (1989). *Parametric Study of Geosynthetic Reinforced Retaining Walls Using the Displacement Method*, Proceedings of Geosynthetic '89 Conference, p. 112-123.

Giroud, J. P. and Beech, J.F., (1989). *Stability of Soil Layers on Geosynthetic Lining Systems.* Proceedings, Geosynthetics '89 Conference, p. 35-46.

Hardin, B.O. and Hardin, K. O.; (September 1984), *A New Statically Consistent Formulation for Slope Stability Analysis* Proceedings of the IV International Symposium on Landslides.

Hadj-Hamoe, T.; Baker, R. M.; and Gwyn, W.W. (1990). *Field Performance of a Geogrid-Reinforced Embankment,* Transportation Research Record 1277, p. 80-89.

Hopkins, T. C., (1984). *Design of Embankments on Clay Foundations,* Kentucky Transportation Research Program, College of Engineering, University of Kentucky (also presented to the Annual Southeastern Conference on Dam Safety, Knoxville, TN, April 1984).

Hopkins, T.C. and Sharpe, G.W., (March 1985). *Unstable Subgrade I 65, Hardin County (I 65-5(17)92); FSP 047-0065-091-094-0396*, University of Kentucky Transportation Center, College of Engineering, Research Report UKTRP 85-9.

Hopkins, T. C., (1986). *A Generalized Slope Computer Program: User's Guide for Hopk-I*, Research Report UKTRP-86-2, University of Kentucky Transportation Center, College of Engineering, Lexington, Kentucky.

Hopkins, T.C. and Allen, D. L., (October 1986). *Lime Stabilization of Pavement Subgrade Soils of Section AA-19 of the Alexandria-Ashland Highway*, Research Report 86-24, University of Kentucky Transportation Center, College of Engineering, Lexington, Kentucky.

Hopkins, T.C., (October 1987). *Lime Stabilization of Kentucky Soils*, University of Kentucky Transportation Center, College of Engineering, Oral presentation to the National Lime Conference, Lexington, Kentucky

Hopkins, T.C., Hunsucker, D., and Sharpe, G.W., (1988). *Highway Field Trials of Chemically Stabilized Soil Subgrades*, Proceedings of the Ohio River Valley Soils Seminar XIX, Lexington, Kentucky.

Hopkins, T.C. and Hunsucker, D., (November 1990). *Interim Design Guidelines for Modified Pavements, University of Kentucky Transportation Center*, College of Engineering (Interim unpublished Report).

Hopkins, T. C. (June 1991). *Bearing Capacity Analyses of Pavements*, Research Report KTC-91-8, University of Kentucky Transportation Center, College of Engineering.

Hopkins, T.C., Hunsucker, D.Q. and Beckham, T.L., (1994a). *Selection of Design Strengths of Untreated Soil Subgrades and Subgrades Treated with Cement and Hydrated Lime***,** Transportation Research Record No. 1440, pp 37-44.

Hopkins, T.C., Hunsucker, D.Q., and Beckham, T.L., (1994b). *Long-term Performance of Untreated Soil Subgrades and Subgrades Treated with Cement and Hydrated Lime***,** Transportation Research Record No. 1440, pp 45-52.

Hopkins, T.C.; (July 1994a), *Minimum Bearing Strength of Soil Subgrades Required to Construct Flexible Pavements***,** Proceedings, The 4th International Conference on the Bearing Capacity of Roads and Airfields, Vol.1, Minneapolis, Minnesota.

Hopkins, T.C., (July 1994b). *Case Studies of Flexible Pavement Failures During Construction***,** Proceedings, The 4th International Conference on the Bearing Capacity of Roads and Airfields, Vol.1, Minneapolis, Minnesota.

Hopkins, T. C. and Beckham, T. L., (June 1995). *Modification of Highway Soil Subgrades*, Research Report KTC-94-11, University of Kentucky Transportation Center, College of Engineering, Lexington, Kentucky.

Hopkins, T. C. and Slepak, M. E. (July 1998). *Estimated Factors of Safety of the AASHO Road Test Flexible Pavement Sections Based on Limiting Equilibrium Methods,* Proceedings, Fifth International Conference on the Bearing Capacity of Roads and Airfields, Trondheim, Norway.

Hopkins, T. C. and Beckham, T. L., (2000). *Influence of Clay Fraction on the Behavior of Soil Subgrades,* Proceedings, Fifth International Symposium on Unbound Aggregates in Roads, Nottingham, UK June 2000.

Hopkins, T. C., Beckham, T. L., and Sun, L. (2004). *Kentucky Geotechnical Database,* Research Report KTC 93-29, Research Report KTC-05-03/SPR227-01-F, College of Engineering, University of Kentucky Transportation Center.

Inglod, T.S., (1982). *An Analytical Study of Geotextile Reinforced Embankments,* Proceedings, 2nd ICG, 3, p. 683-688.

Janbu, N. (1957). *Earth Pressure and Bearing Capacity Calculations by Generalized Procedure of Slices*, Proceedings 4th ICSMFE, 2, p. 207-212.

Jewell, R. A., (1982). *A Limit Equilibrium Design Method for Reinforced Embankments on Soft Foundations*, Proceedings 2nd ICG, 3, p. 671-676.

Huang, Y. H. and Avery, C. M., (1976). *Stability of Slopes by Logarithmic-Spiral Method*, J. of geotechnical Engineering Division, Proceedings, ASCE, 102, No. GT1, p. 41-49.

Kopacsy, J., (1955). Uber Die Bruchflachen und bruchspannungen in den Erdbauten, Gedenbuch-fur Dr. J. Jaky. P. 671-676.

Janbu, N. (1954). *Application of Composite Slip Surface for Stability Analysis, European Conference on Stability of Earth Slopes,* European Conference on Stability of Earth Slopes, Stockholm, Sweden.

Lambe, T. W. and Whitman, R. V., (1969). *Soil Mechanics*, John Wiley and Sons, Inc., New York.

Langston, P. J. and Williams, N. D., (1989). *Design Methods for Reinforced Embankments on Soft Foundations*, Proceedings Geosynthetic '89 Conference, p. 172-183.

Leshchinsky, D., (1984). Geotextile Reinforced Earth, Part I and II, Research Report Nos. CE 84-44/45, University of Delaware.

Leshchinsky, D., (1985). *Design Manual for Geotextile-Retained Earth Walls*, Research Report No. CE 85-51, University of Delaware.

Leshchinsky, D. and Reinschmidth, A. J., (1985). *Stability of Membrane Reinforced Slopes*, Journal of Geotechnical Engineering, Proceedings ASCE, 111, No. 11, p. 1285-1300.

Leshchinsky, D., Baker, R, and Silver, M.L., (1985). *Three -Dimensional Analysis of Slope Stability*, International Journal for Numerical and Analytical Methods in Geomechanics, 9, p. 199-223.

Leshchinsky, D. and Perry, E.B., (1987). *A Design Procedure for Geotextile-Reinforced Walls*, Proceedings Geosynthetic '87 Conference, p. 95-107.

Leshchinsky, D. and Boedeker, R. H., (1989). *Geosynthetic Reinforced Soil Structures*, Journal of Geotectural Engineering, Vol. 115, 10, p. 1459-1478.

Leshchinsky, D., (1990). *Slope Stability Analysis: Generalized Approach*, Journal of Geotechnical Engineering, ASCE, 116(5), p.851-867.

Lowe, J. and Karafiath, L., (1960). *Stability of Earth Dams Upon Drawdown*, Proceedings Pan American Conference on Soil Mechanics and Foundation Engineering, Mexico City, 2, p. 537-552.

Luceno, A. and Castillo, E., (1981). Discussion of *Extreme-Value Problems of Limiting-Equilibrium,* by M. Garber and R. Baker, Journal of the Geotechnical Engineering Division, ASCE, 107(1), p. 118-121.

Morgenstern, N. R. and Price, V. E., (1965). *The Analysis of the Stability of General Slip Surfaces,* Geotechnique, Vol. 15.

McGown, A., Andrawes, K.Z, Yeo, K. C., and DuBois, D. (1984). *The Load-Strain-Time Behavior of Tensar Geogrid*s, Proceedings, Polymer Grid Reinforcement, London, 1984, p. 11-17.

Murray, R., (1982) *Fabric Reinforcement of Embankments and Cuttings*, Proceedings 2nd ICG, 3, p. 707-713.

Meyerhof, G. G., (1951). *The Ultimate Bearing Capacity of Foundations,* Géotechnique, Vol. 2, pp. 301.

Meyerhof, G.G., (1963). *Some Recent Advances on the Bearing Capacity of Foundations*, *Canadian Geotechnical Journal*, Vol. 1, 16-26.

Prandtl, (1921). Hautaufsatze Uber die Eindringungsfestigkrit (Harte) plasticher Baustoffe und die Festigkeit von Schneiden, Zaitschrift Fur Angewandte, Mathematik und Mechanik, Vol.1, No. 1.

Reissner, H., (1924). *Zum Erddruckproblem*, Proceedings, First International Conference on Applied Mechanics, Delft.

Raulin, P., Rouques, G., and Toubol, A., (1974). *Calcul De La Stabilite Des Pente En Rupture Non Circulaire*, Rapport De recherche, No. 36

Rendulic, L., (1935). Ein Beitrag Zur Bestimmung Der gleisicherheit, Bauingenier, No. 19/20.

Rowe, R. K., (1984). *Reinforced Embankments: Analysis and Design,* Journal of the geotechnical Engineering, 110, No. 2, p. 231-246.inc

Rowe, R. K. and Soderman, K. L., (1985). *An Approximate Method for Estimating the Stability of Geotextile-Reinforced Embankments*, Canadian Geotechnical Journal, 22, p. 392-304.

Rowe, R. K. and Soderman, K. L., (1987). *Reinforcement of Embankments on Soils Whose strength Increases with Depth*, Proceedings Geosynthetic '87 conference, p. 266-277.

Rowe, R. K. and Myllerville, B. L. J., (1989). *Consideration of Strain in the Design of Reinforced Embankments,* Proceedings Geosynthetic '89 Conference, p. 124-135.

Schmertmann, G. R., Chouery-Curtis, V.E., Johnson, R. D., and Bonaparte, R. (1987), *Design Charts for Geogrids-Reinforced Soil Slopes*, Proceedings Geosynthetic '87 Conference, p.108-120.

Schneider, H. R. and Holtz, R.D., (1986). *Design of Slopes Reinforced with Geotextiles and Geogrids,* Geotextiles and Geomembranes, 3, p. 29-51.

Seed, H. B. and Sultan, H. A., (1967). Stability Analysis for a Sloping Core Embankment, Journal of the Soil Mechanics and Foundation Divisions, 93, No. SM4, p. 69-83.

Skempton, A.W., (1954). *The Pore Pressure Coefficients A and B*, Geotechnique, Vol. 4, No. 4.

Slepak, M. E. and Hopkins, T.C., (1993). *Computer Program for Stability Analysis of Embankments with Tensile Elements*, Research Report KTC 93-29, University of Kentucky Transportation Center.

Slepak, M. E. and Hopkins, T.C., (January 1995a). *Personal Computer Program for Analysis of Embankments with Tensile Elements,* Research Report KTC 93-29, University of KentuckyTransportation Center, Geotechnology Section, College of Engineering, Lexington, Kentucky.

Slepak, M. E. and Hopkins, T.C., (1995b). *Modified Perturbation Method in Stability Analysis of Reinforced Earth Structures*, Geosynthetics '95, International Conference Proceedings,

Nashville, Tennessee USA.

Southgate, H. F. and Deen, R. C.; (1969), "Temperature Distribution Within Asphalt Pavements and Its Relationship to Pavement Deflection," Highway Research Board, HRB-291, Washington, D.C.

Southgate, H. F. and Deen, R. C., (1975). *Temperature Distributions in Asphaltic Concrete Pavements,* TRB-549, Transportation Research Board, Washington, D.C.

Southgate, H. F., Deen, R. C. and Havens, J. H., (November 1981). *Development of a Thickness Design System for Bituminous Concrete Pavements,* University of Kentucky Transportation Center, College of Engineering, Research Report UKTRP-81-20.

Southgate, H. F., Sharpe, G. W., Deen, R. C. and Havens, J. H., (August 1982). *Structural Capacity of In-Place Asphaltic Pavements from Dynamic Deflections,* Fifth International Conference on the Structural Design of Asphalt Pavements, Proceedings, Vol. 1, The Delft University of Technology, The Netherlands.

Spencer, E., (1967). *A Method of Analysis of the Stability of Embankments Assuming Parallel Inter-Slice Forces,* Geotechnique, Vol 17.

Spencer, E., (1973). *Thrust Line Criterion in Embankment Stability Analysis*, Geotechnique, Vol. 23.

Steward, J. E., Williamson, R., and Mohney, J., (1977). G*uidelines for Use of Fabrics in Construction and Maintenance of Low-volume Road*s, Chapter 5, USDA, Forest Service; Portland, Oregon, Report No. FHWA-TS-78-205.

Sybase PowerBuilder, (1999a). *User's Guide,* Sybase, Inc.

Sybase PowerBuilder, (1999b). *Application Technique,* Sybase, Inc.

Sybase PowerBuilder, (1999c). *PowerBuilder Foundation class Library Object Reference,* Sybase, Inc.

Taylor, D. W., (1937). *Stability of Earth Slopes,* Journal of the Boston Society of Civil Engineering, 24, No. 3, p. 197-246.

Thompson, M. R., (1988). *Admixture Stabilization of Subgrades,* Proceedings, Nineteenth Annual Ohio River Valley Soils Seminar (ORVSS), Lexington, Kentucky.

Traylor, M.L. and Thompson, M. R., (1977). *Sinkage Prediction-Subgrade Stability,* Civil Engineering Studies, Transportation Engineering Studies, Transportation Engineering Series No. 17, Illinois Cooperative Highway and Transportation Series No. 168, Department of Civil Engineering, University of Illinois at Urbana-Champaign.

Tensar®Corporation, Technical Note, (1986a). *Guidelines for the Design of Tensar® Geogrids*. Reinforced Soil Retaining Walls.

Tensar®Corporation, Technical Note, (1986b). *Slope Reinforcement with Tensar® Geogrids*. Design and Construction Guideline.

Terzaghi, K., (1943). *Theoretical Soil Mechanics,* John Wiley and Sons, Incorporated, New York, NY.

Wallace, R. B. and Fluet, J.E., (1987). *Slope Reinforcement Using Geogrids*, Proceedings Geosynthetic '87 Conference, p.121-132.

Winterhorn, H. F. and Fang, H. Y., (1975). *Foundation Engineering Handbook*, Von Nostrand Reinhold Company, New York.

Wright, S. G., (1969). *A Study of Slope Stability and the Undrained Shear Strength of Clay Shales,* Thesis, University of California, Berkley, California.

Wright, S. G. and Duncan, J. M., (1991). *Limit Equilibrium Stability Analyses for Reinforced Slopes,* Transportation Research Board 1330, p. 40-46.

Verduin, J. R. and Holtz, R. D., (1989). *Geosynthetically Reinforced Slopes: A New Procedure*, Proceedings Geosynthetic '87 Conference, p. 279-290.

Vesic', A.S. and Johnson, W. H., (1963). *Model Studies of Beams Resting on a Silt subgrade,* Proceedings, ASCE Journal of the Soil Mechanics and Foundations Division, 89, No. SM1.

Vesic', A. S. and Saxena, S. K., (1970). *Analysis of Structural behavior of AAASHO road Test Rigid Pavements,* Report 97, National Cooperative Highway research Program, National Academy of Science, Washington, D. C.